

MEASUREMENT AND BEHAVIOR OF THE OVERALL VOLUMETRIC OXYGEN TRANSFER COEFFICIENT IN AERATED AGITATED ALKANE BASED MULTIPHASE SYSTEMS

by

Musaida Mercy Manyuchi

Thesis submitted in partial fulfillment
of the requirements for the Degree



MASTER OF SCIENCE IN ENGINEERING
(CHEMICAL ENGINEERING)

in the Department of Process Engineering
at the University of Stellenbosch

Supervised by

Prof. K.G. Clarke

STELLENBOSCH

(December 2010)

Declaration

I, the undersigned, hereby declare that the work contained in this thesis is my own original work and that I have not previously in, its entirety or in part submitted it at any university for a degree.

M.Manyuchi
Signature

November 2010
Date

Abstract

Hydrocarbons provide excellent feed stocks for bioconversion processes to produce value added products using various micro-organisms. However, hydrocarbon-based aerobic bioprocesses may exhibit transport problems where the bioconversion is limited by oxygen supply rather than reaction kinetics. Consequently, the overall volumetric oxygen transfer coefficient (K_{La}) becomes critical in designing, operating and scaling up of these processes. In view of K_{La} importance in hydrocarbon-based processes, this work evaluated K_{La} measurement methodologies as well as quantification of K_{La} behavior in aerated agitated alkane-solid-aqueous dispersions.

A widely used K_{La} measurement methodology, the gassing out procedure (GOP) was improved. This improvement was done to account for the dissolved oxygen (DO) transfer resistances associated with probe. These resistances result in a lag in DO response during K_{La} measurement. The DO probe response lag time, was incorporated into the GOP resulting in the GOP (lag) methodology. The GOP (lag) compared well with the pressure step procedure (PSP), as documented in literature, which also incorporated the probe response lag time.

Using the GOP (lag), K_{La} was quantified in alkane-solid-aqueous dispersions, using either inert compounds (corn flour and CaCO_3) or inactive yeast cells as solids to represent the micro-organisms in a hydrocarbon bioprocess. Influences of agitation, alkane concentration, solids loading and solids particle sizes and their interactions on K_{La} behavior in these systems were quantified.

In the application of an accurate K_{La} measurement methodology, the DO probe response lag time was investigated. Factors affecting the lag, which included process conditions such as agitation (600-1200rpm), alkane concentration (2.5-20% (v/v)), alkane chain length ($n\text{-C}_{10-13}$ and $n\text{-C}_{14-20}$), inert solids loading (1-10g/L) and solids particle sizes (3-14 μm) as well as probe characteristics such as membrane age and electrolyte age (5 day usage), were investigated. K_p , the oxygen transfer coefficient of the probe, was determined experimentally as the inverse of the time taken for the DO to reach 63.2% of saturation after a step change in DO concentration. K_p dependence on these factors was defined using 2^2 factorial design experiments. K_p decreased on increased membrane age with an effect double that of K_p decrease due to electrolyte age. Additionally, increased alkane concentration decreased K_p with an effect 7 times

higher compared to that of K_p decrease due to increased alkane chain length. This was in accordance to Pareto charts quantification.

K_{La} was then calculated, using the GOP (lag), according to equation [1] which incorporates the influence of K_p . Equation 1 is derived from the simultaneous solution of the models which describe the response of the system and of the probe to a step change in DO.

$$\frac{C_p}{C_p^*} = 1 - \frac{1}{K_p - K_{La}} \left[K_p e^{-K_{La}t} - K_{La} e^{-K_p t} \right] \quad [1]$$

The K_{La} values documented in literature from the PSP and K_{La} calculated by the GOP (lag) showed only a 1.6% difference. However K_{La} values calculated by the GOP (lag) were more accurate than K_{La} calculated by the GOP, with up to >40% error observed in the latter according to *t-tests* analyses. These results demonstrated that incorporating K_p markedly improved K_{La} accuracy. Consequently, the GOP (lag) was chosen as the preferred K_{La} measurement methodology.

K_{La} was determined in *n*-C₁₄₋₂₀-inert solid-aqueous dispersions. Experiments were conducted in a stirred tank reactor with a 5L working volume at constant aeration of 0.8vvm, 22°C and 101.3kPa. K_{La} behavior across a range of agitations (600-1200rpm), alkane concentrations (2.5-20% (v/v)), inert solids loadings (1-10g/L) and solids particle sizes (3-14µm) was defined using a 2⁴ factorial design experiment. In these dispersions, K_{La} increased significantly on increased agitation with an effect 5 times higher compared to that of K_{La} increase due to interaction of increased alkane concentration and inert solids loading. Additionally, K_{La} decreased significantly on increased alkane concentration with an effect 4 times higher compared to both that of increased solids particle sizes and the interaction of increased agitation and solids particle size.

In *n*-C₁₄₋₂₀-yeast-aqueous dispersions, K_{La} was determined under narrowed process conditions better representing typical bioprocess conditions. K_{La} behavior across a range of agitations (600-900rpm), alkane concentrations (2.5-11.25% (v/v)) and yeast loadings (1-5.5g/L) using a 5µm-yeast cell was defined using a 2³ factorial design experiment. In these dispersions, K_{La} increased significantly on increased agitation. Additionally, K_{La} decreased significantly on increased yeast loading with an effect 1.2 times higher compared to that of K_{La} decrease due to interaction of increased alkane concentration and yeast loading.

In this study, the importance of K_p for accurate K_La measurement in alkane based systems has been quantified and an accurate and less complex methodology for its measurement applied. Further, K_La behavior in aerated alkane-solid-aqueous dispersions was quantified, demonstrating K_La enhancement on increased agitation and K_La depression on increased alkane concentration, solids loading and solids particle sizes.

Abstract (Afrikaans)

Koolwaterstowwe dien as uitstekende voervoorraad vir 'n verskeidenheid van mikro-organismes wat aangewend word in biologiese omsettingsproesse ter vervaardiging van waardetoevoegende produkte. Hierdie biologiese omsettingsproesse word egter vertraag weens die gebrek aan suurstoftoevoer onder aerobiese toestande. Die tempo van omsetting word dus beheer deur die volumetriese suurstofoordragkoeffisiënt (K_{La}) eerder as die toepaslike reaksiekinetika. Die bepaling van 'n akkurate K_{La} word dus krities tydens die ontwerp en opskaling van hierdie prosesse. Met dit in gedagte het hierdie studie die huidige metodes om K_{La} te bepaal geëvalueer en die gedrag van K_{La} in goed vermengde en belugde waterige alkaanmengsels met inerte vastestowwe, soos gisselle, in suspensie ondersoek.

'n Deesdae populêre metode om K_{La} te bepaal, die sogenaamde gasvrylatingsprosedure (GOP) is in hierdie studie verbeter. Die verbetering berus op die ontwikkeling van 'n prosedure om die suurstofoordragsweerstand van die probe wat die hoeveelheid opgeloste suurstof (DO) meet, in berekening te bring. Hierdie weerstand veroorsaak 'n vertraging in die responstyd van die probe. Die verbeterde metode, GOP (lag), vergelyk goed met die gepubliseerde resultate van die drukstaptegniek (PSP) wat ook die responstyd in ag neem.

GOP (lag) is ingespan om K_{La} te gekwantifiseer vir waterige alkaan-vastestof suspensies. Inerte componente soos meliemeel, kalsiumkarbonaat en onaktiewe gisselle het gedien as die vastestof in suspensie verteenwoordigend van die mikroorganismes in 'n koolwaterstof bio-proses. Die invloed van vermengingstempo, alkaan konsentrasie, vastestof konsentrasie en partikelgrootte asook die interaksie van al die bogenoemde op K_{La} is kwantitatief bepaal in hierdie studie.

Faktore wat die responstyd van die DO probe beïnvloed is ondersoek. Hierdie faktore is onder meer vermengingstempo (600-1200rpm), alkaankonsentrasie (2.5-20% (v/v)), alkaankettinglengte (n-C₁₀₋₁₃ en n-C₁₄₋₂₀), vastestofkonsentrasie (1-10g/L) en partikelgrootte (3-14 μ m). Faktore wat die eienskappe van die probe beïnvloed, naamlik membraan-en elektrolietouderdom (5 dae verbruik), is ook ondersoek. K_p , die suurstofoordragkoeffisiënt, is bepaal deur 'n inkrementele verandering in die suurstofkonsentrasie van die mengsel te maak en die tyd vir 63.2% versadiging van die probelesing te noteer. Die genoteerde tyd is die response tyd van die probe en K_p , die inverse van hierdie tyd. Die afhanklikheid van K_p op die bogenoemde faktore is

ondersoek in 'n 2² faktorieël ontwerpte reeks eksperimente. K_p toon 'n afname met 'n toename in membraanouderdom. Hierdie afname is dubbel in grootte as dit vergelyk word met die afname relatief tot die toename in elektrolietouderdom. Verder toon K_p 'n afname met 'n toename in alkaankonsentrasie. Hierdie afname is 7 keer groter relatief tot die afname gesien met die toename in alkaan kettinglengte. Hierdie is in goeie ooreenstemming met Pareto kaarte as kwantifiseringsmetode.

K_La is bereken met die inagname van K_p volgens vergelyking [1]:

$$\frac{C_p}{C_p^*} = 1 - \frac{1}{K_p - K_{La}} \left[K_p e^{-K_{La}t} - K_{La} e^{-K_p t} \right] \quad [1]$$

Vergelyking [1] is afgelei vanaf die gelyktydige oplossing van die bestaande modelle wat die responstyd van die probe vir 'n stapverandering in DO bereken.

Die K_La waardes van die PSP metode uit literatuur verskil in die orde van 1.6% van dié bereken deur vergelyking [2]. Hierdie verskil is weglaatbaar. Die K_La waardes verkry uit die GOP metode wat nie K_p in berekening bring nie, verskil met meer as 40% van die huidige, verbeterde metode volgens die statistiese *t-test* analiese. Dit bewys dat die inagname van K_p 'n merkwaardige verbetering in die akuraatheid van K_La teweeg bring. GOP (lag) kry dus voorkeur vir die berekening van K_La verder aan in hierdie studie.

K_La is bereken vir n-C₁₄₋₂₀-water mengsels met inerte vastestofsuspensies. Die eksperimente is uitgevoer in 'n 5L geroerde reaktor met 'n konstante belugting van 0.8vvm (volume lug per volume suspensie per minuut), 22°C en 101.3kPa. Die gedrag van K_La met betrekking tot vermengingstempo (600-1200opm), alkaankonsentrasie (2.5-20% (v/v)), vastestofkonsentrasie (1-10g/L) en partikelgrootte (3-14µm) is ondersoek in 'n 2⁴ faktorieël ontwerpte reeks eksperimente. Verder is die invloed van vloeistofviskositeit en oppervlakspanning op K_La ondersoek in 'n 2³ faktorieël ontwerpte reeks eksperimente. K_La het 'n beduidende toename getoon met 'n toename in vermengingstempo. Hierdie toename was 5 keer groter as die toename relatief tot die interaksie van alkaan-en vastestofkonsentrasie. K_La het ook beduidend afgeneem met 'n toename in alkaankonsentrasie. Die toename was 4 keer groter as die toename relatief tot die toename in partikelgrootte en die interaksie van vermengingstempo en partikelgrootte.

In n-C₁₄₋₂₀-water mengsels met gissuspensies is K_La bepaal onder kondisies verteenwoordigend van tipiese biologiese omsettingsprosesse. Die gedrag van K_La

met betrekking tot vermengingstempo (600-900opm), alkaankonsentrasie (2.5-11.25% (v/v)) en giskonsentrasie (1-5.5g/L) met 'n partikelgrootte van 5 μ m is ondersoek in 'n 2³ faktorieel ontwerpte reeks eksperimente. Hierdie eksperimente het 'n beduidende toename in K_{La} met 'n toename in vermengingstempo getoon sowel as 'n beduidende afname met 'n toename in giskonsentrasie. Hierdie afname is in die orde van 1.2 keer groter in vergelyking met die interaksie van alkeen- en giskonsentrasie.

Hierdie studie bring die kritieke rol wat K_p speel in die akkurate bepaling van K_{La} in waterige alkaansisteme met inerte vastestofsuspensies na vore. Dit stel verder 'n metodiek voor vir die akurate meting van en kwantifisering van beide K_p en K_{La} onder aerobiese toestande met betrekking tot vermengingstempo, alkaankonsentrasie, vastestofkonsentrasie en partikelgrootte.

Acknowledgements

I express my gratitude to Prof Clarke for her time, advice, shared expertise on my research work especially for teaching me to think critically, to take charge of my work and to organize my scientific thoughts. Without her it would have been impossible come up with this piece of work.

I also thank Prof Aldrich for his shared knowledge on experimental design and analysis.

Lynette Bresler, Sherry-Lynn Moses and Julian Steyl are thanked for the administrative help. Hanlie Botha for solids samples analysis. The Department of Physical Chemistry is thanked for supply of the tensiometer.

Keenan Bence and Ryno Voigt are thanked for assistance in the lab. Deside Chibwe, Umit Uras, LJ du Preez and Joseph Hamuyuni for being my office mates and for enabling me to have better days in Stellenbosch.

The Manyuchis and the Tichapondwas are thanked for being my family, for their love and constant encouragement. Special thanks go to my mother for seeing me this far in life and to Shep for making my life complete.

DST-NRF Centre of Catalysis (C*-Change) is thanked for funding this work.

My final thanks go to God, for never letting me go in all the seasons of my life.

Table of Contents

DECLARATION	I
ABSTRACT	II
ABSTRACT (AFRIKAANS).....	V
ACKNOWLEDGEMENTS.....	VIII
TABLE OF CONTENTS	IX
1 INTRODUCTION.....	1
2 LITERATURE REVIEW	4
2.1 OXYGEN TRANSFER FROM GAS BUBBLE TO CELL	4
2.1.1 <i>Development of the first order model describing oxygen transfer</i>	5
2.1.2 <i>Development of the second order model describing oxygen transfer</i>	8
2.2 MEASUREMENT METHODS FOR THE OVERALL VOLUMETRIC OXYGEN TRANSFER COEFFICIENT.....	9
2.2.1 <i>Measurement using the gassing out procedure and the first order response model</i>	9
2.2.2 <i>Measurement using the pressure step procedure</i>	10
2.2.3 <i>Measurement using the gassing out procedure and the second order response model</i>	11
2.2.3.1 The probe response lag time	11
2.2.3.2 Influence of the probe response lag time on measurement of the overall volumetric oxygen transfer coefficient.....	16
2.3 BEHAVIOR OF THE OVERALL VOLUMETRIC OXYGEN TRANSFER COEFFICIENT.....	17
2.3.1 <i>Influence of agitation rate</i>	18
2.3.1.1 Influence of agitation rate on the oxygen transfer coefficient.....	19
2.3.1.2 Influence of agitation rate on the gas-liquid interfacial area per unit volume	19
2.3.2 <i>Influence of hydrocarbon addition</i>	21
2.3.2.1 Influence of hydrocarbon addition on the oxygen transfer coefficient....	21
2.3.2.2 Influence of hydrocarbon addition on the gas-liquid interfacial area per unit volume	23
2.3.3 <i>Influence of solids addition</i>	25
2.3.3.1 Influence of solids addition on the oxygen transfer coefficient.....	27

2.3.3.2 Influence of solids addition on the gas-liquid interfacial area per unit volume	28
3 HYPOTHESES, SCOPE OF PROJECT AND OBJECTIVES	30
3.1 HYPOTHESES.....	30
3.2 SCOPE OF RESEARCH PROJECT AND OBJECTIVES.....	31
3.2.1 <i>Evaluation of measurement method for the overall volumetric oxygen transfer coefficient</i>	31
3.2.2 <i>Quantification of the behavior of the overall volumetric oxygen transfer coefficient in alkane-solid-aqueous dispersions</i>	32
4 EXPERIMENTAL MATERIALS AND METHODOLOGY	34
4.1 MATERIALS.....	34
4.1.1 <i>Hydrocarbons</i>	34
4.1.2 <i>Solids</i>	34
4.2 EXPERIMENTAL SYSTEM SET UP AND PROCESS CONDITIONS.....	36
4.3 MEASUREMENT OF THE OVERALL VOLUMETRIC OXYGEN TRANSFER COEFFICIENT ...	37
4.3.1 <i>Measurement using the gassing out procedure and the first order response model</i>	38
4.3.2 <i>Measurement using the gassing out procedure and the second order response model</i>	39
4.3.3 <i>Measurement of the probe response lag time</i>	40
4.4 MEASUREMENT OF FLUID VISCOSITY AND FLUID SURFACE TENSION	42
4.4.1 <i>Homogenization of alkane-solid-aqueous dispersions</i>	42
4.4.2 <i>Measurement of fluid viscosity</i>	43
4.4.3 <i>Measurement of fluid surface tension</i>	44
4.5 EXPERIMENTAL DESIGN AND STATISTICAL ANALYSES	45
4.5.1 <i>Evaluation of measurement methodology</i>	46
4.5.2 <i>Quantification of the behavior of the overall volumetric oxygen transfer coefficient</i>	47
4.5.2.1 <i>Alkane-aqueous dispersions with inert solids</i>	47
4.5.2.2 <i>Alkane-aqueous dispersions with inactive yeast cells</i>	50
5 RESULTS AND DISCUSSION	53
5.1 EVALUATION OF MEASUREMENT METHOD IN ALKANE MULTIPHASE SYSTEMS.....	53
5.1.1 <i>Factors affecting the probe response lag time</i>	53

5.1.1.1	Effect of membrane age, electrolyte age and their interaction.....	53
5.1.1.2	Effect of agitation rate, alkane concentration and their interaction.....	55
5.1.1.3	Effect of alkane chain length, alkane concentration and their interaction	57
5.1.1.4	Effect of solids loading, solids particle size and their interaction.....	59
5.1.2	<i>Influence of the probe response lag time on the overall volumetric oxygen transfer coefficient</i>	61
5.2	QUANTIFICATION OF THE BEHAVIOR OF THE OVERALL VOLUMETRIC OXYGEN TRANSFER COEFFICIENT IN AERATED AGITATED ALKANE-SOLID-AQUEOUS DISPERSIONS....	66
5.2.1	<i>Alkane-aqueous dispersions with inert solids</i>	66
5.2.1.1	Effect of agitation rate.....	68
5.2.1.2	Effect of alkane concentration.....	70
5.2.1.3	Effect of solids loading.....	74
5.2.1.4	Effect of solids particle size	76
5.2.1.5	Effect of interaction between agitation rate and alkane concentration...	76
5.2.1.6	Effect of interaction between agitation rate and solids loading	77
5.2.1.7	Effect of interaction between agitation rate and solids particles size	77
5.2.1.8	Effect of interaction between alkane concentration and solids loading..	77
5.2.1.9	Effect of interaction between alkane concentration and solids particle size	78
5.2.1.10	Effect of interaction between solids loading and solids particle size...	78
5.2.2	<i>Alkane-aqueous dispersions with inactive yeast cells</i>	78
5.2.2.1	Effect of agitation rate.....	80
5.2.2.2	Effect of alkane concentration.....	81
5.2.2.3	Effect of yeast loading	83
5.2.2.4	Effect of interaction between agitation rate and alkane concentration...	84
5.2.2.5	Effect of interaction between agitation rate and yeast loading.....	84
5.2.2.6	Effect of interaction between alkane concentration and yeast loading...	84
5.2.3	<i>Comparison of trends in systems with inert solids to those with inactive yeast</i>	84
6	CONCLUSIONS	87
6.1	EVALUATION OF MEASUREMENT METHODOLOGY.....	87
6.2	QUANTIFICATION OF THE BEHAVIOR OF THE OVERALL VOLUMETRIC OXYGEN TRANSFER COEFFICIENT IN ALKANE- SOLID-AQUEOUS DISPERSIONS	89

6.2.1	<i>Alkane-aqueous dispersions with inert solids</i>	89
6.2.2	<i>Alkane-aqueous dispersions with inactive yeast</i>	90
6.2.3	<i>Comparison of trends in systems with inert solids to those with inactive yeast</i>	91
7	RECOMMENDATIONS	92
8	REFERENCES	93
	APPENDICES	104
A.1:	DERIVATION OF FIRST ORDER RESPONSE MODEL USED FOR MEASUREMENT OF THE OVERALL VOLUMETRIC OXYGEN TRANSFER COEFFICIENT	104
A.2:	LAPLACE TRANSFORMS SOLUTION FOR SECOND ORDER RESPONSE MODEL USED FOR MEASUREMENT OF THE OVERALL VOLUMETRIC OXYGEN TRANSFER COEFFICIENT ...	108
A.3:	ANALYTICAL DERIVATION OF SECOND ORDER RESPONSE MODEL USED FOR MEASUREMENT OF THE OVERALL VOLUMETRIC OXYGEN TRANSFER COEFFICIENT ...	112
A.4:	CHARACTERISTICS OF THE PROBE AND DERIVATION OF THE PROBE RESPONSE LAG TIME	117
	<i>A4.1: Probe characteristics</i>	117
	<i>A4.2: Derivation of the probe response lag time</i>	118
A.5:	SAMPLE CALCULATION OF THE OVERALL VOLUMETRIC OXYGEN TRANSFER COEFFICIENT USING THE SECOND ORDER RESPONSE MODEL	120
A.6:	THEORY ON FLUID VISCOSITY AND SURFACE TENSION MEASUREMENT	121
	<i>A.6.1 The homogenization process</i>	121
	<i>A.6.2 Theory on fluid viscosity and surface tension</i>	122
A.7:	REPRODUCIBILITY OF RAW DATA IN THE ALKANE MULTIPHASE SYSTEMS	124
A.8:	STATISTICAL VALIDATION OF EXPERIMENTAL RESULTS	145

List of Figures

Figure 2.1	Steps for transfer of oxygen from gas bubble to cell.....	4
Figure 2.2	Concentration gradients for gas-liquid oxygen transfer associated with the two film theory	7
Figure 2.3	K_La measurement by the PSP using imposed pressure change to yield DO response data	10
Figure 2.4	Comparison of K_La values between the GOP and PSP in 2.5-20%..... (v/v) $n\text{-C}_{10-13}$ -aqueous dispersions for agitation 600-1200rpm.....	11
Figure 2.5	Resistances encountered by DO from fluid film to cathode surface ...	13
Figure 2.6	Influence of agitation rate and CMC concentration on DO diffusion film lag time	15
Figure 2.7	K_p impact on K_La estimation in water and 0.05% (v/v) propanol-..... aqueous solutions	17
Figure 2.8	Influence of increased agitation rate on K_La in distilled water	19
Figure 2.9	Influence of increased agitation rate on gas hold-up at various gas velocities	20
Figure 2.10	Influence of increased agitation rate on D_{32} at various gas velocities	20
Figure 2.11	Relationship between fluid surface tension and viscosity at varying $n\text{-C}_{10}\text{H}_{22} + n\text{-C}_{20}\text{H}_{42}$ mole fractions	21
Figure 2.12	Influence of increased hydrocarbon chain length and hydrocarbon concentration on K_L	23
Figure 2.13	Influence of 0.5% (v/v) hydrocarbon at constant liquid velocity of 0.063m/s on gas hold up	24
Figure 4.1	CaCO_3 particle size distribution	35
Figure 4.2	Yeast particle size distribution	36
Figure 4.3	Corn flour particle size distribution.....	36
Figure 4.4	Experimental bioreactor system geometry.....	37
Figure 4.5	DO concentration profiles during N_2/air sparging in the GOP (no lag)	38
Figure 4.6	Experimental measurement of K_La by the GOP (no lag) first order response model.....	39

Figure 4.7	Experimental determination of τ_p by solving the equation of line when $C_p/C_p^* = 0.632$	41
Figure 4.8	Experimental determination of K_p by non-linear regression from DO .. probe first order response model.....	42
Figure 4.9	Double gap system used for fluid viscosity measurements	44
Figure 5.1	Pareto chart for effect of membrane age, electrolyte age and their..... interaction on K_p in 2.5% (v/v) $n-C_{14-20}$ -aqueous dispersions at	54
Figure.5.2	Surface response for effect of membrane age, electrolyte age and their interaction on K_p in 2.5% (v/v) $n-C_{14-20}$ -aqueous dispersions at	55
Figure 5.3	Pareto chart for effect of agitation rate, alkane concentration and their interaction on K_p in 2.5-20% (v/v) $n-C_{14-20}$ -aqueous dispersions	56
Figure 5.4	Surface response for effect of agitation rate and alkane concentration on K_p in 2.5-20% (v/v) $n-C_{14-20}$ -aqueous dispersions at 1000rpm.....	57
Figure 5.5	Pareto chart for effect of alkane chain length, alkane concentration and their interaction on K_p in 2.5-20% (v/v) $n-C_{14-20}$ -aqueous	58
Figure 5.6	Surface response for effect of alkane chain length and alkane	59
Figure 5.7	Pareto chart for effect of solids loading, solids particle size and their ... interaction on K_p in 2.5% (v/v) $n-C_{14-20}$ -solid-aqueous dispersions at ...	60
Figure 5.8	Surface response for effect of solids loading and particle size on K_p in 2.5% (v/v) $n-C_{14-20}$ -solid-aqueous dispersions at 1000rpm.....	61
Figure 5.9	Comparison of K_La results from GOP (no lag) and GOP (lag) in 0- 20% (v/v) $n-C_{14-20}$ -aqueous dispersions for agitation 600-1200rpm.....	62
Figure 5.10	Comparison of K_La results from GOP (no lag) and GOP (lag) in 0-20% (v/v) $n-C_{10-13}$ -aqueous dispersions for agitation 600-1200rpm.....	62
Figure 5.11	Difference in K_La results from the GOP (no lag) and GOP (lag) in 0- 20% (v/v) $n-C_{14-20}$ -aqueous dispersions for agitation 600-1200rpm....	64
Figure 5.12	Difference in K_La results from GOP (no lag) and GOP (lag) in 0-	64

Figure 5.13	Comparison of K_La results from the PSP by Correia and Clarke (2009) and GOP (lag) in 0-20% (v/v) $n-C_{10-13}$ -aqueous dispersions for agitation 600-1200rpm.....	65
Figure 5.14	Pareto chart for effect of agitation, alkane concentration, inert solids ... loading, particle size and their interactions on K_La	67
Figure 5.15	Pareto chart for effect of alkane concentration, inert solids loading, particle size and their interactions on fluid viscosity.....	67
Figure 5.16	Pareto chart for effect of alkane concentration, inert solids loading, particle size and their interactions on fluid surface tension.....	68
Figure 5.17	Surface response for effect of agitation and alkane concentration on .. K_La at constant inert solids loading of 5.5g/L and particle size of 9 μ m	69
Figure 5.18	Surface response for effect of agitation and inert solids loading on K_La at constant 11.25% (v/v) $n-C_{14-20}$ alkane and particle size of 9 μ m	69
Figure 5.19	Surface response for effect of agitation and particle size on K_La at constant 11.25% (v/v) $n-C_{14-20}$ alkane and inert solids loading of 5.5g/L	70
Figure 5.20	Surface response for effect of alkane concentration and inert solids loading on K_La at constant agitation of 900rpm and particle size of 9 μ m	71
Figure 5.21	Surface response for effect of alkane concentration and particle size on K_La at constant agitation of 900rpm and inert solids loading of 5.5g/L.....	72
Figure 5.22	Surface response for effect of alkane concentration and inert solids loading on fluid viscosity at constant particle size of 9 μ m.....	72
Figure 5.23	Surface response for effect of alkane concentration and particle size on fluid viscosity at constant solids loading of 5.5g/L.....	73
Figure 5.24	Surface response for effect of alkane concentration and inert solids loading on fluid surface tension at constant particle size of 9 μ m	73
Figure 5.25	Surface response for effect of inert solids loading and particle size on K_La at constant agitation of 900rpm and 11.25% (v/v) $n-C_{14-20}$ alkane	75
Figure 5.26	Surface response for effect of inert solids loading and particle size on fluid viscosity at constant 11.25% (v/v) $n-C_{14-20}$ alkane	75
Figure 5.27	Surface response for effect of inert solids loading and particle size on fluid surface tension at constant 11.25% (v/v) $n-C_{14-20}$ alkane	76

Figure 5.28	Pareto chart for effect of agitation, alkane concentration, yeast loading and their interactions on K_La	79
Figure 5.29	Pareto chart for effect of alkane concentration, yeast loading and their interaction on fluid viscosity	79
Figure 5.30	Pareto chart for effect of alkane concentration, yeast loading and their interaction on fluid surface tension	80
Figure 5.31	Surface response for effect of agitation and alkane concentration on K_La at constant yeast loading of 3.25g/L.....	81
Figure 5.32	Surface response for effect of agitation and yeast loading on K_La at constant 6.88% (v/v) <i>n</i> -C ₁₄₋₂₀ alkane	81
Figure 5.33	Surface response for effect of alkane concentration and yeast loading on K_La at constant agitation of 750rpm.....	82
Figure 5.34	Surface response for effect of alkane concentration and yeast loading on fluid surface tension.....	83
Figure 5.35	Surface response for effect of alkane concentration and yeast loading on fluid viscosity.....	83

List of Tables

Table 2.1:	Steps occurring during oxygen transfer from oxygen bubble to cell ..	5
Table 2.2:	DO probe response lag times reported in literature for various fluid properties and K_La calculation methods	14
Table 2.3:	K_La behavior due to differences in solids properties, liquid properties and operating conditions	26
Table 4.1:	$n-C_{10-13}$ Sasol alkane cut composition	34
Table 4.2:	$n-C_{14-20}$ Sasol alkane cut composition	34
Table 4.3:	Solid particles average properties	35
Table 4.4:	Factors affecting K_p at two levels	46
Table 4.5:	2^2 Experimental design used to quantify factors affecting K_p at two levels	47
Table 4.6:	Factors affecting K_La in alkane-inert solid-aqueous dispersions at two levels	48
Table 4.7:	2^4 Experimental design used to quantify factors affecting K_La in alkane-inert solid-aqueous dispersions	49
Table 4.8:	Factors affecting fluid viscosity and fluid surface tension at two levels in alkane-inert solid-aqueous dispersions	50
Table 4.9:	2^3 Experimental design used to quantify factors affecting fluid surface tension and fluid viscosity in alkane-inert solid-aqueous dispersions	50
Table 4.10:	Factors affecting K_La at two levels in alkane-yeast-aqueous dispersions	51
Table 4.11:	2^3 Experimental design used to quantify factors affecting K_La in alkane-yeast-aqueous dispersions	51
Table 4.12:	Factors affecting on fluid viscosity and fluid surface tension at two levels in alkane-yeast-aqueous dispersions	52
Table 4.13:	2^2 Experimental design used to quantify factors affecting on fluid viscosity and fluid surface tension at two levels in alkane-yeast-aqueous dispersions	52
Table 5.1:	K_La behavior due to density differences in 2.5% (v/v) $n-C_{14-20}$ -solid aqueous dispersions	85

Nomenclature

a	Gas-liquid interfacial area per unit volume ($\text{m}^2.\text{m}^{-3}$)
A	Integration constant (-)
B	Integration constant (-)
C	Integration constant (-)
C	Oxygen concentration in solution ($\text{mol}.\text{m}^{-3}$)
C*	Oxygen concentration in solution at saturation ($\text{mol}.\text{m}^{-3}$)
C _o	Oxygen concentration in solution at initial conditions ($\text{mol}.\text{m}^{-3}$)
C ₁	Oxygen concentration in solution at t ₁ ($\text{mol}.\text{m}^{-3}$)
C ₂	Oxygen concentration in solution at t ₂ ($\text{mol}.\text{m}^{-3}$)
C _L	Oxygen concentration in bulk liquid phase ($\text{mol}.\text{m}^{-3}$)
C _G	Oxygen concentration in bulk gas phase ($\text{mol}.\text{m}^{-3}$)
C _{Gi}	Oxygen concentration at gas-liquid interface ($\text{mol}.\text{m}^{-3}$)
C _{Li}	Oxygen concentration at liquid-gas interface ($\text{mol}.\text{m}^{-3}$)
C _L *	Oxygen concentration in liquid phase at saturation ($\text{mol}.\text{m}^{-3}$)
C _G *	Oxygen concentration in gas phase at saturation ($\text{mol}.\text{m}^{-3}$)
C _E	Oxygen concentration due to probe electrolyte resistance ($\text{mol}.\text{m}^{-3}$)
C _F	Oxygen concentration due to fluid film resistance ($\text{mol}.\text{m}^{-3}$)
C _M	Oxygen concentration due to probe membrane resistance ($\text{mol}.\text{m}^{-3}$)
C _p	Oxygen concentration indicated by oxygen probe ($\text{mol}.\text{m}^{-3}$)
C _{po}	Oxygen concentration indicated by oxygen probe at initial conditions ($\text{mol}.\text{m}^{-3}$)
C _p *	Oxygen concentration indicated by oxygen probe at saturation ($\text{mol}.\text{m}^{-3}$)
D	Integration constant (-)
D _i	Impeller diameter (cm)
D _L	Liquid phase diffusivity ($\text{m}^2.\text{s}^{-1}$)
D _{O₂}	Oxygen diffusion coefficient ($\text{m}^2.\text{s}^{-1}$)
d _p	Solids particle size (μm)
D _t	Bioreactor diameter (cm)
D ₃₂	Sauter mean diameter of bubble (mm)
f (t)	Laplace transforms linear operator of an original function with $t \geq 0$ (-)
F(s)	Laplace transforms image function with complex argument s (-)

H_i	Distance between lower turbine and bottom of bioreactor (cm)
H_t	Dispersion height (cm)
l	Perimeter of platinum ring (mm)
J_{O_2}	Oxygen flux ($\text{mol.m}^{-2}.\text{s}^{-1}$)
K	Process gain (-)
KM	Lumped constant for process gain and the step input magnitude (-)
K_1	Process gain constant for oxygen transfer first order response model (s)
K_2	Process gain constant for oxygen probe first order response model (s)
K_1K_2	Lumped process gain constant for two first order models (s^2)
k_{Ga}	Volumetric oxygen transfer coefficient in gas phase (s^{-1})
k_{La}	Volumetric oxygen transfer coefficient in liquid phase (s^{-1})
k_G	Oxygen transfer coefficient in gas phase (m.s^{-1})
k_L	Oxygen transfer coefficient in liquid phase (m.s^{-1})
K_{Ga}	Overall volumetric oxygen transfer coefficient in gas phase (s^{-1})
K_{La}	Overall volumetric oxygen transfer coefficient in liquid phase (s^{-1})
K_G	Overall oxygen transfer coefficient in gas phase (m.s^{-1})
K_L	Overall oxygen transfer coefficient in liquid phase (m.s^{-1})
K_p	Inverse oxygen probe response lag time (s^{-1})
m	Oxygen distribution coefficient (-)
m	Mass of piece of paper (g)
M	Step input magnitude (-)
N	Impeller speed (rpm)
N_{O_2}	Rate of oxygen transfer ($\text{mol.m}^{-3}.\text{s}^{-1}$)
N_{O_2G}	Rate of oxygen transfer in gaseous phase ($\text{mol.m}^{-3}.\text{s}^{-1}$)
N_{O_2L}	Rate of oxygen transfer in liquid phase ($\text{mol.m}^{-3}.\text{s}^{-1}$)
OTR	Oxygen transfer rate ($\text{mol.m}^{-3}.\text{s}^{-1}$)
P_t	Total power input (W)
P/V	Total power input per unit volume (W.m^{-3})
Q_G	Gas aeration rate per unit volume of liquid (vvm)
R	Differences in Tensiometer readings with and without paper (mN.m^{-1})
R	Regression coefficient (-)

r_E	Oxygen transfer resistance due to electrolyte solution ($\text{cm}^2 \cdot \text{s} \cdot \text{cmHg} \cdot \text{gmol}^{-1}$)
r_F	Oxygen transfer resistance due to fluid properties ($\text{cm}^2 \cdot \text{s} \cdot \text{cmHg} \cdot \text{gmol}^{-1}$)
r_M	Oxygen transfer resistance due to membrane characteristics ($\text{cm}^2 \cdot \text{s} \cdot \text{cmHg} \cdot \text{gmol}^{-1}$)
S_i	Distance between upper and lower turbine (cm)
t	Time of experiment (s)
t_o	Initial time of experiment (s)
t_1	Time of experiment at condition 1 (s)
t_2	Time of experiment at condition 2 (s)
t_f	Characteristic time of oxygen transfer (s)
U_G	Gas velocity ($\text{m} \cdot \text{s}^{-1}$)
U_L	Liquid velocity ($\text{m} \cdot \text{s}^{-1}$)
V_s	Aeration rate (vvm)
V_{SL}	Volume of slurry (m^3)
x	Distance over which a concentration gradient exist (cm)

Greek letters

τ_p	Oxygen probe response lag time (s)
ϵ_G	Gas hold-up (-)
τ	Shear stress (Pa)
γ	Shear rate (s^{-1})
τ_F	Oxygen probe response lag time due to fluid film resistance (s)
σ	Fluid surface tension ($\text{mN} \cdot \text{m}^{-1}$)
μ	Fluid viscosity (mPa.s)
μ_{SL}	Slurry viscosity (mPa.s)
μ_L	Pure liquid viscosity (mPa.s)
ρ_p	Solid particle density ($\text{kg} \cdot \text{m}^{-3}$)

Abbreviations

CF	Correction factor
CMC	Carboxymethyl cellulose
DO	Dissolved oxygen
GOP	Standard gassing out procedure

GOP (no lag)	Gassing out procedure neglecting the probe response lag time
GOP (lag)	Gassing out procedure incorporating the probe response lag time
LPM	Litres per minute
PA	Sodium polyacrylate
PGME	Polyglycol methyl ether
PSP	Pressure step procedure
rpm	Revolutions per minute
v/v	Volume of dispersion per volume of distilled water in dispersion
vvm	Volume of air per volume of dispersion in bioreactor per minute

1 INTRODUCTION

Hydrocarbon processes for the production of synthetic fuels are becoming increasingly popular globally. However these processes result in the formation of large amounts of *n*-paraffin or alkane by-products with relatively low fuel value. These hydrocarbons have been identified as potential feed stocks in aerobic bioprocesses where bacteria and fungi can convert the alkane under moderate temperatures and pressures, unlike analogous chemical processes (Shennan and Levi, 1974; Singer and Finnerty, 1984). This means that a variety of products can be produced at low operating costs in these hydrocarbons based bioprocesses. High value marketable products which include amino acids, antibiotics, vitamins, nucleic acids, lipids, carbohydrates and organic acids have been reported to be produced from hydrocarbon based bioprocesses (Fukui and Tanaka, 1980). Recently produced products from these hydrocarbon based bioprocesses include biosurfactants (Kosaric 1996; Mukherjee *et al.*, 2006) and dioic acids (Chan and Kuo, 1997).

The oxygen transfer rate (OTR) has been identified as a key process parameter in aerobic hydrocarbon based bioprocesses (equation 1.1) (Mimura *et al.* 1973; Hassan and Robinson, 1977a; Clarke *et al.*, 2006; Correia and Clarke, 2009). The OTR is dependent on the oxygen concentration driving force (C^*-C) and the overall volumetric oxygen transfer coefficient (K_La) during the bioprocess (equation 1.1). This has resulted in K_La being a very important parameter in optimum operation, design and scale up of hydrocarbon based bioprocesses (Mimura *et al.*, 1973; Hassan and Robinson, 1977a; Bi *et al.*, 2001; Nielsen *et al.*, 2003; Clarke *et al.*, 2006; Correia and Clarke, 2009).

$$OTR = \frac{dC}{dt} = K_La(C^* - C) \quad [1.1]$$

Although hydrocarbons significantly increase the oxygen solubility in alkane-aqueous dispersions, resulting in enhanced oxygen transfer, the viscous nature of the alkane plays an important part on K_La behavior due to viscosity effects on oxygen diffusivity (Clarke and Correia, 2008). K_La behavior has thus been reported to be dependent on the pressures imposed by the alterations in fluid properties upon hydrocarbon addition (Clarke and Correia, 2008). Moreover, difficulty in supplying adequate oxygen in alkane based bioprocesses has been suggested due to the absence of the oxygen molecule in the molecular structure of the substrate. Therefore, the oxygen demand must be met solely through oxygen transfer to the media. Oxygen transfer, therefore,

becomes more critical in alkane-based bioprocesses in comparison with carbohydrate based media where the hydroxyl functional group ($-OH$) in the carbohydrate structure supplies about 2/3 of the oxygen requirement (Shennan and Levi, 1974; Moo-Yang 1975). Previous studies by Mimura *et al.* (1971) showed a 250% higher oxygen requirement for *Candida petrophilum* grown on *n*-hexane in comparison with growth on glucose. Another 250% higher oxygen requirement was observed by Preusting *et al.* (1993) to grow *Pseudomonas oleovarius* on octane compared to *Escherichia coli* grown on glucose at the same growth rate.

From these studies it is evident that sufficient oxygen transfer rate in alkane based bioprocesses is very critical. In fact, the limiting regime in alkane based bioprocesses is therefore likely to change from being kinetic control to transport control (Shuler and Kargi, 2002).

Clarke and Correia (2008) reviewed K_La behavior in hydrocarbon-aqueous dispersions and showed that there are three types of K_La behavior depending on the reactor type, aqueous phase, hydrocarbon concentration and hydrocarbon chain length. In type 1, K_La increased with increase in hydrocarbon concentration to a maximum value then decreased upon further hydrocarbon addition, in type 2, K_La increased with increase in hydrocarbon concentration and lastly in type 3, K_La was constant or decreased upon hydrocarbon addition. Correia *et al.* (2010) further showed that turbulence and fluid properties were important parameters in quantifying K_La in alkane-aqueous dispersions due to their impact on the volumetric oxygen transfer coefficient (K_L), Sauter mean diameter of the gas bubble (D_{32}) and the gas hold up (ϵ_G), the last two which will effectively influence the bubbles' interfacial area per unit volume (a).

Recent studies by Correia and Clarke (2009) also drew attention to finding an accurate K_La measurement method in alkane based bioprocesses. K_La was measured using two different physical methods: the pressure step procedure (PSP) and the gassing out procedure (GOP). The GOP methodology measured K_La according to a response to a step change in the amount of oxygen supplied in the sparge gas to the system. In this method, K_La was calculated from linearization of equation 1.1 which neglected the influence of the resistances associated with the dissolved oxygen probe. The PSP methodology measured K_La by introducing a step change in the partial pressure of the sparge gas and calculated K_La from mass balances which incorporated the effect of a probe response lag (Correia and Clarke,

2009). This study by Correia and Clarke (2009) confirmed that the PSP was superior to the GOP especially at 1200rpm and higher alkane concentrations. Correia and Clarke (2009) attributed this predominantly to the effects of the response lag time of the probe used to measure dissolved oxygen (DO). However, the PSP was considerably more complex, both practically and experimentally, than the GOP.

From the work that has been done on alkane-aqueous dispersions it is evident there is need to first find an accurate and less complex K_{La} measurement method which will give comparable results to the PSP but is less complex to use. Furthermore, since bioprocesses contain solids in the form of microorganisms, there is need to quantify the influence of solids loading and solids particle sizes on K_{La} behavior in alkane-aqueous dispersions. To date, K_{La} trends have only been reported in cell free alkane-aqueous dispersions (Correia *et al.*, 2010) there is also need to understand the interactions of these solid particles with agitation rate and alkane concentration.

Evaluation of an accurate and less complex K_{La} measurement with critical assessment of the DO probe response lag time and thereafter quantification of K_{La} behavior in aerated agitated alkane-solid-aqueous dispersions will form the basis of this study. Alkanes cuts of C_{10-13} and C_{14-20} used in this study were obtained from Sasol SA.

2 LITERATURE REVIEW

2.1 Oxygen transfer from gas bubble to cell

Oxygen transfer occurs when there is non-uniformity in DO concentration in a fluid resulting in a concentration gradient. The concentration gradient causes transport of DO from a region of high concentration to a region of low concentration. Due to this non-uniformity, DO concentration is therefore high at the oxygen bubble surface compared to the rest of the fluid. This results in oxygen transfer from the gas bubble to the fluid then ultimately to the site of oxidative phosphorylation in the cells (Doran, 1995).

There are a possible 8 steps during DO transfer from a rising gas bubble into a fluid containing cells under turbulent conditions (Bailey and Ollis, 1986; Doran, 1995; Nielsen *et al.*, 2002) (Figure 2.1). DO therefore pass through a number of transport resistances before it reaches the cell where the biochemical reaction can take place (Figure 2.1).

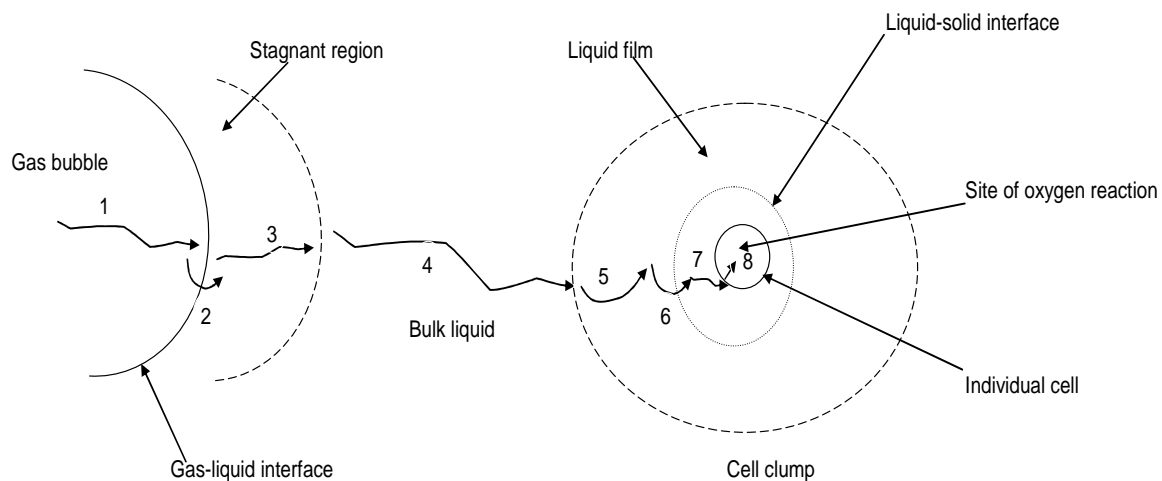


Figure 2.1 Steps for transfer of oxygen from gas bubble to cell (Redrawn from Doran, 1995)

The magnitude of DO resistance to transfer is dependent on temperature, fluid composition, agitation intensity, cell-clump size, interfacial phenomena and gas bubble hydrodynamics (Bailey and Ollis, 1986) (Table 2.1). These steps for DO transfer (Figure 2.1) are individually described in Table 2.1. Resistances due to the gas boundary layer on the inside of the oxygen bubble are negligible because of oxygen's high diffusivity. Bulk resistance is also assume negligible because of the relatively high turbulence. If individual cells are dispersed in the fluid rather than in

clumps (as is the case here), the resistance due to diffusion through the cell clump (Step 7) becomes negligible (Doran, 1995).

The diffusion through the liquid-film surrounding the gas bubble (Step 3), which takes place via molecular diffusion, is therefore assumed to dominate the major resistance in gas-liquid oxygen transfer (Doran, 1995).

Table 2.1: Steps occurring during oxygen transfer from oxygen bubble to cell (Doran, 1995)

Step	Oxygen transfer	Contribution to oxygen transfer resistance
1	Transport through interior of gas bubble.	Negligible
2	Movement through gas-liquid interface	Negligible
3	Diffusion through the relatively stagnant liquid film surrounding the gas bubble to the bulk liquid	Major resistance
4	Transfer through bulk liquid	Negligible only in turbulent and less viscous media
5	Transfer through the relatively stagnant liquid film surrounding the cells	Negligible only if the cells are much smaller than the oxygen bubbles
6	Movement through liquid-cell interface	Negligible
7	Diffusion through cell intra-particle resistance	Magnitude of resistance related to the cell clump size
8	Diffusion through intracellular interface	Negligible due to small distances involved

2.1.1 Development of the first order model describing oxygen transfer

Since the resistance to oxygen transfer is defined by molecular diffusion through the stagnant liquid film surrounding the gas bubble to the bulk liquid, flux of DO molecules during oxygen transfer is described by Fick's law which states that the oxygen flux is proportional to the oxygen concentration gradient (equation 2.1) (Doran, 1995).

$$J_{O_2} = -\frac{N_{O_2}}{a} = -D_{O_2} \frac{dC}{dx} \quad [2.1]$$

Where J_{O_2} is the oxygen flux ($\text{mol.m}^{-2}.\text{s}^{-1}$), N_{O_2} is the rate of oxygen transfer in the solution ($\text{mol.m}^{-3}.\text{s}^{-1}$), D_{O_2} is the oxygen diffusion coefficient ($\text{m}^2.\text{s}^{-1}$), a is the gas-liquid interfacial area per unit volume ($\text{m}^2.\text{m}^{-3}$), x is the distance over which the concentration gradient exists (m) and C is the oxygen concentration (mol.m^{-3}).

Fick's law is based on DO transfer through molecular diffusion due to a concentration gradient, direction of oxygen transfer from a region of high concentration to low concentration and DO transfer across an area which is perpendicular to the direction of DO diffusion (equation 2.2) (Doran, 1995).

$$N_{O_2} = -D_{O_2} a \frac{dC}{dx} \quad [2.2]$$

Oxygen transfer between the gas and liquid phases is therefore best modeled by the two film theory (Lewis, 1916; Whitman, 1923). This theory suggests that a stagnant boundary forms at both sides of the interfaces where there is contact between the liquid and the gaseous phases (Doran, 1995) (Figure 2.2). Oxygen transfer will then involve transport of oxygen molecules from the gas bulk phase to the interface then to the liquid bulk phase. The resistance to oxygen transfer at the boundary layer is assumed negligible at moderate oxygen transfer rate and when there is no accumulation of surfactants at the interface (Doran, 1995). Thus the gas-liquid phases will be in equilibrium at the contact plane. According to the two film theory, oxygen transfer rate increases with decrease of the phase boundary layer between the two phases i.e. at higher turbulence. Fick's law can be modified for the oxygen transfer between the gas phase boundary layer (equation 2.3) and liquid phase boundary layer (equation 2.4) if it is assumed that the rate of DO transfer is directly proportional to the concentration gradient and the area available for transport.

$$N_{O_2G} = k_G a (C_G - C_{Gi}) \quad [2.3]$$

$$N_{O_2L} = k_L a (C_{Li} - C_L) \quad [2.4]$$

Where k_G and k_L are the volumetric oxygen transfer coefficient in gas phase and liquid phase respectively ($m.s^{-1}$), C_{Gi} and C_{Li} are gas and liquid interfacial oxygen concentrations ($mol.m^{-3}$) and C_G and C_L are oxygen concentration in bulk gas and liquid phase ($mol.m^{-3}$) respectively.

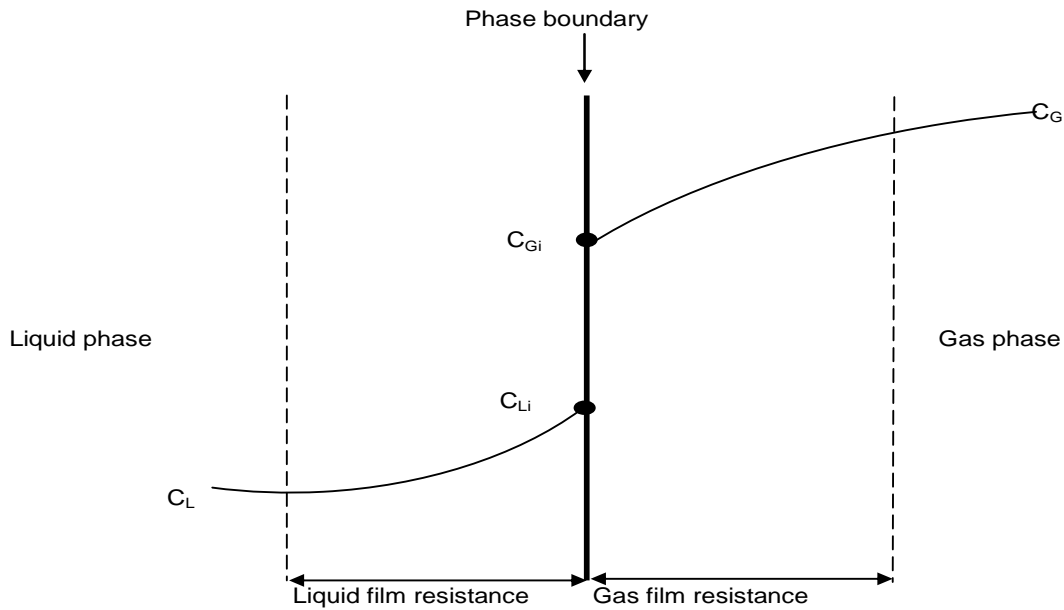


Figure 2.2 Concentration gradients for gas-liquid oxygen transfer associated with the two film theory (Redrawn from Doran, 1995)

If oxygen transfer occurs at steady state, there will be no DO accumulation at the interface therefore the rate of oxygen transfer through the gas phase will equal that through the liquid phase hence $N_{O_2G} = N_{O_2L}$. Therefore the OTR will be referred as N_{O_2} only.

The interfacial terms (C_{Gi} and C_{Li}) will be eliminated from the gas phase boundary layer equation 2.3 and liquid phase boundary layer equation 2.4 since they are difficult to measure. Elimination of the interfacial terms are described in a detailed derivation in Appendix 1. The OTR in gas-liquid systems will then be represented by equation 2.5 for the liquid phase resistance and equation 2.6 for the gas phase resistance. C_G^* and C_L^* represent the oxygen equilibrium concentration at saturation (mol.m^{-3}). The derivation of these equations is provided in Appendix 1.

$$N_{O_2} = K_G a (C_G - C_G^*) \quad [2.5]$$

$$N_{O_2} = K_L a (C_L^* - C_L) \quad [2.6]$$

Since the liquid phase DO transfer resistance will dominate due to oxygen poor solubility, the DO transfer rate in the fluid is therefore defined by equation 2.7.

$$N_{O_2} = OTR = \frac{dC}{dt} = K_L a (C^* - C) \quad [2.7]$$

This rate of oxygen transfer (equation 2.7), is a first order response model that has been widely used for K_La measurement. The first order response model has been used for K_La measurement according to the GOP. Specifically, it has been used in hydrocarbon-aqueous dispersions by Mimura *et al.* (1973); Hassan and Robinson, (1977a); Clarke *et al.* (2006) and Correia and Clarke (2009). A detailed derivation of the first order response model has been provided in Appendix A.1.

2.1.2 Development of the second order model describing oxygen transfer

During K_La measurement a DO probe is used to measure the rate of change of DO over time in the fluid. The characteristics of the DO probe are provided in Appendix A4.1. This probe has been reported to have a first order response (equation 2.8). This was under the assumption that the membrane is firmly attached to the cathode and that there are no contaminants on the membrane surface (Aiba and Huang, 1969; Godbole *et al.*, 1984). This probe response is associated with the resistance to oxygen transfer inside the probe will in turn affect the actual amount of DO measured in the fluid at a particular time. This then results in a lag in the DO measurement

$$\frac{dC_p}{dt} = K_p (C_p^* - C_p) \quad [2.8]$$

where K_p is the oxygen transfer coefficient of the probe (s^{-1}), C_p is the DO concentration indicated by the probe ($mol.m^{-3}$) and C_p^* is the DO concentration indicated by the probe at saturation ($mol.m^{-3}$)

Nielsen *et al.* (2003) confirmed that the change in DO concentration indicated by the DO probe, dC_p/dt , cannot be used to represent the change in actual DO concentration, dC/dt , according to equation 1.1, due to K_p effects. Instead, dC_p/dt represents the concentration driving force between the DO in the solution and the DO indicated by the probe (equation 2.9).

$$\frac{dC_p}{dt} = K_p (C - C_p) \quad [2.9]$$

Simultaneous solution of equations 1.1 and 2.9 yields the second order response model given by equation 2.10 (Nielsen *et al.*, 2003). Detailed derivations are provided in Appendices A.2 and A.3 according to different procedures. This second order response model forms the basis for the modified gassing out procedure that has been widely used for K_La measurement in aqueous systems.

$$\frac{C_p}{C_p^*} = 1 - \frac{1}{K_p - K_{La}} \left[K_p e^{-K_{La}t} - K_{La} e^{-K_p t} \right] \quad [2.10]$$

2.2 Measurement methods for the overall volumetric oxygen transfer coefficient

K_{La} has been widely measured experimentally by physical methods in bioprocesses (Mimura *et al.*, 1973; Hassan and Robinson, 1977a; Clarke *et al.*, 2006; Correia and Clarke, 2009). These physical methods include the gassing out procedure (GOP) and the pressure step procedure (PSP) (Garcia-Ochoa and Gomez, 2009). Physical methods have been reported to be the most appropriate to measure K_{La} in bioprocesses since there is no chemical usage which can affect physico-chemical properties of fluid which result in erroneous K_{La} values (Garcia-Ochoa and Gomez, 2009). Physical methods involve the dynamic response of the DO probe in the fluid under turbulent conditions to a step change in the oxygen in the inlet gas (Garcia-Ochoa and Gomez, 2009).

2.2.1 Measurement using the gassing out procedure and the first order response model

The gassing out procedure without incorporation of the DO probe response lag time (GOP (no lag)) is the most widely used method for determining K_{La} in bioprocesses and was first developed by Bandyopadhyay *et al.* (1967). This is also known as the dynamic method. This method uses the first order response model for K_{La} measurement. Mimura *et al.* (1973) and Hassan and Robinson (1977a) were the first to use the GOP (no lag) for K_{La} measurement in hydrocarbon-aqueous dispersions containing *n*-dodecane and *n*-hexadecane. Recently this method was used for K_{La} measurement in *n*-C₁₂₋₁₃-aqueous dispersions by Clarke *et al.* (2006) and in *n*-C₁₀₋₁₃-aqueous dispersions by Correia and Clarke (2009). The DO change over time in this method is measured when a step change is created when the fluid is de-aerated with nitrogen then sparged with air (Garcia-Ochoa and Gomez, 2009). The air sparging phase known as oxygen absorption has been widely used for K_{La} measurement. K_{La} was obtained upon linearising the OTR first order response model (equation 1.1); assuming zero DO probe response lag time.

Although the GOP (no lag) has been extensively used for K_{La} measurement in bioprocesses, its accuracy has been reported to be questionable by Correia and Clarke (2009) since the DO probe response lag time is not accounted for.

2.2.2 Measurement using the pressure step procedure

The pressure step procedure (PSP) was first developed by Linek *et al.* (1989) and has been used for K_La measurement in aqueous systems only until recently. Correia and Clarke (2009) were the first to use this method for K_La measurement in a hydrocarbon based system. This method is based on measuring the change in DO concentration over time by introducing a step change in the bioreactor pressure by either decreasing or increasing the pressure by 20% of the initial value (Linek *et al.*, 1993; Linek *et al.*, 1994; Correia and Clarke, 2009). A range of response profiles are then generated according to the pressure changes (Figure 2.3). K_La was then obtained when the calculated response fits the experimental profile using mass balance equations which incorporate different transport rates for nitrogen and oxygen from air as they are absorbed in the liquid across the gas-liquid interface (Figure 2.3) (Linek *et al.*, 1989; Linek *et al.*, 1993; Linek *et al.*, 1994; Correia and Clarke, 2009). The DO profile which equals the response profile used for K_La determination is adjusted to incorporate the dynamics of the DO probe response lag time according to the model of Linek *et al.* (1984).

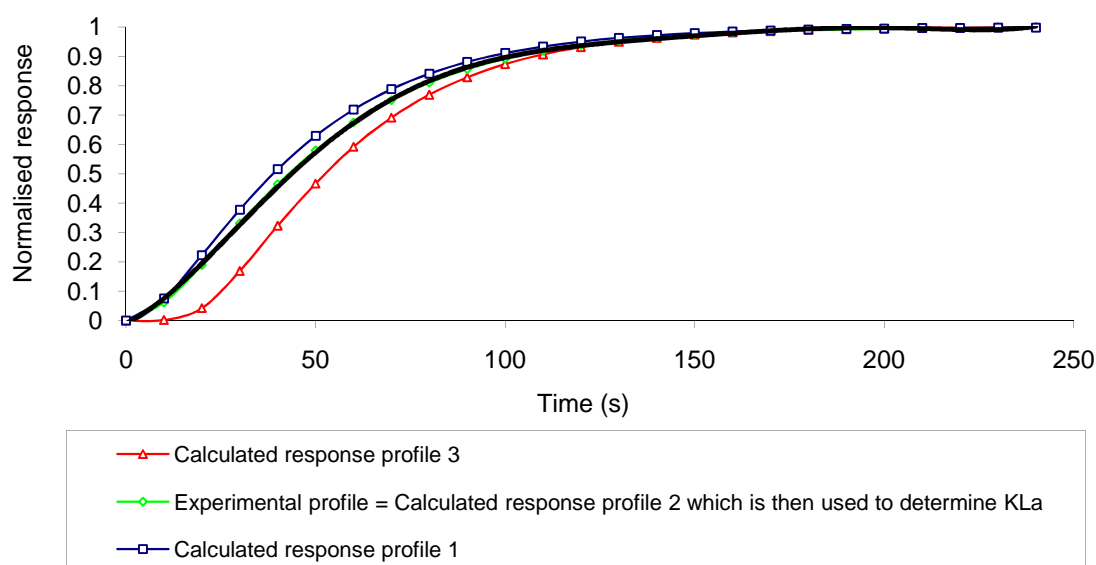


Figure 2.3 K_La measurement by the PSP using imposed pressure change to yield DO response data (Linek *et al.*, 1989)

Correia and Clarke (2009) reported that the PSP gave accurate K_La values in hydrocarbon-aqueous dispersions mainly because it addressed the issue of the DO probe response lag time in its methodology. Comparison of K_La values from both the GOP (no lag) and the PSP in 2.5-20% (v/v) n -C₁₀₋₁₃-aqueous dispersions for an agitation range of 600rpm to 1200rpm confirmed this accuracy. They indicated that

the PSP became increasingly superior over the GOP (no lag) as agitation rate and alkane concentration increased, K_{La} values from the GOP (no lag) became more dampened at higher agitations and alkane concentrations with deviations of up to 49% at 1200rpm and 5% (v/v) (Figure 2.4). This deviation indicated that K_{La} inaccuracies were more pronounced using the GOP (no lag) in hydrocarbon based systems than aqueous systems possibly due to the viscous nature of the alkanes.

However, the PSP is complex to use both experimentally and practically so there is need to develop an alternative method that will give comparable K_{La} results to those from the PSP in hydrocarbon based systems.

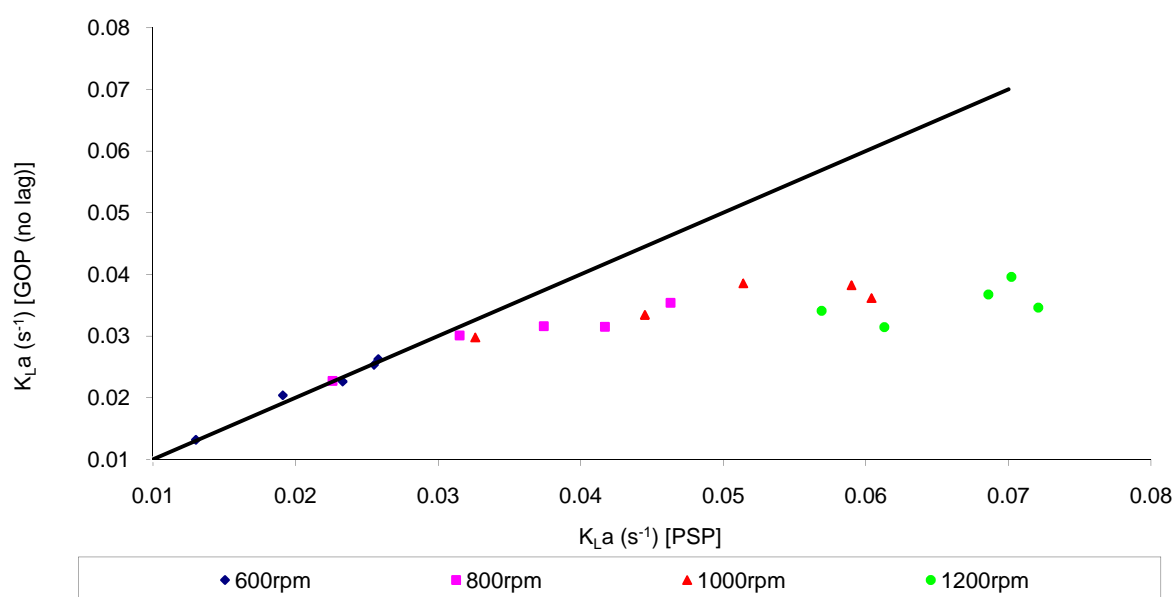


Figure 2.4 Comparison of K_{La} values between the GOP and PSP in 2.5-20% (v/v) n -C₁₀₋₁₃-aqueous dispersions for agitation 600-1200rpm (Redrawn from Correia and Clarke, 2009)

2.2.3 Measurement using the gassing out procedure and the second order response model

A study by Correia and Clarke (2009) indicated that in hydrocarbon-aqueous dispersions there are large discrepancies in K_{La} results between the PSP and the GOP (no lag) methodologies. There is therefore a need to investigate ways of incorporating K_p effects on K_{La} measurement, hence the GOP (lag) methodology was examined.

2.2.3.1 The probe response lag time

The DO probe response lag time (τ_p) is defined as the time taken for the DO concentration to reach 63.2% of its saturation value after an experimental step

change (Van't Riet, 1979; Ruchti *et al.*, 1981; Tribe *et al.*, 1994; Luyben and Luyben, 1997; Nikolov *et al.*, 2000; Juarez and Orians, 2001). The derivation of the probe response lag time is detailed in Appendix A.4.2. An alternative notation, K_p , has also been widely used in literature indicating the inverse of the DO probe response lag time (Merchuk *et al.*, 1990) or the DO resistance associated with the probe.

τ_p has been measured by two methods, either by transferring the DO probe from a sulphite saturated fluid to an air-saturated fluid (Benedek and Heideger, 1970; Fuchs *et al.*, 1971) or by transferring the DO probe from a nitrogen saturated fluid to an air saturated one (Nakanoh and Yoshida, 1980; Godbole *et al.*, 1984). In both cases the initial fluid was de-oxygenated by oxidation of sulphite or nitrogen sparging respectively.

Dang *et al.* (1977) and Merchuk *et al.* (1990) suggested that τ_p occurred due to resistance when DO molecules diffused through the fluid film, membrane and electrolyte solution to cathode where DO reacts with the anode to produce a current (which is proportional to the DO partial pressure in the fluid). This was in agreement to the work of Aiba and Huang (1969) and Benedek and Heideger (1970) who indicated that this DO movement from the fluid film to the cathode is on its own a mass transfer process which eventually results in the lag (Figure 2.5). This DO transfer resulted in a delay in measuring the sudden changes in actual DO concentration in the fluid, resulting in underestimated $K_L a$ values in the GOP (no lag), especially at high aeration rates (Benedek and Heideger, 1970).

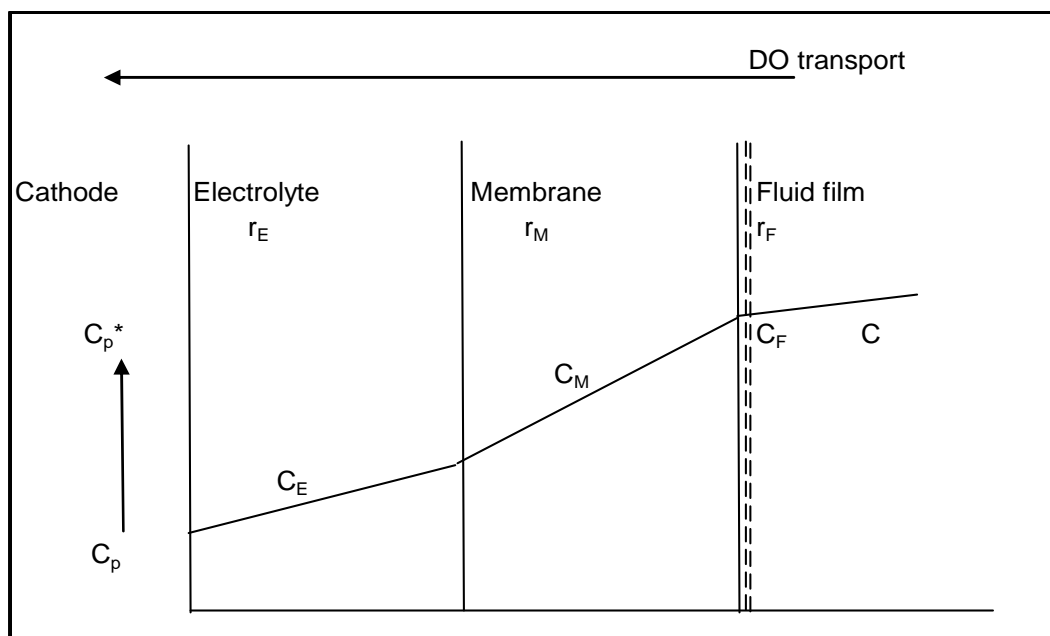


Figure 2.5 Resistances encountered by DO from fluid film to cathode surface
(Redrawn from Aiba and Huang, 1969)

The magnitude of τ_p has been reported to be a function of membrane type, membrane thickness, membrane age, electrolyte usage and electrochemical reactions that occur within the DO probe (Aiba and Huang, 1969; Benedek and Heideger, 1970; Fuchs *et al.*, 1971). $\tau_p = 1/K_p$ values in literature also varied depending on fluid properties (Table 2.2).

Table 2.2: DO probe response lag times reported in literature for various fluid properties and K_La calculation methods

Reference	Response lag time	K_La range (s^{-1})	Fluid	Calculation of K_La
Dang <i>et al.</i> (1977)	14.2s (dead time of 3s subtracted from the data)	0.01-0.015	water, CMC solutions	Dynamic model moment analysis
Godbole <i>et al.</i> (1984)	4.7s in water, 3 times increase in CMC solutions (14.1 s)	0.01-0.04	water, CMC solutions	1 st order model
Gourich <i>et al.</i> (2008)	7s	0.01-0.025	water and propanol solutions	2 nd order model. Mat lab 6.5 (The Math works)
Nakanoh and Yoshida (1980)	5-6s in water, 9-10s in 60% sucrose solutions	1.36-4.76 (ratio)	water, sucrose, CMC and PA solutions	1 st order model
Nielsen <i>et al.</i> (2003)	11.2s	0-0.556	hexadecane organic phase	2 nd order model
Ruchti <i>et al.</i> (1981)	10-13s \pm 0.3-0.5s	0.021-0.19	water, CMC solutions	Dynamic model moment analysis

Dang *et al.* (1977) further proposed a second order DO probe response model for viscous fluids which accounts for both the probe membrane response time and the diffusion film lag time ($\tau_p + \tau_F$) (equations 2.11 and 2.12). This implied that the DO probe response lag time resulted from these two lags. The second order model was also used by Ruchti *et al.* (1981) who indicated that the diffusion film lag was dependent on the agitation rate as well as the CMC (carboxymethyl cellulose) concentration and that effects of the lag were more pronounced at low agitations (Figure 2.6). The effect of agitation rate is a likely consequence of increased turbulence with increased agitation which would result in a decrease liquid film thickness around the bubble. At the same time increasing the CMC concentration increased the liquid film diffusion lag time due to increase in thickness of the fluid film (Figure 2.6).

$$\frac{dC_F}{dt} = \frac{C - C_F}{\tau_p} \quad [2.11]$$

$$\frac{dC_p}{dt} = \frac{C_F - C_p}{\tau_p} \quad [2.12]$$

where C_F is the DO concentration due to fluid film resistance lag time (mol.m^{-3})

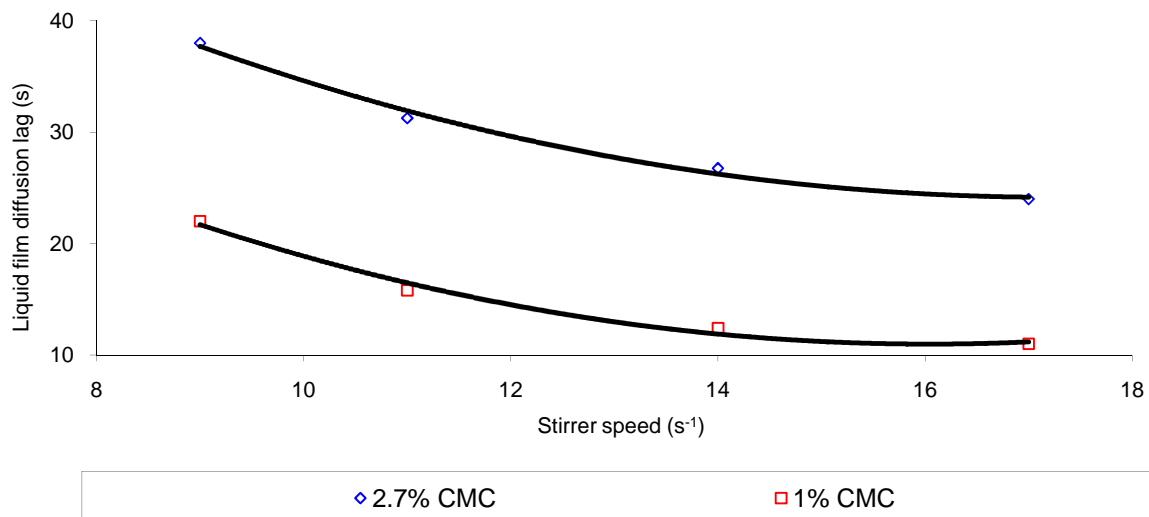


Figure 2.6 Influence of agitation rate and CMC concentration on DO diffusion film lag time (Redrawn from Ruchti *et al.*, 1981)

Aiba and Huang (1969) found a 25.4 μm membrane to have a 3 times longer τ_p compared to a 12.7 μm membrane in aqueous solutions. The τ_p values also increased with membrane usage. A thin membrane had a τ_p equal to that of a thick

membrane due to continual usage which resulted in membrane stretching. Benedek and Heideger (1970) had the same observations in aqueous solutions and attributed the increased slowdown in τ_p with usage to membrane stretching. They also indicated that an artificial space formed between the membrane and the cathode due to continual usage which resulted in the DO probe response deviating from the first order response model. Benedek and Heideger (1970) further showed that as the probe electrolyte usage increased, a reduction product, AgCl, formed at the probe anode which also contributed to increased τ_p . Additionally Aiba and Huang (1969) showed that different membrane materials with the same thickness have different oxygen diffusivities in water which in turn affected τ_p . A 53 μm polypropylene membrane had a 5 times higher DO diffusivity of $2.4 \times 10^7 \text{ cm}^2/\text{s}$ in air and $2.6 \times 10^7 \text{ cm}^2/\text{s}$ in water as compared to a 51 μm triacetyl cellulose membrane which had a DO diffusivity of $0.50 \times 10^7 \text{ cm}^2/\text{s}$ in air and $0.53 \times 10^7 \text{ cm}^2/\text{s}$ in water.

From the information reported on the DO probe response lag time, it is evident that the K_p values are dependent on the probe characteristics and process conditions. However there is still need to understand how K_p values will be affected in alkane multiphase systems since these data were mostly collected in aqueous systems.

2.2.3.2 Influence of the probe response lag time on measurement of the overall volumetric oxygen transfer coefficient

The DO probe response lag time has been accounted for in a few studies for $K_{L,a}$ measurement using the GOP by modifying the GOP (no lag) (Fuchs *et al.*, 1971, Letzel *et al.*, 1999; Nielsen *et al.*, 2003, Vandu and Krishna, 2004). This response lag is a consequence of the resistance to DO transfer across the probe membrane.

Further, in the systems where the K_p value was incorporated, a constant value was used irrespective of process conditions. Nielsen *et al.* (2003) reported an increase of more than 25% for $K_{L,a}$ values greater than 0.25 s^{-1} when a τ_p of 11.2s was incorporated in aqueous-hexadecane phases but did not observe any difference at low agitation rates of 400rpm in $K_{L,a}$ from the GOP (no lag) and the GOP (lag). Gourich *et al.* (2008) observed the same behavior in $K_{L,a}$ due to τ_p when they measured $K_{L,a}$ in propanol-aqueous systems. After incorporating a τ_p of 7s their $K_{L,a}$ values increased significantly by more than 40% for both water and propanol at higher gas velocities of 0.087m/s when the GOP (lag) was used (Figure 2.7). However their $K_{L,a}$ from the GOP (no lag) and the GOP (lag) did not show significant

differences at low gas velocities of 0.007m/s. They attributed this to K_{La} and K_p having the same magnitude hence the effects of τ_p became pronounced. This was in agreement to conditions set by Van't Riet (1979) and Ruchti *et al.* (1981) that τ_p should only be considered when determining K_{La} in the GOP if τ_p is of the same magnitude as the inverse of the K_{La} i.e. $\tau_p = 1/K_p \approx 1/K_{La}$. Gourich *et al.* (2008) also indicated that the characteristic time of DO transfer; $t_f = 1/K_{La}$ should be lower than $10\tau_p$ otherwise the K_p effects are negligible.

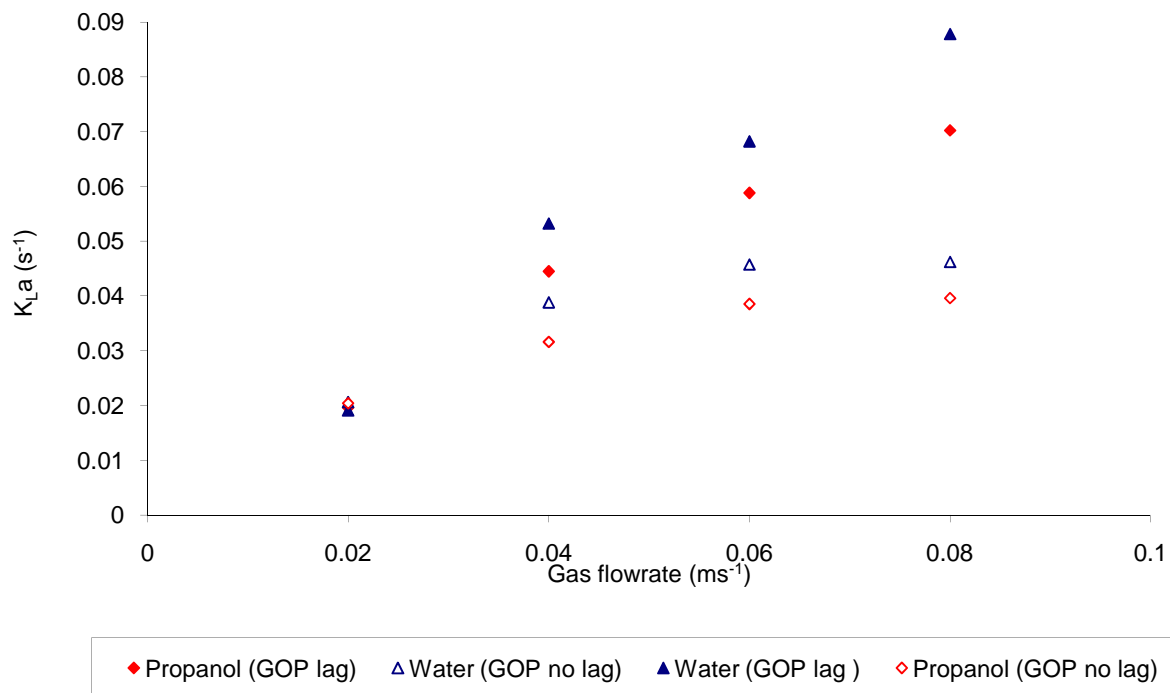


Figure 2.7 K_p impact on K_{La} estimation in water and 0.05% (v/v) propanol-aqueous solutions (Redrawn from Gourich *et al.*, 2008)

There is need to modify the GOP by incorporating the K_p effects and further to quantify the impact of K_p on K_{La} measurement in view of the particularly critical role of the correct K_p in hydrocarbon based systems (Correia and Clarke, 2009).

2.3 Behavior of the overall volumetric oxygen transfer coefficient

K_{La} behavior has been reported to be dependent on individual process conditions such as agitation rate, hydrocarbon type, concentration and chain length (or other related hydrocarbon derivatives) but their interactions have not been quantified (Mimura *et al.*, 1973; Hassan and Robinson, 1977a; Clarke *et al.*, 2006; Clarke and Correia, 2008). Furthermore different K_{La} trends have been identified upon hydrocarbon addition and attributed to either to effect of fluid surface tension or fluid

viscosity but their interactions have also not been quantified (Correia *et al.*, 2010). Importantly the effect of solids loading and solids particle size has not been quantified in alkane multiphase systems. Although rheological alterations have been reported upon solids loading in aqueous systems (Khare and Joshi, 1990; Salvacion *et al.*, 1995), no quantitative information on the effect of fluid surface tension as well as the solids' interaction with the other process parameters on K_La has been reported.

2.3.1 Influence of agitation rate

Increases in agitation rate have been reported to enhance K_La in hydrocarbon multiphase systems by several authors (Bartos and Satterfield, 1986; Ju and Sundararajan, 1994; Ozbek and Gayik, 2001; Clarke *et al.*, 2006; Clarke and Correia, 2008; Correia and Clarke, 2009; Correia *et al.*, 2010) (see also Figure 2.8). K_La is however a lumped factor comprising of the volumetric oxygen transfer coefficient (K_L) and the gas-liquid interfacial area per unit volume (a) so increasing the agitation rate will therefore enhance K_La by either affecting K_L , a or both parameters. The gas-liquid interfacial area per unit volume is directly related to the gas hold up (ϵ_G) and inversely related the DO Sauter mean bubble diameter (D_{32}) (equation 2.13). K_L is a measure of the inverse of resistance to DO transfer.

$$a = \frac{6\epsilon_G}{D_{32}} \quad [2.13]$$

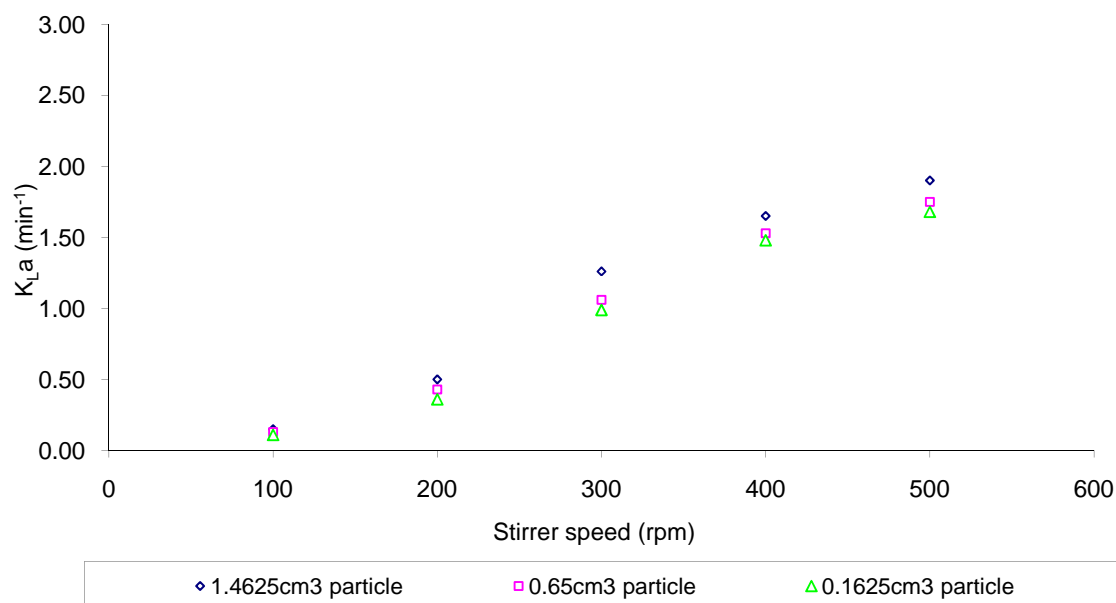


Figure 2.8 Influence of increased agitation rate on K_La in distilled water containing 25wt% biomass support particles (Redrawn from Ozbek and Gayik, 2001)

2.3.1.1 Influence of agitation rate on the oxygen transfer coefficient

K_L has been reported to be enhanced by an increase in agitation rate through decreased D_{32} due to the shearing action exerted by agitation on the DO bubbles (Alves *et al.*, 2004). Alves *et al.* (2004) indicated that K_L was approximately 5 times bigger for smaller bubbles with 2.5mm diameter compared to larger bubbles with diameter greater than 2.5mm. Increased agitation rates have also been reported to decrease the resistance to molecular diffusion due to a decrease in the stagnant layer thickness at high turbulence, as suggested by Lewis (1916) and Whitman (1923)'s two film theory resulting in K_L increases. A number of correlations have also been reviewed by Clarke and Correia (2008) which predict K_L increases with increases in turbulence resulting in enhanced K_La .

2.3.1.2 Influence of agitation rate on the gas-liquid interfacial area per unit volume

Increasing turbulence effects have been reported to increase the gas-liquid interfacial area per unit volume in hydrocarbon multiphase systems as indicated by the various correlations between the impeller speed (N), aeration rate (V_s) and the input power per unit volume (P/V) reviewed by Clarke and Correia (2008). Increased agitation rate increases the turbulent shear rate for DO bubble breakage resulting in a smaller D_{32} (Parthasarathy and Ahmed, 1994) thus increasing ϵ_G (Figure 2.9) due to lower DO bubble rise velocities thereby enhancing the gas-liquid interfacial area per unit

volume (equation 2.13) and hence the overall $K_L a$ (Sridhar and Potter, 1980; Yoshida and Miura, 1963; van Dierenolonck *et al.*, 1968; Hassan and Robinson, 1977b; Correia *et al.*, 2010).

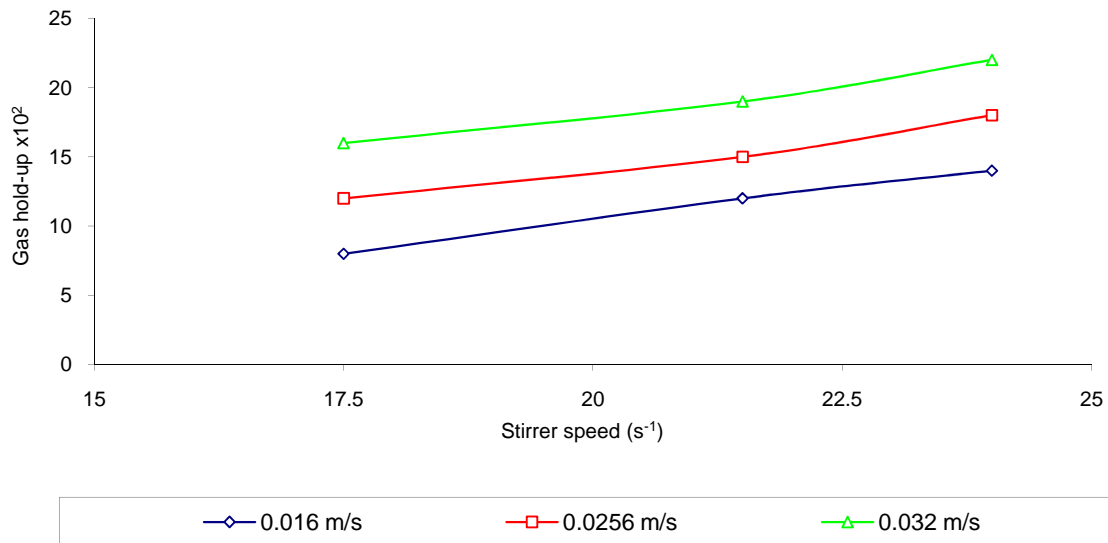


Figure 2.9 Influence of increased agitation rate on gas hold-up at various gas velocities (Redrawn from Sridhar and Potter, 1980)

Sridhar and Potter (1980) confirmed the linear relationship between increase in ε_G and increased agitation rate (Figure 2.9). They also indicated that increasing agitation will decrease D_{32} and went on further to show that at high agitations D_{32} becomes almost constant (Figure 2.10) which was in agreement to the work of Calderbank (1958), Westerterp *et al.* (1963) and Correia *et al.* (2010).

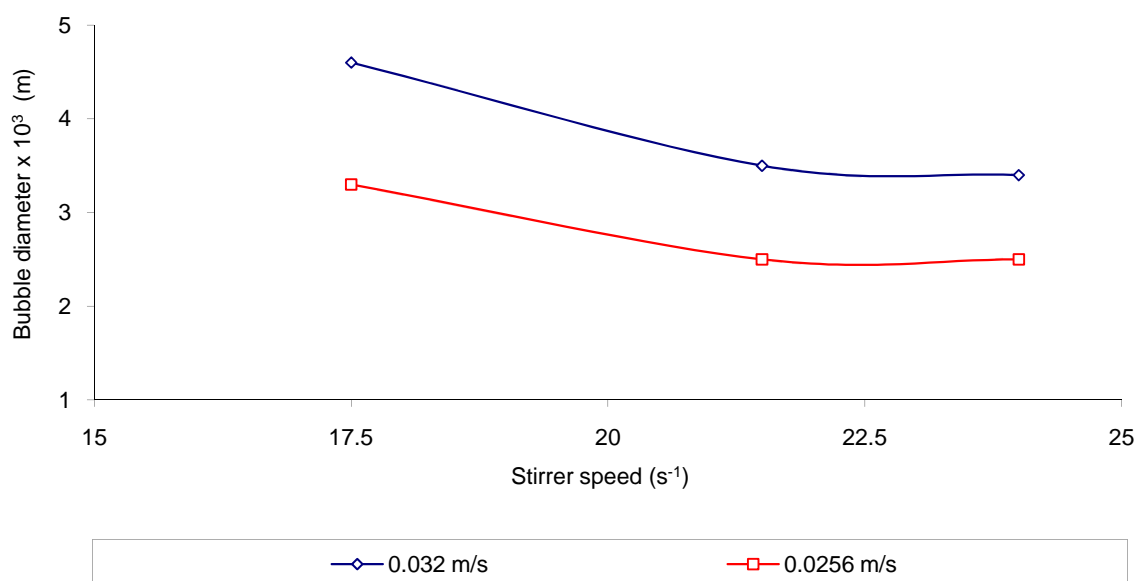


Figure 2.10 Influence of increased agitation rate on D_{32} at various gas velocities (Redrawn from Sridhar and Potter, 1980)

2.3.2 Influence of hydrocarbon addition

Hydrocarbon addition has been reported to alter $K_L a$ due to the influence on the fluid viscosity (μ) and fluid surface tension (σ) depending on hydrocarbon concentration, hydrocarbon type as well as hydrocarbon chain length (Koide *et al.*, 1976; Zahradnik *et al.*, 1999; Clarke and Correia, 2008). Hydrocarbon addition decreased the fluid surface tension whilst the fluid viscosity was increased (Queimada *et al.*, 1976) (Figure 2.11). This inverse linear relationship between the fluid viscosity and fluid surface tension upon hydrocarbon addition had been earlier reported by Pelofsky (1966) (equation 2.14).

$$\ln \sigma = \ln A + \frac{B}{\mu} \quad [2.14]$$

where A and B are constants of proportionality

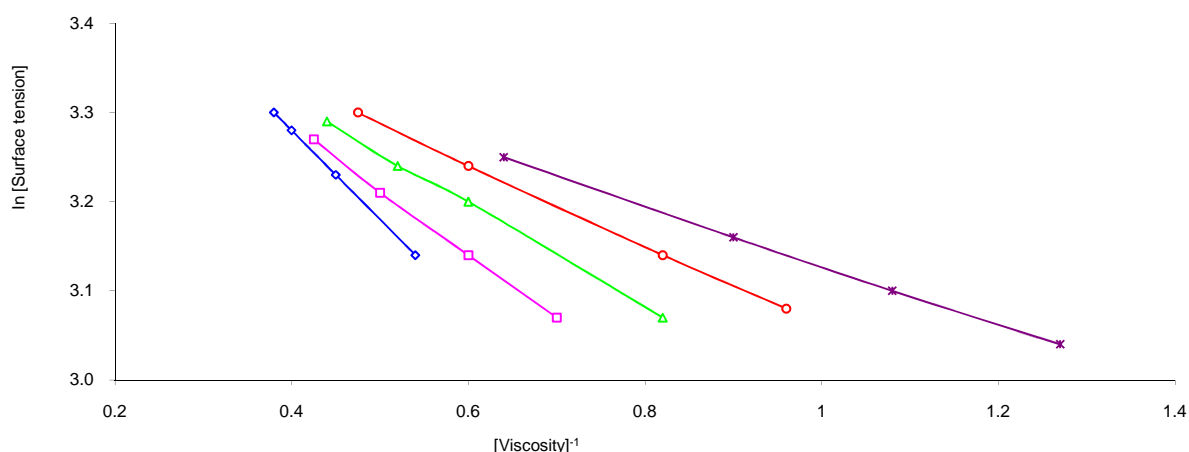


Figure 2.11 Relationship between fluid surface tension and viscosity at varying n - $C_{10}H_{22}$ + n - $C_{20}H_{42}$ mole fractions (Redrawn from Queimada *et al.*, 1976)

2.3.2.1 Influence of hydrocarbon addition on the oxygen transfer coefficient

Increased hydrocarbon concentration or hydrocarbon chain length resulted in increased fluid viscosities which caused a decrease in the diffusivity of DO in the fluid thereby decreasing K_L (Calderbank, 1958; Clarke and Correia, 2008). The decrease in K_L increased resistance to DO diffusion through the gas-liquid interface. K_L was found to be largely dependent on the diffusion coefficient (D_L) for oscillating and rigid bubbles (equations 2.15 and 2.16) (Calderbank and Moo-Yang, 1961; Juretzek *et al.*, 2000; Garcia-Ochoa and Gomez, 2005). Kilonzo and Margaritis (2004) also indicated that increase in fluid viscosity had an inverse relationship with K_L (equations 2.17 and

2.18) resulting in decreased $K_L a$. Elgozalia *et al.* (2002) reported $K_L a$ decreases of up to 60% due to K_L decreases when the fluid viscosity was continually increased by adding a polymer based thickener and this was attributed to the coalescing behavior of the thickener.

$$K_L = D_L^{2/3} \quad [2.15]$$

$$K_L = D_L^{1/2} \quad [2.16]$$

$$K_L \propto \mu^{-0.333} \quad [2.17]$$

$$K_L \propto \mu^{-0.167} \quad [2.18]$$

Raymond and Zieminski (1997) reported a decrease in fluid surface tension due to hydrocarbon addition which resulted in decreased bubble surface mobility. This caused the bubbles to act as rigid spheres causing the internal motion inside the bubbles to decrease, hence a negative effect on K_L . Linek *et al.* (2005) also observed a 0.8 decrease in K_L upon addition of ocnol and CMC solutions which are fluid surface tension reducing substances. This was in agreement with Koide *et al.* (1976) (Figure 2.12) who used aqueous solutions of *n*-hexanol, *n*-heptanol and *n*-octanol and indicated that addition of an alcohol acted as barriers for passage of gaseous molecules on the gas-liquid interface since they were absorbed at the interface, thereby reducing K_L .

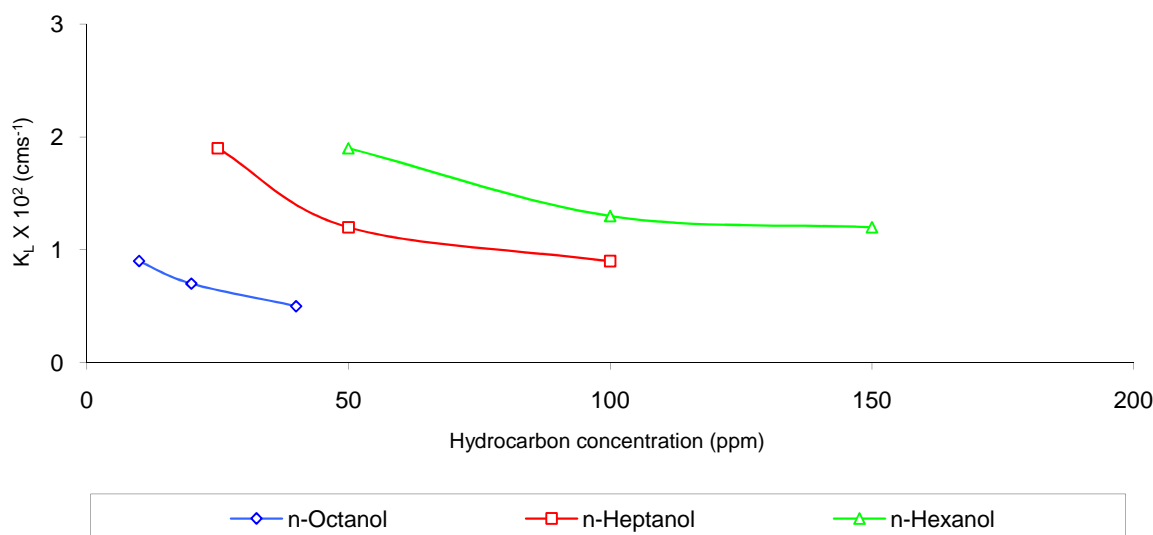


Figure 2.12 Influence of increased hydrocarbon chain length and hydrocarbon concentration on K_L (Redrawn from Koide *et al.* 1976)

Contrary to this, van der Meer *et al.* (1992) indicated that small concentrations of octanol enhanced K_L especially when the octanol drop diameter was sufficiently smaller than the gas-liquid film thickness. Due to this smaller octanol size, no accumulation occurred at the gas-liquid interface since the octanol drops were sufficiently small hence increased K_L .

2.3.2.2 Influence of hydrocarbon addition on the gas-liquid interfacial area per unit volume

Alterations in fluid physico-chemical properties due to hydrocarbon addition determine the gas-liquid interfacial area per unit volume based on ε_G and D_{32} through their influence on coalescence and bubble break-up (equation 2.13).

Increases in fluid viscosity due to hydrocarbon addition have been reported to reduce the turbulence effects in the fluid due to increased bubble coalescence which results in a reduced degree of bubble break-up, and slower formation of liquid films causing more air to be trapped in the bubbles (Khare and Joshi, 1990; O'Connor *et al.*, 1990; Schafer *et al.*, 2002; Correia *et al.*, 2010). This resulted in larger D_{32} values and lowering gas-liquid interfacial area per unit volume values (equation 2.28) hence lowered $K_L a$ (Schumpe and Deckwer, 1982; Garcia-Ochoa and Gomez, 2004; Kilonzo and Margaritis, 2004; Mehria *et al.*, 2005; Correia *et al.*, 2010).

Al Taweel and Chang (1995) reported a fluid surface tension decrease in water from 73mN/m to about 66mN/m upon addition of up to 100ppm of polyglycol methyl ether (PGME). This lowered fluid surface tension tended to decrease D_{32} , resulting in larger

gas-liquid interfacial area per unit volume. ε_G also increased due to inhibition of bubble coalescence and promotion of gas dispersions with lower rising velocities thus enhancing K_{La} (Das *et al.*, 1985; Koide *et al.*, 1985; Parthasarathy *et al.*, 1991). Hu *et al.* (2005) reported a fluid surface tension decrease upon addition of diethylene glycol and decanol in aqueous solutions which led to D_{32} reduction due to coalescence inhibition thereby increasing K_{La} . Kelkar *et al.* (1983) also showed that ε_G increased with increase in alcohol chain length thereby increasing K_{La} and attributed this to decrease in fluid surface tension (Figure 2.13).

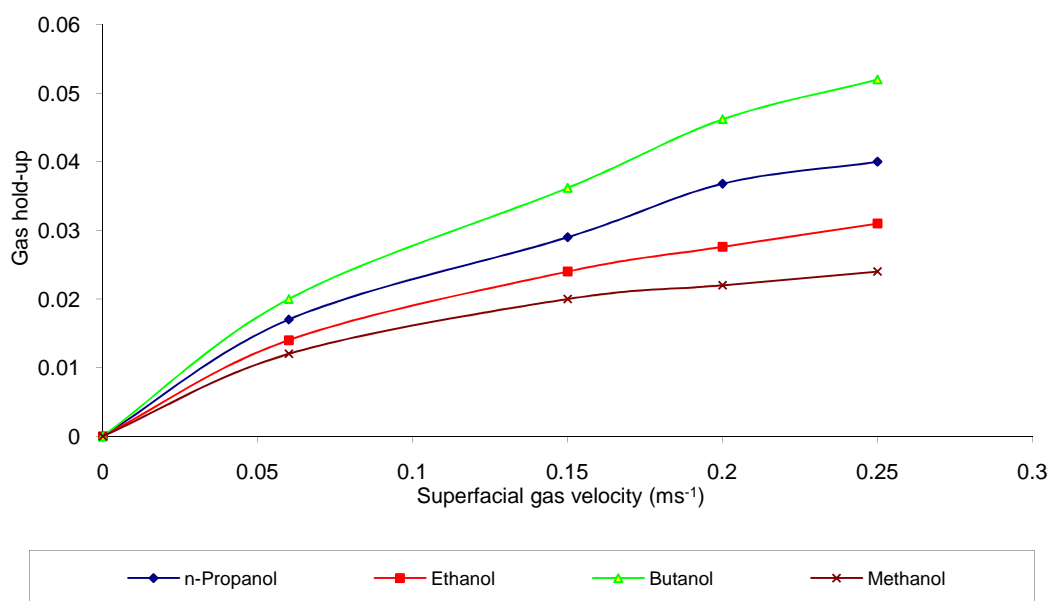


Figure 2.13 Influence of 0.5% (v/v) hydrocarbon at constant liquid velocity of 0.063m/s on gas hold up (Redrawn from Kelkar *et al.*, 1983)

However, in highly viscous hydrocarbon-aqueous dispersions, the effect of increased fluid viscosity has been reported to override the effect of fluid surface tension. This effectively lowered the gas-liquid interfacial area per unit volume and hence the overall K_{La} . Hu *et al.* (2005) reported a bigger D_{32} in a highly viscous air-decanol system as compared to a low viscous air-propanol system though their fluid surface tension was not significantly different. Das *et al.* (1985) indicated an increase in D_{32} for both toluene and 2-ethyl hexanol dispersions with increase in alcohol concentration above 10% although both alcohols had comparable fluid surface tensions. Recently Correia *et al.* (2010) reported the same trend in 2.5-20% (v/v) *n*-C₁₀₋₁₃-aqueous dispersions when both D_{32} and ε_G decreased due to the almost doubling effect of increase in fluid viscosity from 1.01mPa.s to 1.95mPa.s while the fluid surface tension decreased from 26.0mN/m to 17.7mN/m.

2.3.3 Influence of solids addition

Solids addition has been reported to affect K_{La} depending on solids particle size (d_p), solids loading (wt %) and solids density (ρ_p) (Table 2.3). K_{La} studies in aqueous systems containing solids have been widely carried out with inert particles informing on K_{La} trends upon solids addition mostly in aqueous dispersions. Several K_{La} trends upon solids addition have been identified in literature depending on the process conditions, liquid medium and the solid particle properties.

As with hydrocarbon addition, solids addition affects K_{La} through K_L (Alper *et al.*, 1980; Chapman *et al.*, 1983; Ju and Sundararajan, 1994) and the gas-liquid interfacial area per unit volume (Joosten *et al.*, 1977; Quicker *et al.*, 1984; Bartoes and Satterfield, 1986; Hwang and Lu, 1997; Kawase *et al.*, 1997) or through both parameters (Miyachi *et al.*, 1981; Chisti and Moo-Yang, 1988; Kim and Kim, 1990; Benchapattarapong *et al.*, 2005; Mena *et al.*, 2005).

Table 2.3: K_{La} behavior due to differences in solids properties, liquid properties and operating conditions

Reference	Medium and operating conditions	Particle type	d_p (μm)	ρ_p (kgm^{-3})	Solids loading (wt%)	K_{La} behavior
Vandu and Krishna (2003)	Ethanol $U_G: 0-0.11\text{ms}^{-1}$	Cobalt catalyst	25.4	1177	1.0 and 3.8	K_{La} and gas hold-up decreased with increase in the catalyst concentration.
Albal <i>et al.</i> (1983)	Water; 10wt% glycerin; CMC solutions N:100-1200rpm	Glass beads Oil shale particles	150 140	2700 2270	0-25 0-25	K_{La} increased by 10-20% for 0-2.5wt% solids loading and then decreased thereafter until 25wt%.
Sada <i>et al.</i> (1986)	NaCl Distilled water $Q_G=2\text{cm}^3\text{s}^{-1}$ for 2h	Aluminum oxide Calcium hydroxide Calcium carbonate	<3 7 10	3850 2240 varying	<1.0 <1.0 <1.0	K_{La} remained constant for all low particles loading. K_{La} increased for particles lower than $10\mu\text{m}$ then decreased for $10\mu\text{m}$ particles depending on the solids loading.
Ozturk and Schumpe (1987)	Ligroin and tetralin-aqueous systems	Aluminum oxide Polyvinylchloride Polyethylene A Polyethylene B	10.5 82 106 124.6	3180 1380 940 965		Fine high density solids in small concentration increased K_{La} in this case aluminum due to increase in K_L .
Joosten <i>et al.</i> (1977)	Kerosene-helium-nitrogen $U_G=2.5\text{cms}^{-1}$ $P_T=1.5\text{kWm}^{-3}$	Glass beads Glass beads Sugar Polypropylene Polypropylene	88 53 74-105 53-105 250	0-40 0-40 0-40 0-40 0-40		K_{La} increased with small loadings of 10-20wt%, stayed constant at 20wt% loading and decreased sharply thereafter to 40wt% depending on the solids type and size.

$K_L a$ behavior was reported to be governed by higher solids loadings at the bottom of the reactor thereby significantly altering the rheological properties of the fluid (Joosten *et al.*, 1977; Frijlink and Smith, 1986; Oguz *et al.*, 1987; Mandersloot and Scott, 1990; Ozbek and Gayik, 2001). Correlations showing the relationship between the fluid viscosity and solids addition for various power per unit volume (P/V) and air flow rates (Q_G) have been formulated by Oguz *et al.* (1987) (equation 2.19) and van Weert *et al.* (1995) (equation 2.20) in slurry systems. Khare and Joshi (1990) and Salvacion *et al.* (1995) further showed that the rheological alterations upon solids addition were also dependent on the rheological properties of the liquid.

$$K_L a = 6.6 \times 10^{-4} \left(\frac{\mu_{SL}}{\mu_L} \right)^{-0.39} \left(\frac{P_t}{V_{SL}} \right)^{0.75} Q_G^{0.5} \quad [2.19]$$

$$K_L a = 0.036 \left(\frac{\mu_{SL}}{\mu_L} \right)^{-0.22} \left(\frac{P_t}{V_{SL}} \right)^{0.39} Q_G^{0.5} \quad [2.20]$$

where μ_{SL}/μ_L is the ratio between the slurry viscosity and the liquid viscosity, P_t is the total power input (W) and V_{SL} is the volume of slurry (m^3)

2.3.3.1 Influence of solids addition on the oxygen transfer coefficient

Solids addition have been reported to affect K_L either by creating a diffusion blocking effect on the gas-liquid interface, thereby increasing the diffusion film layer thickness, or by altering the interfacial turbulence of fluid (Chisti and Moo-Yang, 1988; Mena *et al.*, 2005).

Joosten *et al.* (1977) showed that an increased interfacial turbulence was observed with low solids loading of 0.1-2.5% (v/v) therefore increasing K_L resulting in a small $K_L a$ increase in kerosene-helium-nitrogen systems with polypropylene, sugar and glass beads particles. This was in agreement to Miyachi *et al.* (1981) who indicated a K_L increase in aqueous- $CaCO_3$ systems for solid particle sizes $>1.75\mu m$ and indicated this was due to larger turbulence on the gas-liquid film caused by larger particles relative to smaller ones also within the same solids loading range. Albal *et al.* (1983) confirmed this trend in aqueous systems with glass beads and oil shale particles with $K_L a$ increases of 10-30% for 0-2.5% (v/v) solids loading. They demonstrated that low solids loadings do not alter the fluid viscosity but enhance the surface renewal rate and mobility thereby increasing K_L . Chandrasekaran and Sharma (1977) had also reported a 60% $K_L a$ increase in a sulfite system with 0.2wt% activated carbon and 150% $K_L a$ increase in slurries containing 0.1-0.33wt% activated

carbon compared to powdered quartz, sand and oxirane-acrylic beads at the same loading. They had attributed this $K_L a$ enhancement to physical absorption of oxygen by activated carbon increasing K_L . Quicker *et al.* (1984) had had similar observations for an aqueous system containing activated carbon, but no enhancement for quartz and beads solids particles as they were less porous.

However, Albal *et al.* (1983) also showed that high solids loadings of >2.5% (v/v) decreased $K_L a$ due to increased fluid viscosity which increased the diffusion film thickness lowering K_L with the largest particles showing the greatest decrease. This was in agreement to Ju and Sundararajan (1994) who observed a decrease in $K_L a$ for >0.45 μm baker's yeast particles. They attributed this to physical blockage by cells accumulated on the gas-liquid interface decreasing K_L .

2.3.3.2 Influence of solids addition on the gas-liquid interfacial area per unit volume

Solids addition also determines the gas-liquid interfacial area per unit volume based on ε_G and D_{32} through their influence on coalescence and bubble break-up (equation 2.19). Sada *et al.* (1986) observed that addition of <10 μm solids particles at 0.1wt% loadings increased ε_G in aqueous systems containing aluminum oxide, calcium hydroxide and calcium carbonate. They indicated that fine particles hindered bubble coalescence hence maintained low D_{32} . This was in agreement to the work of Khare and Joshi (1990) in aliphatic alcohol/electrolytic solutions with 12-1300 μm particles with loadings of 0-10wt% but reached a maximum value upon further increase in solids particle size and solids loading. However Khare and Joshi (1990)'s ε_G increased with non-coalescing behavior of the fluid and they argued that the ε_G behavior was due to the synergetic effect of solids particle size, solid loading, fluid surface tension and fluid viscosity of liquid. This result was in agreement to Kawase *et al.* (1997) who also showed that $K_L a$ decreased upon addition of 0.002 μm polymeric particles at 5-15wt% but increased on 0.15-0.5wt% CMC addition due to reduced coalescence in the fluid properties and decreased D_{32} .

Decreases in gas-liquid interfacial area per unit volume have been reported upon increased solids addition (Yagi and Yoshida, 1974; Lee *et al.*, 1982; Gollakotta and Guin, 1984; Fukuma *et al.*, 1987; Mills *et al.*, 1987; Chisti and Moo-Yang, 1988; Sun and Furusaki, 1988; O'Connor *et al.*, 1990; Zahradnik *et al.*, 1992; Reese *et al.*, 1996; van Weert *et al.*, 1999; Krishna *et al.*, 1997; Nicolella *et al.*, 1998; Freitas and Teixeira, 2001; Mena *et al.*, 2005). Hwang and Lu (1997) demonstrated a decrease

in K_{La} on addition of 0.0024 μm polystyrene cylinder particles in an air-water system and concluded that the decrease was attributed to a decrease in ε_G due to solids loading resulting in formation of larger D_{32} and lower rise velocities. Vandu and Krishna (2003) had the same observation when they investigated the influence of 25.4 μm cobalt loading of 1.0-3.8wt% in ethanol solutions whereby both K_{La} and ε_G decreased with increase in cobalt loading despite the increase in the superficial gas velocities from 0-0.11m/s. Vandu and Krishna (2003) attributed this to increased coalescence of smaller bubbles to form larger bubbles with increase in catalyst loading.

Sada *et al.* (1986) investigated an aqueous system containing aluminum oxide, calcium hydroxide and calcium carbonate; K_{La} values for the slurries were the same as those without any solids. They argued that the degree of influence of suspended particles in the bubble column depended on the solids particle sizes. Particles $>50\mu\text{m}$ decreased ε_G with increasing solids loading but at low loadings they showed no appreciable influence. This was in agreement to the work of Miyachi *et al.* (1981) who reported K_{La} decreases for particles $>1.75\mu\text{m}$ due to reduction in gas-liquid interfacial area per unit volume due to the occupation of the bubbles by solids which resulted in larger D_{32} .

In addition to the influence of solids loading and solids particle sizes on K_{La} , solids density particles were also found to alter K_{La} behavior. High solid particle densities were shown to cause more coalescence in systems with bronze spheres with density of 8770kg/m³ compared to systems with glass spheres with density of 2500kg/m³ by Koide *et al.* (1984). These included aqueous systems with glycerol, glycol, barium chloride and sodium sulfate solutions. The coalescence resulted in lower gas-liquid interfacial area per unit volume, ε_G and lower K_{La} . Freitas and Teixeira (2001) had the same observation with a K_{La} decrease of up to 30% in aqueous systems containing a 2.151mm particle with density of 1048kg/m³ compared to a 2.131mm calcium alginate beads with density of 1023kg/m³. The 1048kg/m³ particle had the lowest K_{La} due to increase in coalescence which was reflected by smaller gas-liquid interfacial area per unit volume.

3 HYPOTHESES, SCOPE OF PROJECT AND OBJECTIVES

The hypotheses formulated for this work, scope of project and objectives were based on the two areas of study which are evaluation of an accurate and less complex K_{La} measurement methodology and quantification of K_{La} behavior in alkane systems with solids.

3.1 Hypotheses

From the literature survey it is evident that there is need to apply an accurate and less K_{La} measurement method in alkane multiphase systems which accounts for K_p effects. K_p has been shown to play a significant role in K_{La} measurements in aqueous systems using the GOP (lag) and also in alkane systems through the PSP, the latter methodology is relatively complex to use. Moreover, according to the literature survey, the magnitude of K_p cannot be generalized but is dependent on the DO probe characteristics, process conditions and fluid properties.

There is therefore a need to first quantify the factors affecting K_p in the viscous alkane multiphase systems and see what parameters really affect the probe response lag time. There is then need to modify the GOP (no lag) to incorporate K_p effects per each process condition during K_{La} measurement. Secondly, there is need to benchmark the GOP (lag) methodology to the alternative PSP methodology. Both methodologies account for the DO transfer limitations associated with the probe. Hypothesis one was then formulated according to the literature study of K_{La} measurement methodology.

Hypothesis 1: Oxygen transfer resistance associated with the probe has to be accounted for when measuring the DO

It is also evident that the behavior of K_{La} upon hydrocarbon and solids addition is dependent on the agitation rate and the impact of hydrocarbon addition and solids addition on the fluid properties. Although there is a lot of information on K_{La} trends upon increasing agitation rate and hydrocarbon addition there is no explicit information on how these process parameters will interact with each other upon solids addition in a viscous alkane multiphase system. There is therefore need to quantify K_{La} behavior in aerated agitated alkane-solid-aqueous dispersions using an accurate measurement method. Furthermore influences of fluid properties through alterations in fluid viscosity and fluid surface tension on K_{La} due to alkane addition

and solid addition need to be quantified to fully underpin K_{La} behavior in these systems. Additionally to that there is a need to assess the influence of cells as well as inert solids on K_{La} behavior. Hypotheses two was then formulated according to the literature study of the K_{La} behavior in hydrocarbon based systems.

Hypothesis 2: K_{La} behaviour in alkane-solid-aqueous dispersions is dependent on agitation rate, alkane concentration, inert solids loading, solids particle size and their interactions

3.2 Scope of research project and objectives

This project firstly evaluates an accurate K_{La} measurement method in alkane multiphase systems which accounts for K_p effects and, secondly, quantifies K_{La} behavior in aerated agitated alkane-solid-aqueous dispersions and the influence of agitation rate, alterations in fluid properties and their interactions on the K_{La} behavior. Moreover the influence of inactive yeast cells as well as inert solids on K_{La} behavior in hydrocarbon based systems is evaluated.

3.2.1 Evaluation of measurement method for the overall volumetric oxygen transfer coefficient

In evaluation of an accurate and less complex K_{La} measurement in alkane multiphase systems, factors thought to affect K_p and their interactive effects will be investigated according to the literature review. These factors will include the probe membrane age (5 day usage), probe electrolyte age (5 day usage), agitation rate (600-1200rpm), alkane concentration (2.5-20% (v/v)), alkane chain length (n -C₁₀₋₁₃ and n -C₁₄₋₂₀), solids loading (1-10g/L) and solids particle size (3-14 μ m). Since K_p was a sensitive parameter, independent experiments on investigating the parameters affecting K_p will be carried out and the influence of only two parameters was investigated at a time.

K_{La} values in n -C₁₀₋₁₃ and n -C₁₄₋₂₀-aqueous dispersions from the GOP (no lag) and the GOP (lag) will then be compared to quantify the degree of difference in K_{La} due to K_p effects. Furthermore K_{La} values measured with the GOP (lag) in n -C₁₀₋₁₃-aqueous dispersions will be compared to those previously reported by Correia and Clarke (2009) measured with the relatively complex PSP.

3.2.2 Quantification of the behavior of the overall volumetric oxygen transfer coefficient in alkane-solid-aqueous dispersions

Quantification of K_La behavior firstly, in alkane multiphase systems with inert solids is necessary and see if it follows any trends in literature. Secondly, cells with properties almost similar to the inert solids will be introduced and resultant K_La behavior recorded. Comparison of K_La trends in these systems will help identify optimum operating conditions in systems with solids.

K_La will be measured in alkane-inert solid-aqueous dispersions for varying agitation rates (600-1200rpm), alkane concentrations (2.5-20% (v/v)), solids loading (1-10g/L) and solids particle sizes (3-14 μ m) in n -C₁₄₋₂₀ alkane, at constant aeration of 0.8vvm (volume of air per volume of dispersion per minute), at 22°C and 101.3kPa. The measurement method used will be dependent on the outcome of the first objective. The fluid viscosity and fluid surface tension will then be measured in the alkane-inert solid-aqueous dispersions at the same process conditions where K_La values will be measured to fully quantify K_La behavior due to alterations in alkane concentration, solids loading and solids particle sizes.

In dispersions with inert solids, corn flour and CaCO₃ will be employed as solids since they had the same density but had different particle sizes. This enables the investigation of various solids loading and solids particle sizes at constant density. The challenge encountered for this experiment is that it is difficult to obtain an inert solid with a particle size of 9 μ m yet with the same density as corn flour and CaCO₃ so center conditions could not be investigated with the inert solids experiments. Further K_La measurement will be done using the 5 μ m yeast particle to better represent a typical hydrocarbon based bioprocess. Alkane-yeast-aqueous dispersions at various agitation rates (600-900rpm), alkane concentrations (2.5-11.25% (v/v)) and yeast loadings (1-5.5g/L) in n -C₁₄₋₂₀ alkane also at constant aeration of 0.8vvm, at 22°C and 101.3kPa will be used. The fluid viscosity and fluid surface tension will also be measured in the alkane-yeast-aqueous dispersions to fully quantify K_La behavior due to alterations in alkane concentration and solids loading. The yeast cells will be inactivated since if they are respiring there will be a possibility of our K_La being affected as well.

Finally $K_L a$ behavior will be explained through the effect of agitation rate, the impact of fluid properties due to alterations in alkane concentration, solids loading and solids particle size and their interactions in the alkane multiphase systems.

4 EXPERIMENTAL MATERIALS AND METHODOLOGY

4.1 Materials

4.1.1 Hydrocarbons

n-C₁₀₋₁₃ and *n*-C₁₄₋₂₀ alkane cuts (Sasol Ltd; South Africa) were used with alkane concentrations of 2.5-20% (v/v) in alkane-aqueous dispersions and alkane-solid-aqueous dispersions with inert solids. Alkane concentrations of 2.5-11.25% (v/v) were used in the alkane-solid-aqueous dispersions with inactive yeast. Alkane compositions were obtained by gas chromatographic analysis (Table 4.1) (Correia, 2007) and (Table 4.2) (Pennels, 2008). The alkane-solid-aqueous dispersions and the alkane-aqueous dispersions were made by adding solids and alkanes to distilled water at concentrations indicated in the text.

Table 4.1: *n*-C₁₀₋₁₃ Sasol alkane cut composition (Correia, 2007)

Alkane	Chain length	% Composition
<i>n</i> -Decane	<i>n</i> -C ₁₀	10.3
<i>n</i> -Undecane	<i>n</i> -C ₁₁	29.3
<i>n</i> -Dodecane	<i>n</i> -C ₁₂	30.0
<i>n</i> -Tridecane	<i>n</i> -C ₁₃	30.4

Table 4.2: *n*-C₁₄₋₂₀ Sasol alkane cut composition (Pennels, 2008)

Alkane	Chain length	% Composition
<i>n</i> -Tetradecane	<i>n</i> -C ₁₄	49.0
<i>n</i> -Pentadecane	<i>n</i> -C ₁₅	33.3
<i>n</i> -Hexadecane	<i>n</i> -C ₁₆	7.1
<i>n</i> -Heptaecane	<i>n</i> -C ₁₇	6.8
<i>n</i> -Octadecane	<i>n</i> -C ₁₈	3.2
<i>n</i> -Nonadecane	<i>n</i> -C ₁₉	0.4
<i>n</i> -Eicosane	<i>n</i> -C ₂₀	0.2

4.1.2 Solids

Solids used in the alkane-inert solid-aqueous dispersions were corn flour with density of 670kg/m³ and CaCO₃ with density of 700kg/m³. The solids loading was varied from

1-10g/L for varying particle sizes of 3-14 μm . Yeast with an average particle size of 5 μm and density of 900 kg/m^3 was used in the alkane-yeast-aqueous dispersions. The yeast loadings employed were 1-5.5g/L. The solids particle size distributions were analyzed by a Saturn Digisizer 5200 V1.10 analyzer (Micrometrics Instrument Company) (Figures 4.1-4.3). The solid particles were sampled 3 times to determine the average particle size (Table 4.3). The solids densities were obtained at <http://www.powderandbulk.com>. Corn flour and CaCO_3 were naturally inert. The yeast cells were de-activated by soaking them in 70% ethanol for 24 hours before use and filtered before use.

Nitrogen gas (>99.5% purity) was used as the nitrogen source, compressed air was used as source of oxygen.

Table 4.3: Solid particles average properties

Solid	Mean (μm)	Median (μm)	Mode (μm)	Density (kg/m^3)
CaCO_3	3.3 \pm 0.13	2.9 \pm 0.07	3.2 \pm 0.11	700
Yeast	4.8 \pm 0.12	4.9 \pm 0.07	5.3 \pm 0.00	970
Corn flour	13.6 \pm 0.03	14.3 \pm 0.02	16.0 \pm 0.00	670

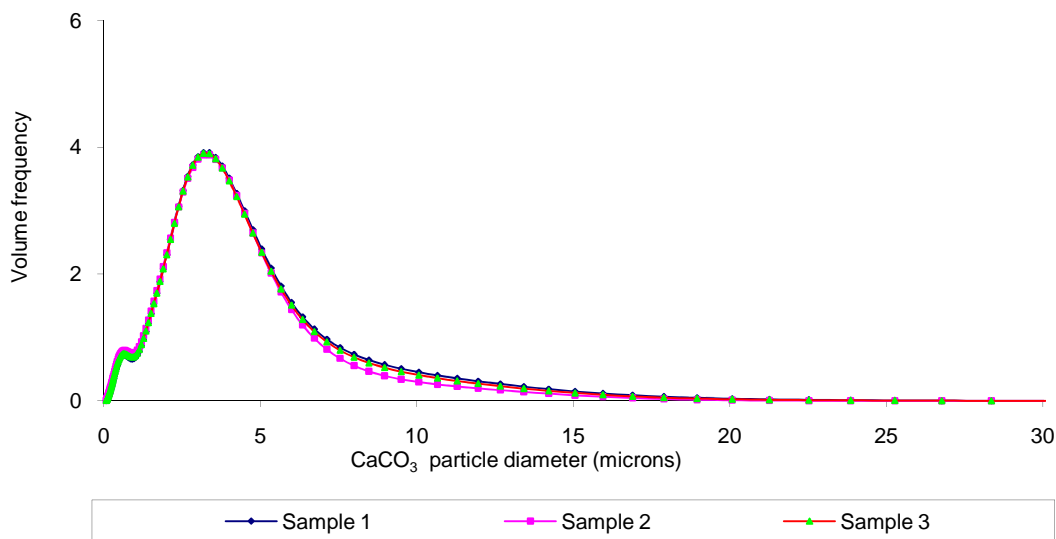


Figure 4.1 CaCO_3 particle size distribution

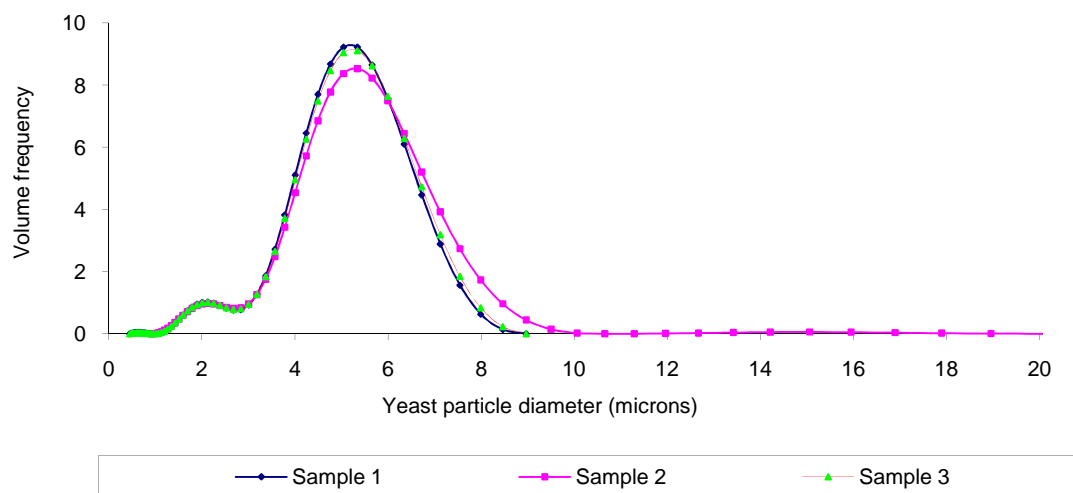


Figure 4.2 Yeast particle size distribution

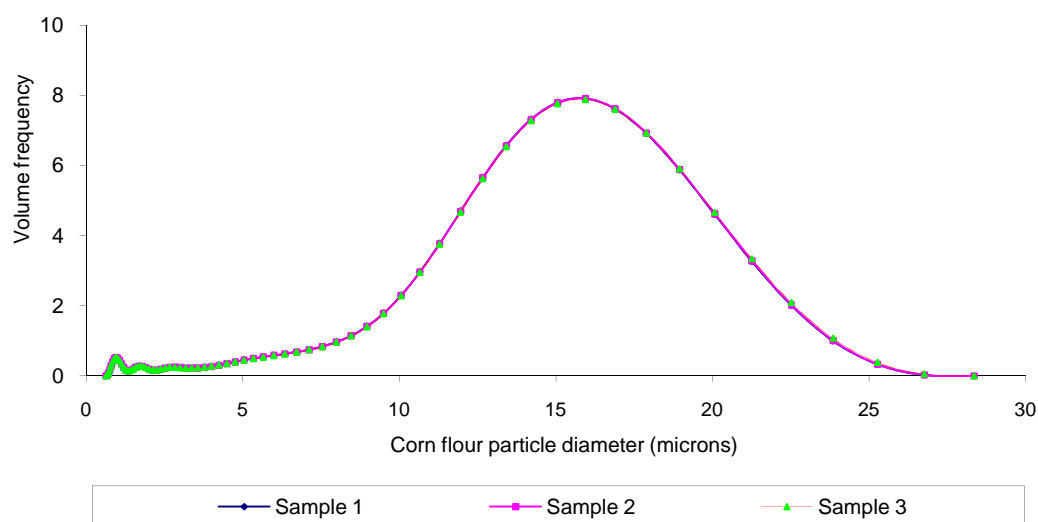


Figure 4.3 Corn flour particle size distribution

4.2 Experimental system set up and process conditions

Experimental work was carried out in a 7.5L New Brunswick Bioflo 110 stirred bioreactor with a working volume of 5L. The geometry was as defined by Correia *et al.* (2010) (Figure 4.4). Agitation was provided by two six flat bladed Rushton turbines driven by an electric motor with adjustable speed (Figure 4.4). Agitation was varied between 600-1200rpm in alkane-aqueous dispersions and in alkane-inert solid-aqueous dispersions. Agitation was varied between 600-900rpm in alkane-yeast-aqueous dispersions. Aeration was constantly provided at 0.8vvm (volume of air per volume of dispersion per minute) by a stainless steel ring sparger located directly below the lower turbine. The sparger was 5mm in diameter and had 7X1mm diameter equally spaced holes around the ring. Temperature was controlled at $22\pm 1^{\circ}\text{C}$ by circulating cooling water below the sparger and the system pressure was

kept constant at 101.3kPa for all experiments. A 12mm Teflon membrane diameter probe was used for DO measurement (Mettler Toledo InPro® 6800, 2005) (see Appendix A4.1 for the DO probe characteristics).

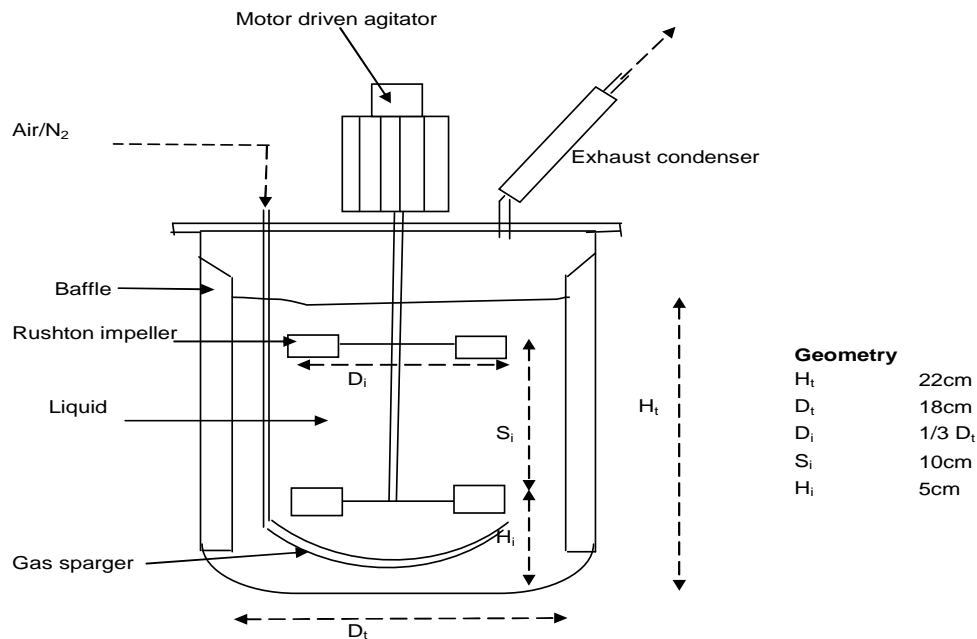


Figure 4.4 Experimental bioreactor system geometry (Redrawn from Correia *et al.* 2010)

K_{La} , K_p , fluid viscosity and fluid surface tension values were measured for all process conditions. Experiments were replicated 5 times and low standard deviations were observed i.e. the experiments were reproducible. The standard deviations values obtained during the experiments are noted in Appendices A7.1-A7.20.

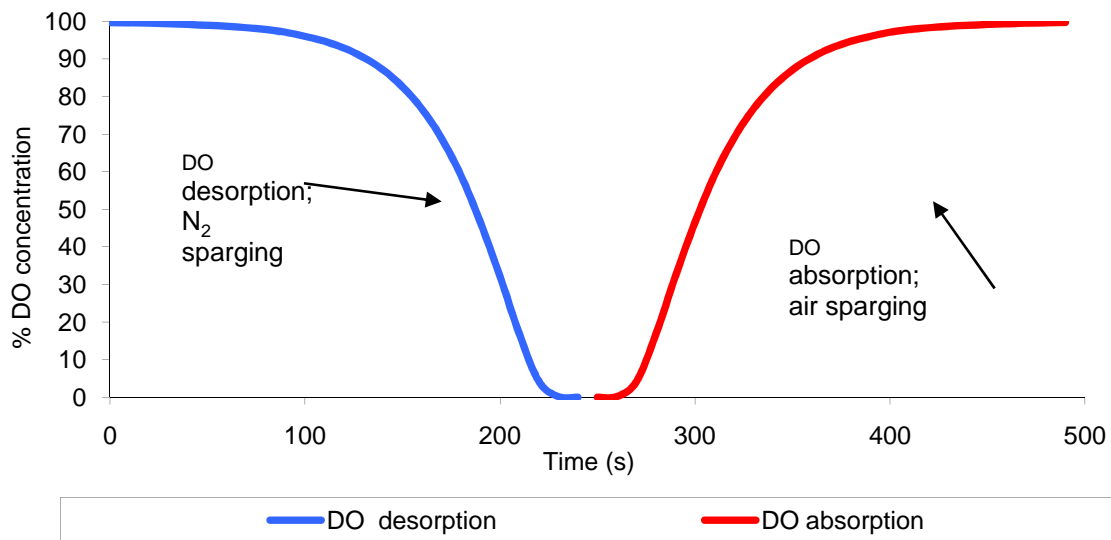
4.3 Measurement of the overall volumetric oxygen transfer coefficient

K_{La} was measured by both the gassing out procedure neglecting the DO probe response lag time (GOP (no lag)) according to the first order response model and the gassing out procedure incorporating the DO probe response lag time (GOP (lag)) according to the second order response model. The DO probe was calibrated before K_{La} measurement in the dispersion K_{La} was to be measured. This was done by first sparging the dispersion in the bioreactor with nitrogen until the raw input data on the DO meter was stable at a low value when the DO concentration was set to 0% (New Brunswick Bioreactor manual, 2005). Air was then sparged into the dispersion until the DO raw input data on the DO meter became stable again value and the DO value was then set to 100% (New Brunswick Bioreactor manual, 2005).

4.3.1 Measurement using the gassing out procedure and the first order response model

After calibration DO concentration was measured over time during the absorption of oxygen (Figure 4.5). DO absorption involves the re-sparging of air into the dispersion from 0% (after first de-oxygenating with nitrogen) until 100% DO saturation was reached (Figure 4.5). The probe then monitored DO change over time as C/C^* over 10s intervals until DO saturation was reached.

Figure 4.5 DO concentration profiles



during N_2 /air sparging in the GOP (no lag) (Redrawn from Garcia-Ochoa and Gomez, 2009)

The OTR first order response model was used for K_La measurement in the dispersion assuming zero DO probe response lag time (equation 1.1, equation 2.13). This first order response model is reduced to the form represented by equation 4.1 upon linearization. During oxygen absorption, the linearised OTR equation (equation 4.1) reduces to a form represented by equation 4.2 under conditions $C_1 = 0$ and $t_1 = 0$.

$$\ln\left(\frac{C^* - C_2}{C^* - C_1}\right) = -K_L a(t_2 - t_1) \quad [4.1]$$

$$\ln\left(1 - \frac{C}{C^*}\right) = -K_L a t \quad [4.2]$$

A graph of $\ln\left(1 - \frac{C}{C^*}\right)$ vs. time was plotted over 20s intervals and K_La was then obtained as the gradient of the line of this response (Figure 4.6).

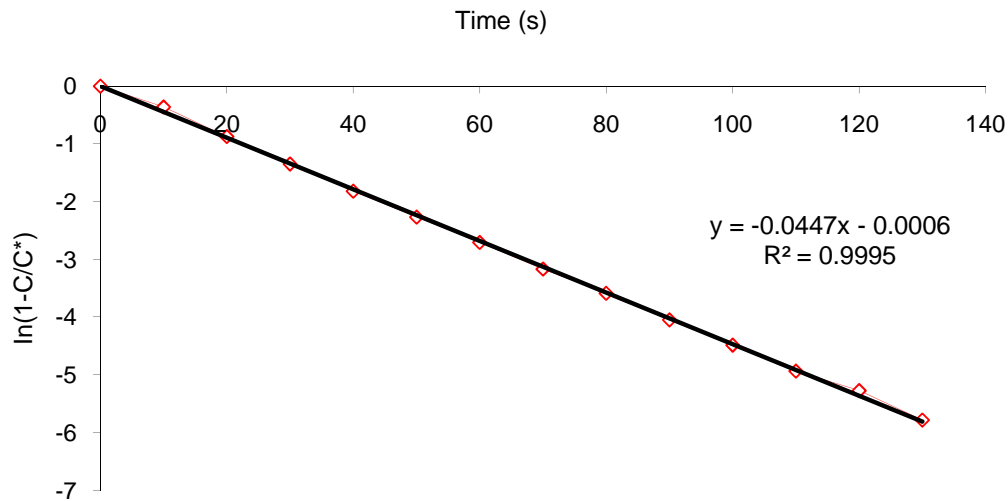


Figure 4.6 Experimental measurement of K_{La} by the GOP (no lag) first order response model

4.3.2 Measurement using the gassing out procedure and the second order response model

Since DO concentrations output indicated by the DO probe over time cannot be used to represent the actual change in DO concentration due to K_p effects, K_p had to be incorporated in DO measurement. The DO in the solution (equation 1.1, equation 2.7) and the DO indicated by the probe per particular time (equation 2.9) were convoluted to yield a second order response model (equation 2.10). This was used to accurately determine K_{La} in alkane multiphase systems. This second order response model was derived by using Laplace transforms (see Appendix A.2) and analytically (see Appendix A.3) under conditions that $C_{p0} = C_o$ at initial conditions with $t_o = 0$ and $C_p^* = C^*$ at saturation conditions.

The K_p value for each process condition was measured and incorporated in the calculation of K_{La} . K_{La} was determined by minimizing the total sum of errors between the measured DO and the DO calculated from the second order response model (equation 2.10) at each time interval. That is, the total sum of errors was determined from the sum of the square of the difference between the measured DO and the DO calculated from the second order model. The DO change error was determined according to equation 4.3 per each finite time. The DO over 10s intervals for the second order response model were calculated according to equation 4.4, using K_{La} from the first order response model as the initial K_{La} .

The K_La from the first order response model was set as the initial K_La and changed according to K_p effects. If the K_p effects were minimal, the sum of errors (the total sum of the squared differences between the two methodologies per each 10s interval) obtained between the two OTR measurement methods will be small. However if K_p effects are significant then a high sum of errors will be obtained. The actual K_La was then attained by changing K_La obtained from the first order response model until the sum of errors between these two methods was minimal using Equation Solver in Excel (see Appendix A.5 for a sample calculation).

$$\sum (Errors)^2 = \sum (\%DO_{2^{nd} \text{ order model}}) - \sum (\%DO_{1^{st} \text{ order model}}) \quad [4.3]$$

$$\%DO_{(2^{nd} \text{ order model})} = \left(\frac{C_p}{C_p^*} \right) * 100\% = \left[1 - \frac{1}{K_p - K_La} \left[K_p e^{-K_Lat} - K_La e^{-K_p t} \right] \right] * 100\% \quad [4.4]$$

4.3.3 Measurement of the probe response lag time

The DO probe was calibrated before measuring τ_p and K_p . This was done by immersing the probe in a solution of excess Na_2SO_3 in a 500ml beaker. Na_2SO_3 was converted to Na_2SO_4 thereby reducing the oxygen to zero. Zero oxygen was achieved by continual addition of excess Na_2SO_3 until there was no further decrease in the DO raw input on the DO meter and the zero value had stabilized. The DO probe was then quickly transferred to the pre-aerated oxygen saturated dispersion in the bioreactor and calibrated to 100% DO.

After calibration, the DO probe was immersed back to the sulfite solution (0% DO concentration). Then DO probe was transferred back to the oxygen saturated dispersion in the bioreactor and readings for %DO change were recorded as C_p/C_p^* over 10s intervals until 100% DO saturation was reached.

A graph of C_p/C_p^* vs. time was then plotted over 10s intervals. The time taken to transfer the DO probe from the DO-free sulfite solution to the DO-saturated dispersion in the bioreactor (dead time) was accounted for by omitting DO values obtained during this dead time when calculating K_p . The dead time was defined as the initial time which needed to be deleted so as to obtain a DO vs. time trend line with $R^2 \approx 1$. The dead time was typically less than 8s.

τ_p is defined as the time taken by the DO to undergo 63.2% of DO saturation after an experimental step change. At this condition, $C_p/C_p^* = 0.632$ and the time of experiment, t , is equal to the DO probe response time, τ_p i.e. $t = \tau_p$ (Luyben and

Luyben, 1997). Appendix A4.2 provides the analytical solution for the DO probe response lag time. Consequently, τ_p was determined from the graph of C_p/C_p^* vs. time by solving the equation of the line when $C_p/C_p^* = 0.632$ with $y = 0.632$ and x as τ_p (Nakanoh and Yoshida, 1980; Luyben and Luyben, 1997; Juarez and Orians, 2001) (Figure 4.7).

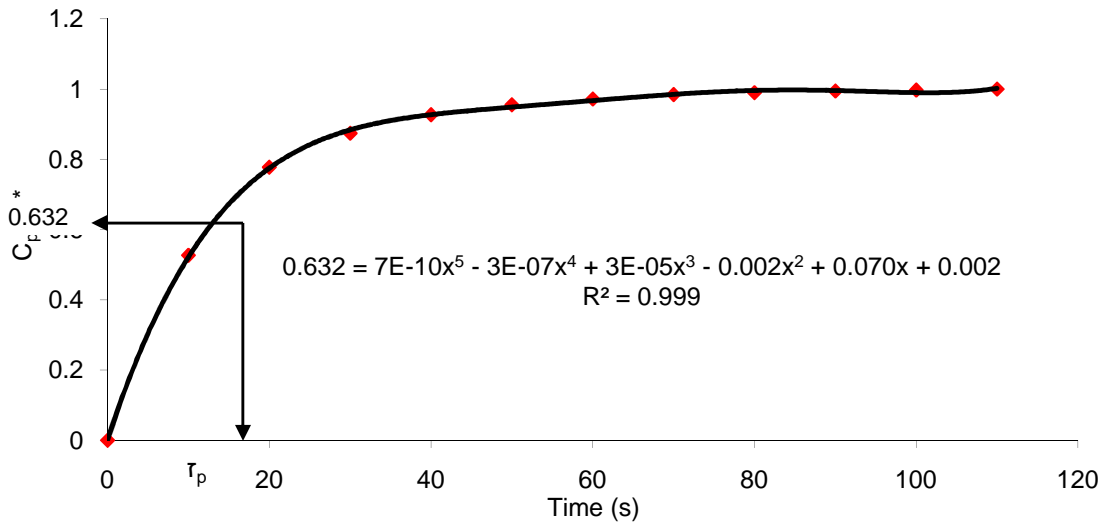


Figure 4.7 Experimental determination of τ_p by solving the equation of line when $C_p/C_p^* = 0.632$

τ_p which can also be expressed as: $\tau_p = 1/K_p$ (Merchuk *et al.* 1990), where K_p is the inverse DO probe response lag time was alternatively determined by non-linear least squares regression from a graph of $\ln\left(1 - \frac{C_p}{C_p^*}\right)$ vs. time using the DO probe first order response model (equation 2.24) as the slope of the line (Figure 4.8) (Letzel *et al.*, 1999; Bi *et al.*, 2001; Vandu and Krishna 2004). The τ_p and K_p values obtained from both methods were similar with slight deviations as low as 5%. For example in Figure 4.7 τ_p is about 17s and the inverse K_p from non-linear regression in Figure 4.8 gives 17.8s.

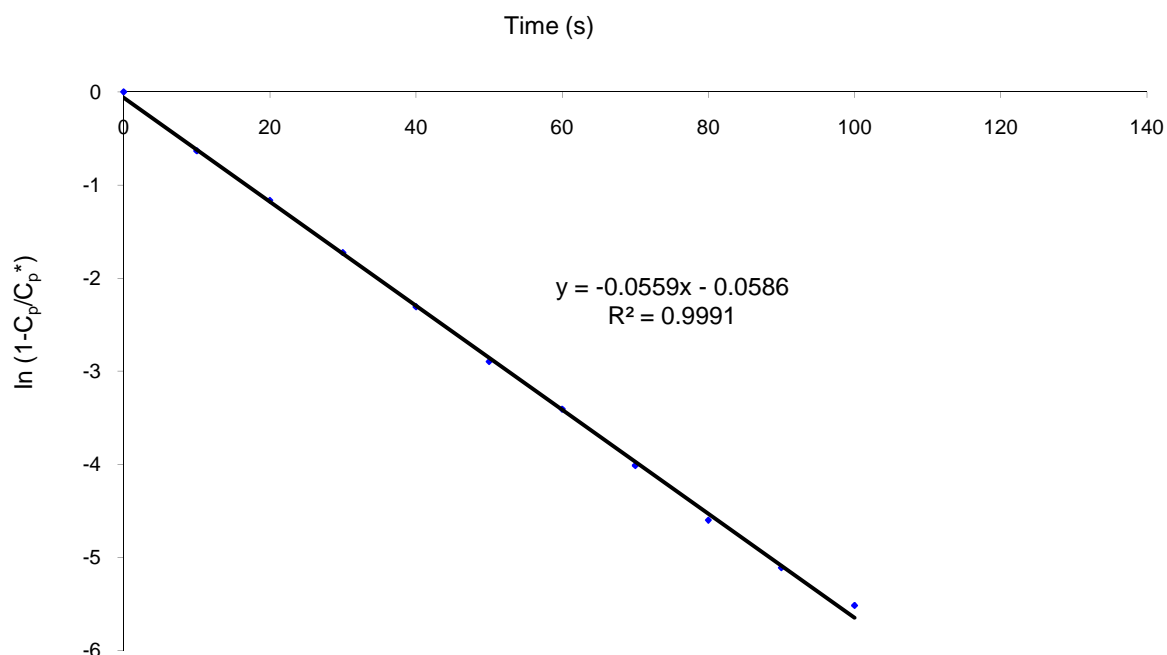


Figure 4.8 Experimental determination of K_p by non-linear regression from DO probe first order response model

4.4 Measurement of fluid viscosity and fluid surface tension

Fluid viscosity and fluid surface tension were measured to fully underpin K_La behavior due to influences of fluid properties in alkane-solid-aqueous dispersions at the same conditions K_La was measured. Prior to taking fluid viscosity and fluid surface tension measurements the alkane-solid-aqueous dispersions samples were homogenized. Samples were analyzed immediately after homogenization. Homogenization followed by analysis was repeated 5 times for each sample with reproducible results.

4.4.1 Homogenization of alkane-solid-aqueous dispersions

A lab bench model homogenizer which is ideal for preparing laboratory samples was used for homogenization (Figure A6.1). 100cm^3 of the alkane-solid-aqueous dispersion were homogenized at a time. The dispersion was poured into the feeding cone at a time after vigorous shaking. 20cm^3 of sample were then drawn in the feeding cone at a time to ensure uniformity in the sample. 10cm^3 of the dispersion were then used during viscosity and surface tension measurements soon after homogenization.

Cleaning of the homogenizer was carried out with 70% ethanol after every experimental run to ensure no blockages occurred and to ensure consistent operation of the homogenizer. The theory on the homogenization process is detailed in Appendix A6.1.

4.4.2 Measurement of fluid viscosity

Fluid viscosity measurements were carried out at shear rates from 0-1000s⁻¹ using a Paar Physica MCR 501 Rheometer. Viscosity measurements were carried out using 5cm³ of fluid for each process condition then readings at 600s⁻¹ were only considered since the dispersions showed a Newtonian behavior. A double gap method (DG 26.7) was used for viscosity determination (Figure 4.9). This method is useful in measuring low viscosity fluids with viscosities close to that of water and it also increases the surface area of the fluid enabling measurements to be done at low torques (Mezger, 2002). The DG 26.7 system consists of a bob and a cylindrical central part that allows an annular gap for the alkane-solid-aqueous dispersion (Figure 4.9).

The sample was placed in the cup annular gap and the inner cylinder was then rotated within the cup. The rheometer then measured the cylindrical cup's angular velocity and torque of rotation within the fluid. These quantities were then used to measure the shear stress (τ) and the shear rate (γ) after which the viscosity was determined from Newton's Law of Viscosity for Newtonian fluids (equation 4.5) for each process condition. A computer program Rheoplus was used for viscosity analysis. The theory on fluid viscosity is detailed in Appendix A6.2.

$$\frac{\tau}{\gamma} = \mu = \text{constant} \quad [4.5]$$

Where τ is the shear stress, the shear rate (γ) the shear rate which is constant for Newtonian fluids.

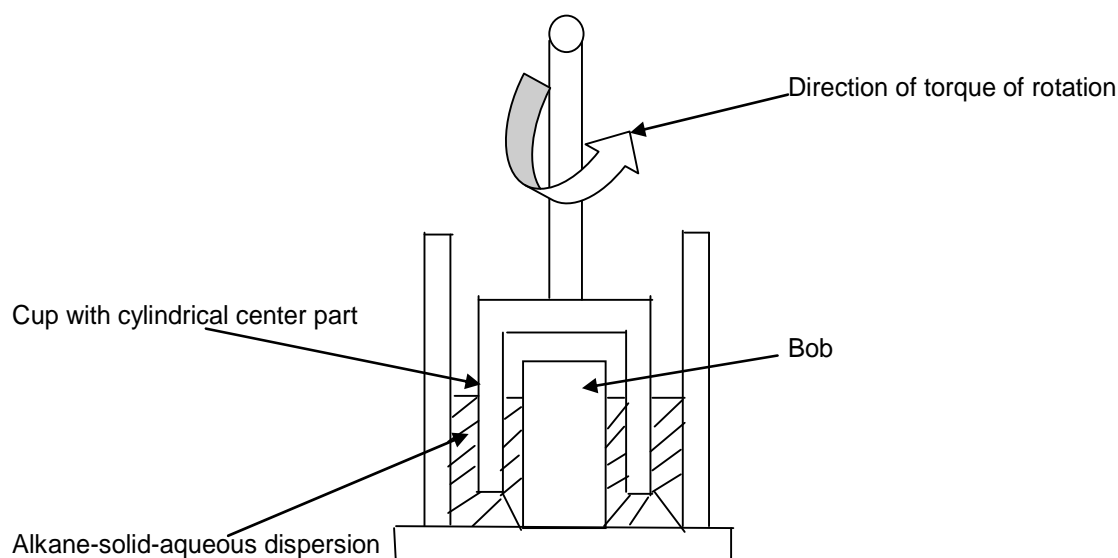


Figure 4.9 Double gap system used for fluid viscosity measurements (Mezger, 2002)

4.4.3 Measurement of fluid surface tension

A Du Noüy tensiometer with a 6mm radius platinum ring was used for surface tension measurements. The tensiometer was placed at a level surface and was calibrated before taking measurements. During calibration the bar attached to the platinum ring was aligned horizontally to the torsion balance using the fine adjustment screw and a surface tension reading was taken. A small piece of paper (78g) was weighed and placed on the platinum ring then a second surface tension reading was taken. The correction factor (CF) was then obtained by multiplying the mass of the paper with the acceleration due to gravity and dividing it by the perimeter of the ring and the differences in surface tension readings with and without the paper (equation 4.6). The effectiveness of calibration was tested by measuring the surface tension of distilled water which was found to be 71.8mN/m at 22°C.

$$CF = \frac{mg}{RI} \quad [4.6]$$

where m is the mass of piece of paper (g), g is the acceleration due to gravity (m^2/s), R is the difference in tensiometer readings with and without paper (mN/m) and I is the perimeter of ring which is equal to $4\pi r$ with r as radius of the ring (mm)

The platinum ring was cleaned with distilled water between measurements for accurate results. The ring was handled with care to avoid deformations and it was made sure that the ring did not touch the sides of the beaker for accurate results. Surface tension readings were then taken after calibration. 10cm³ of fluid were

poured into a beaker which was placed on the sample platform directly beneath the platinum ring. The ring was suspended in the dispersion by raising the sample platform until the ring was 5mm immersed in the dispersion. Using the fine adjustment screw, the platinum ring was continuously lifted up until the ring was within the surface of the fluid and the torsion balance scale was zeroed. The torsion that supports the wire was increased by turning the torsion balance scale upwards. This increased the torsion on the ring until the ring broke away from the surface of the fluid. The force required to break through the fluid/air surface was directly proportional to the surface tension of the fluid. Measurements obtained when the ring broke free from the fluid surface were multiplied by the correction factor to obtain the actual fluid surface tension. The correction factor used for this analysis was 0.46 and the torsion balance was zeroed at 21mN/m.

4.5 Experimental design and statistical analyses

All experiments done in this work were carried out through experimental designs and analyses were carried out statistically. Experimental design and analyses is necessary in using experiments to gain maximum knowledge at minimum cost and time (Vining, 1998). Factorial designs were used in evaluation of an accurate and less complex K_La measurement method in alkane multiphase systems as well the quantification of K_La behavior in these systems. This allowed the simultaneous examination of the effects of various parameters on K_p , K_La , μ and σ as well as their degree of interaction. In addition to that the *t-test* was used for comparing K_La values from the different measurement methods. The *t-test* assesses whether there is a statistically significant difference between two groups. This tested the significant difference between the average K_La values in each of the different methodologies. The F-variance ratio is a part of the *t-test* and it assesses if the variance between groups are statistically different. The influence of K_p on K_La as agitation rate increased was quantified by the F-variance ratio at each individual agitation rate.

All experimental designs were carried out at 99% confidence interval. The low levels and high levels applied in the factorial designs were based on reported process conditions from literature, with the low level being the minimum process condition reported and the high level being the maximum process condition employed. The low levels and high levels used for the K_p , K_La , μ and σ experiments are shown in Tables 4.4, 4.6, 4.8, 4.10 and 4.12.

Pareto charts, which show the relative effects of the different process parameters in their decreasing order on K_p , K_{La} , μ and σ as well as their degree of interaction, were used for results analyses. The 99% confidence interval value used for analyses was represented by a probability value (p-value) of 0.1 on the Pareto chart. Any effect crossing the vertical line on the Pareto chart for the p-value of 0.1 was significant. The number relating to each variable on the Pareto charts signifies the calculated effect of that parameter, relative to the other parameters for that particular factorial experimental design. The negative sign shows it has a decreasing effect and the positive sign an increasing effect on the response variables.

In addition, surface response curves were drawn to represent the information indicated by the Pareto charts at the low and high levels, giving possible trends in K_p , K_{La} , μ and σ . The effect of two parameters and their interaction were evaluated at a time during which the other parameters (if any) were kept constant at the average conditions of the experiment.

4.5.1 Evaluation of measurement methodology

Factors underpinning K_p which related to the DO probe characteristics and process conditions were first investigated using 2^2 factorial experimental designs. The influences of various parameters on K_p which included the probe membrane age (5 day usage), probe electrolyte age (5 day usage), agitation rates (600-1200rpm), alkane concentrations (2.5-20% (v/v)), alkane chain lengths (n -C₁₀₋₁₃ and n -C₁₄₋₂₀), solids loadings (1-10g/L), solids particle sizes (3-14 μ m) and their interactions were investigated at the chosen low level (-1) and high level (1) (Table 4.4). Four independent 2^2 factorial experimental designs were used to statistically quantify the effects of these factors on K_p using an analysis tool pack (STATISTICA) which led to the analysis of the first hypothesis. The K_p values obtained according to the series of designs are listed in Appendices A7.1-A7.4. A 2^2 experimental design is a two level factorial experiment with two factors under investigation showing all possible treatment combinations at the two levels (-1 and 1) (Vining, 1998) (Table 4.5).

Table 4.4: Factors affecting K_p at two levels

Experiment	Factor	Low level	High level
1	A. Membrane age	Day 1	Day 5
	B. Electrolyte age	Day 1	Day 5
2	A. Agitation rate	600rpm	1200rpm
	B. Alkane concentration	2.5% (v/v)	20% (v/v)

3	A. Alkane chain length	$n\text{-C}_{10-13}$	$n\text{-C}_{14-20}$
	B. Alkane concentration	2.5% (v/v)	20% (v/v)
4	A. Solids loading	1g/L	10g/L
	B. Solids particle size	3 μm	14 μm

Table 4.5: 2² Experimental design used to quantify factors affecting K_p at two levels

Factor		Treatment Combination	
A	B		
-1	-1	A low,B low	
1	-1	A high,B low	
-1	1	A low,B high	
1	1	A high,B high	

After evaluating factors affecting K_p , K_{La} was measured in $n\text{-C}_{10-13}$ -aqueous dispersions and $n\text{-C}_{14-20}$ -aqueous dispersions for varying alkane concentrations of 2.5-20% (v/v) and agitation rates of 600-1200rpm. Average K_{La} results from the second order response model, GOP (lag) and the first order response model, GOP (no lag) in the alkane-aqueous dispersions were compared using a *t-test* to statistically quantify K_p effects on K_{La} measurement in alkane multiphase systems leading to further analysis of the first hypothesis. Also the effect of agitation rate on K_{La} differences due to K_p effects in these dispersions was also quantified using the *t-test* in these dispersions. Additionally, average K_{La} results from the PSP and the GOP (lag) in the $n\text{-C}_{10-13}$ -aqueous dispersions were compared using the *t-test* to statistically quantify if the PSP and GOP (lag) methodologies resulted in the same K_{La} values since they both account for K_p effects. This also led to the analysis of the first hypothesis.

4.5.2 Quantification of the behavior of the overall volumetric oxygen transfer coefficient

4.5.2.1 Alkane-aqueous dispersions with inert solids

The influences of various parameters on K_{La} in alkane-solid-aqueous dispersions with inert solids including agitation rates (600-1200rpm), alkane concentrations (2.5-20% (v/v)), solids loadings (1-10g/L) and solids particle sizes (3-14 μm) were investigated at both the low level (-1) and the high level (1) (Table 4.6). A 2⁴ factorial experimental design was used to statistically quantify the effects of these factors and their interactions on K_{La} considering the low level (-1) and the high level (1) (Vining,

1998) (Table 4.7). This led to the analysis of the second hypothesis. A 2^4 experimental design is a two level factorial experiment with four factors under investigation showing all possible treatment combinations at the two levels (Vining 1998). The effect of two factors and their interaction was determined when the other two factors were kept constant at the center conditions i.e. agitation of 900rpm, alkane concentration of 11.25% (v/v), solids loading of 5.5g/L and solids particle size of $9\mu\text{m}$.

The centre conditions in this system could not be investigated due to the absence of a solid particle with similar density to corn flour and CaCO_3 but with a particle size of $9\mu\text{m}$. So the data from the experiments only show K_La behavior at the low and high levels but does not conclusively show the actual K_La trend since no center conditions were investigated. However, this was enabled the estimation of the range of parameters to use in the experiments with inactive yeast cells where process conditions at the centre point could be evaluated.

Table 4.6: Factors affecting K_La in alkane-inert solid-aqueous dispersions at two levels

Factor	Low level (-1)	High level (1)
A. Agitation rate	600rpm	1200rpm
B. Alkane concentration	2.5% (v/v)	20% (v/v)
C. Solids loading	1g/L	10g/L
D. Solids particle size	$3\mu\text{m}$	$14\mu\text{m}$

Table 4.7: 2⁴ Experimental design used to quantify factors affecting K_La in alkane-inert solid-aqueous dispersions

Factor				Treatment Combination
A	B	C	D	
-1	-1	-1	-1	A low,B low,C low,D low
1	-1	-1	-1	A high,B low,C low,D low
-1	1	-1	-1	A low,B high,C low,D low
1	1	-1	-1	A high,B high,C low,D low
-1	-1	1	-1	A low,B low,C high,D low
1	-1	1	-1	A high,B low,C high,D low
-1	1	1	-1	A low,B high,C high,D low
1	1	1	-1	A high,B high,C high,D low
-1	-1	-1	1	A low,B low,C low,D high
1	-1	-1	1	A high,B low,C low,D high
-1	1	-1	1	A low,B high,C low,D high
1	1	-1	1	A high,B high,C low,D high
-1	-1	1	1	A low,B low,C high,D high
1	-1	1	1	A high,B low,C high,D high
-1	1	1	1	A low,B high,C high,D high
1	1	1	1	A high,B high,C high,D high

Additionally, influences of alkane concentrations (2.5-20% (v/v)), solids loadings (1-10g/L), solids particle sizes (3-14 μ m) and their interactions on fluid viscosity and fluid surface tension were quantified at the low level (-1) and the high level (1) (Table 4.8). A 2³ factorial design was used to quantify effects of alkane concentration, solids loading, solids particle size and their interaction on fluid viscosity and fluid surface tension at two levels in alkane-inert solid-aqueous dispersions (Table 4.9).

The effect of individual parameters and interaction between two factors was determined when one of the factors was kept constant i.e. at alkane concentration of 11.25% (v/v), solids loading of 5.5g/L and solids particle size of 9 μ m. The factorial design on influences of fluid viscosity and surface tension in systems with inert solids helped in analysis of the second hypothesis.

Table 4.8: Factors affecting fluid viscosity and fluid surface tension at two levels in alkane-inert solid-aqueous dispersions

Factor	Low level (-1)	High level (1)
A. Alkane concentration	2.5% (v/v)	20% (v/v)
B. Solids loading	1g/L	10g/L
C. Solids particle size	3 μ m	14 μ m

Table 4.9: 2³ Experimental design used to quantify factors affecting fluid surface tension and fluid viscosity in alkane-inert solid-aqueous dispersions

		Factor		Treatment Combination
A	B	C		
-1	-1	-1	A low,B low,C low	
1	-1	-1	A high,B low,C low	
-1	1	-1	A low,B high,C low	
1	1	-1	A high,B high,C low	
-1	-1	1	A low,B low,C high	
1	-1	1	A high,B low,C high	
-1	1	1	A low,B high,C high	
1	1	1	A high,B high,C high	

4.5.2.2 Alkane-aqueous dispersions with inactive yeast cells

The influences of various parameters on K_La in alkane-solid-aqueous dispersions with inactive yeast including of agitation rates (600-900rpm), alkane concentrations (2.5-11.25% (v/v)) and yeast loadings (1-5.5g/L) as typical on K_La were investigated in alkane-yeast-aqueous dispersions at both the low level (-1) and high level (1) as well as the centre run (0) (Table 4.10). In the yeast experiment, the parameter range

was narrowed to more accurately represent conditions in a bioprocess. A centre run was done at an alkane concentration of 6.88% (v/v), agitation rate of 750rpm and yeast loading of 3.25g/L for the alkane-yeast-aqueous dispersions to check for any curvature in K_La behavior.

A 2^3 factorial experimental design was used to statistically quantify effects of agitation rate, alkane concentration, yeast loading and their interaction on K_La considering the low level and the high level (Table 4.11). This led to the analysis of the third hypothesis. A 2^3 experimental design is a two level factorial experiment with three factors under investigation showing all possible treatment combinations at the two levels (Vining, 1998) (Table 4.11).

Table 4.10: Factors affecting K_La at two levels in alkane-yeast-aqueous dispersions

Factor	Low level (-1)	Center point (0)	High level (1)
A. Agitation rate	600rpm	750rpm	900rpm
B. Alkane concentration	2.5% (v/v)	6.88% (v/v)	11.25% (v/v)
C. Yeast loading	1g/L	3.25g/L	5.5g/L

Table 4.11: 2^3 Experimental design used to quantify factors affecting K_La in alkane-yeast-aqueous dispersions

Factor			Treatment Combination
A	B	C	
-1	-1	-1	A low,B low,C low
1	-1	-1	A high,B low,C low
-1	1	-1	A low,B high,C low
1	1	-1	A high,B high,C low
-1	-1	1	A low,B low,C high
1	-1	1	A high,B low,C high
-1	1	1	A low,B high,C high
1	1	1	A high,B high,C high
0	0	0	Center point

Additionally, influences of alkane concentrations (2.5-11.25% (v/v)), yeast loadings (1-5.5g/L) and their interactions on fluid viscosity and fluid surface tension were also quantified in the alkane-yeast-aqueous dispersions at the low level (-1) and high level (1) (Table 4.12). A centre run (0) was done at an alkane concentration of 6.88% (v/v) and yeast loading of 3.25g/L to check for any curvature in fluid viscosity and fluid surface tension behavior in these systems (Table 4.12). A 2^2 factorial design with a centre point (Table 4.13) was used to quantify effects of alkane concentration; yeast loading and their interaction on fluid viscosity and fluid surface tension at two levels in alkane-yeast-aqueous dispersions (Table 4.13). The factorial design on influences of fluid viscosity and surface tension in systems with inactive yeast helped in analysis of the third hypothesis.

Table 4.12: Factors affecting on fluid viscosity and fluid surface tension at two levels in alkane-yeast-aqueous dispersions

Factor	Low level (-1)	Center point (0)	High level (1)
A. Alkane concentration	2.5% (v/v)	6.88% (v/v)	11.25% (v/v)
B. Yeast loading	1g/L	3.25g/L	5.5g/L

Table 4.13: 2^2 Experimental design used to quantify factors affecting on fluid viscosity and fluid surface tension at two levels in alkane-yeast-aqueous dispersions

Factor		Treatment Combination
A	B	
-1	-1	A low,B low
1	-1	A high,B low
-1	1	A low,B high
1	1	A high,B high
0	0	Center point

5 RESULTS AND DISCUSSION

Results and discussion are divided into two parts which are, firstly, the evaluation of an accurate K_{La} measurement method in alkane multiphase systems, which accounts for K_p effects and, secondly, the quantification of K_{La} behavior in aerated agitated alkane-solid-aqueous dispersions in systems with inert solids and inactive yeast using this accurate measurement method. When quantifying K_{La} , the influence of fluid viscosity and fluid surface tension on K_{La} was also evaluated in alkane-solid-aqueous dispersions with both inert solids and inactive yeast. Analysis software (STATISTICA) was used for results analysis at 99% confidence interval and the *t-test* was used for comparing K_{La} results from different measurement methods. The details of the statistical analyses are detailed in section 4.5.

5.1 Evaluation of measurement method in alkane multiphase systems

The DO probe response lag time and how it impacts K_{La} measurement in an alkane based system was investigated. Influences of membrane age, electrolyte age, agitation rate, alkane concentration, alkane chain length, solids loading, solids particle size and their interactions on K_p were investigated. The effects of these parameters will be explained in accordance with the individual experiments carried out.

Additionally, K_p was incorporated into K_{La} measurement for each process condition according to the GOP (lag) second order response model, and the results were compared to those from the GOP (no lag) first order response model in which K_p was neglected. Lastly the K_{La} calculated from the second order response model and the PSP were compared since both methods incorporate K_p effects in their methodology.

5.1.1 Factors affecting the probe response lag time

5.1.1.1 *Effect of membrane age, electrolyte age and their interaction*

Increase in membrane age and electrolyte age contributed to K_p decrease over a period of 5 days in 2.5% (v/v) *n*-C₁₄₋₂₀-aqueous dispersions at 1000rpm (see Table A7.1 for results). Membrane age caused the major decrease with an effect of -21.34 compared to electrolyte age which had approximately half the effect. Their interactive effect on K_p was insignificant at 99% confidence interval (Figure 5.1).

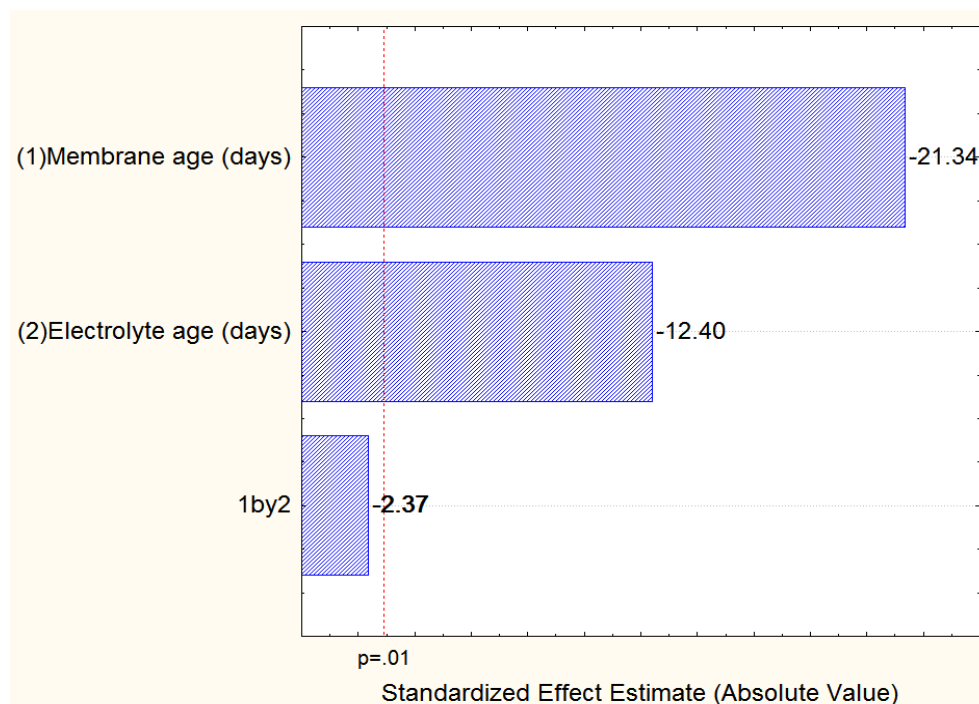


Figure 5.1 Pareto chart for effect of membrane age, electrolyte age and their interaction on K_p in 2.5% (v/v) $n\text{-C}_{14-20}$ -aqueous dispersions at 1000rpm

The influence of the membrane and electrolyte age is demonstrated by means of a surface plot (Figure 5.2). K_p had a maximum value of 0.0559s^{-1} when both membrane and electrolyte were new and gradually decreased to 0.0329s^{-1} with an increase in membrane age and electrolyte usage. This behavior is in agreement to the work of Aiba and Huang (1969) who studied oxygen permeability and diffusivity in polymer membranes immersed in aqueous solutions and to that of Benedek and Heideger (1970) who studied the effect of the response lag time in non-steady state aeration aqueous systems. They demonstrated that when the membrane was continuously used, an artificial space formed between the DO probe membrane and cathode due to stretching which resulted in longer probe response times. This artificial space also resulted in the formation of excess platinum oxides at the cathode which resulted in an over potential, making the platinum oxides behave like contaminants at the cathode, thus the DO probe's slow response. Also as the DO probe electrolyte usage increased, a reduction product, AgCl, formed at the probe anode which also contributes to the slow response of the probe and possibly reduction in conductivity of electrolyte.

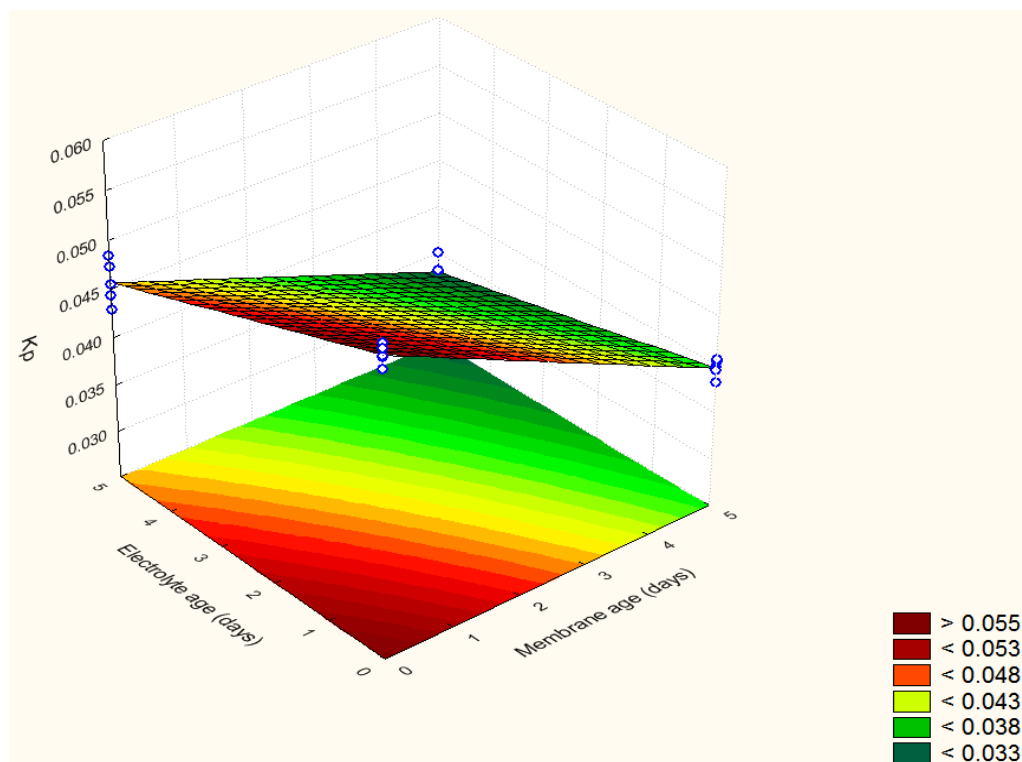


Figure.5.2 Surface response for effect of membrane age, electrolyte age and their interaction on K_p in 2.5% (v/v) n -C₁₄₋₂₀-aqueous dispersions at 1000rpm

5.1.1.2 Effect of agitation rate, alkane concentration and their interaction

An increase in alkane concentration decreased K_p with an effect of -9.12 whilst an increase in agitation rate was insignificant at 99% confidence interval (Figure 5.3) (see Table A7.2 for results). Secondly the interactive effect between increasing agitation rate and alkane concentration was insignificant at 99% confidence interval (Figure 5.3).

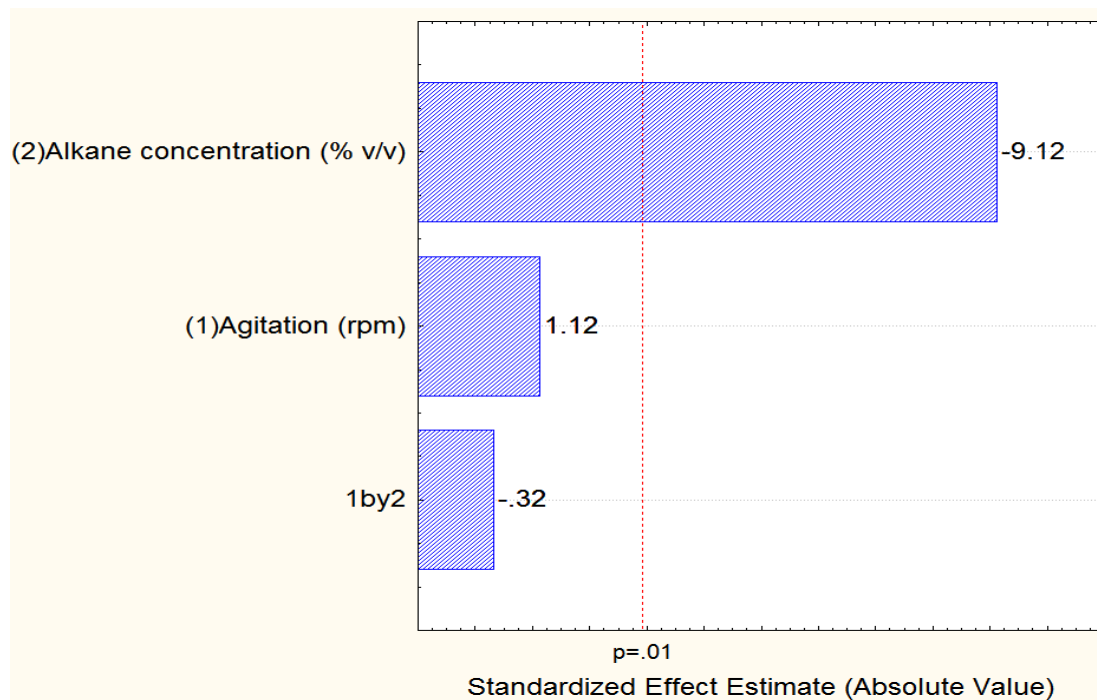


Figure 5.3 Pareto chart for effect of agitation rate, alkane concentration and their interaction on K_p in 2.5-20% (v/v) n -C₁₄₋₂₀-aqueous dispersions

K_p had a maximum value of 0.0434s^{-1} when the alkane concentration in the dispersion was 2.5% (v/v) and agitation rate was at 1200rpm. As the alkane concentration increased to 20% (v/v), K_p decreased to 0.0373s^{-1} at 600rpm and 0.0377s^{-1} at 1200rpm (Figure 5.4). This was possibly because, as the alkane concentration increased, the fluid viscosity increased as indicated by Queimada *et al.* (2004) and Correia *et al.* (2010). This thickened the liquid film increasing the resistance to DO transfer through the liquid film. This same result was obtained by Dang *et al.* (1977) in 2% (v/v) CMC solution and they indicated that for very viscous systems the film diffusion contributes to higher probe response lag times which cannot be neglected. They also indicated that the probe response times in 2% (v/v) CMC additive can be 15% higher than that free from any additives which was in agreement to Godbole *et al.* (1980)'s findings who reported a threefold increase in the probe response lag time in CMC solutions compared to water.

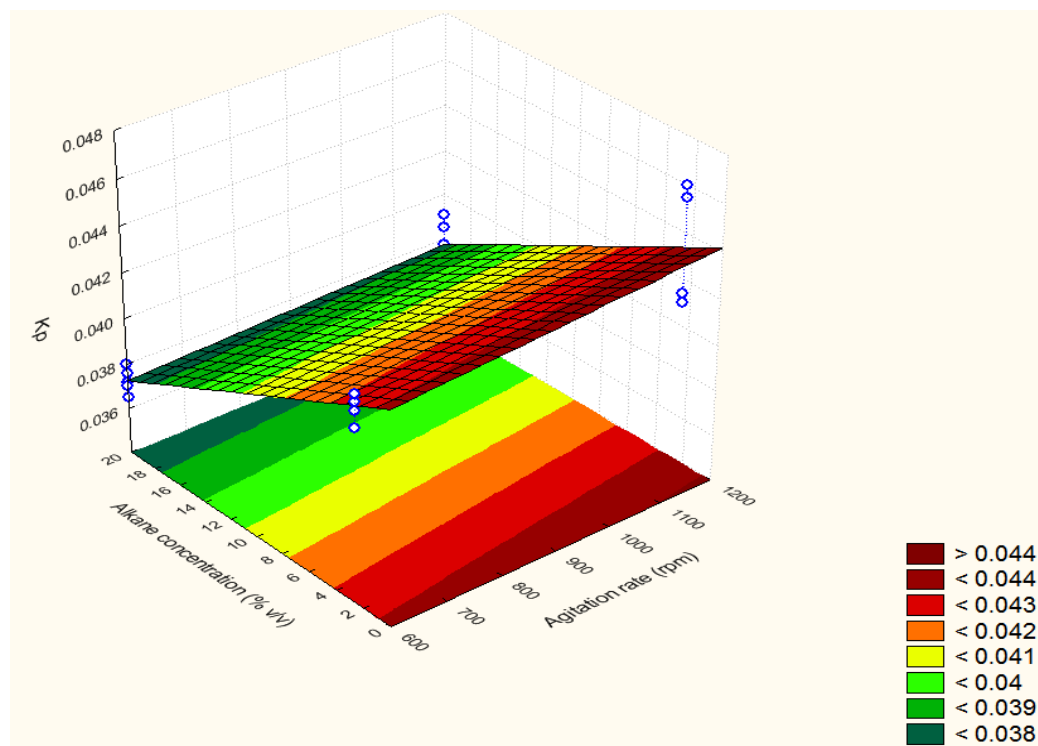


Figure 5.4 Surface response for effect of agitation rate and alkane concentration on K_p in 2.5-20% (v/v) n -C₁₄₋₂₀-aqueous dispersions at 1000rpm

5.1.1.3 Effect of alkane chain length, alkane concentration and their interaction

K_p decreased with increase in alkane chain length from n -C₁₀₋₁₃ to n -C₁₄₋₂₀ and alkane concentration from 2.5% (v/v) to 20% (v/v) with alkane concentration having the major effect of -44.8, about 7 times greater than the effect of the average alkane chain length (Figure 5.5) (see Table A7.3 for results). The interaction between these two factors on K_p was insignificant at 99% confidence interval (Figure 5.5).

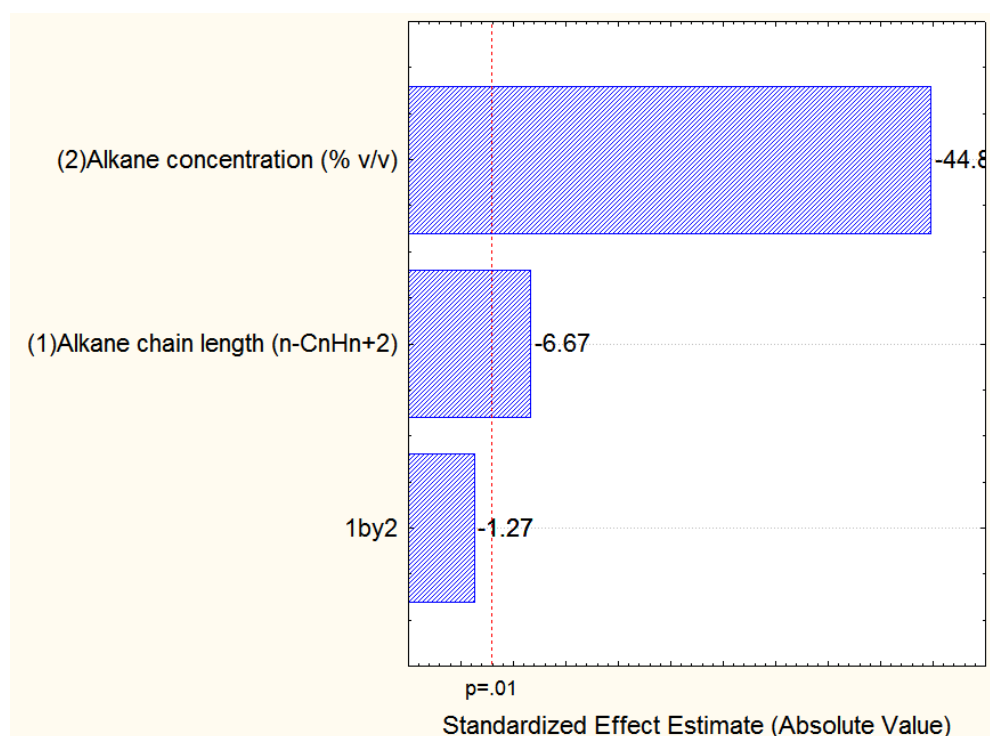


Figure 5.5 Pareto chart for effect of alkane chain length, alkane concentration and their interaction on K_p in 2.5-20% (v/v) n -C₁₄₋₂₀-aqueous dispersions at 1000rpm

K_p had a maximum value of 0.0589s^{-1} in 2.5% (v/v) n -C₁₀₋₁₃-aqueous dispersions and slightly decreased to 0.0556s^{-1} in 2.5% (v/v) n -C₁₄₋₂₀-aqueous dispersions. However at an alkane concentration of 20% (v/v) K_p decreased from 0.0327s^{-1} in n -C₁₀₋₁₃-aqueous dispersions to 0.0280s^{-1} in n -C₁₄₋₂₀-aqueous dispersions (Figure 5.6). This was attributed to an increase in the fluid viscosity with increase in both alkane chain length alkane concentration as indicated by Koide *et al.* (1976) and Correia *et al.* (2010), resulting in more time required by the DO to diffuse through the liquid film hence longer DO probe response lag times. The same result was obtained by Ruchti *et al.* (1981) when their response lag time due to the film diffusion effect increased from 21s in 1% (v/v) CMC to about 40s in 2.7% (v/v) CMC solution. This was also in agreement to the work of Nakanoh and Yoshida (1980) who indicated that K_p was very much dependent on fluid properties.

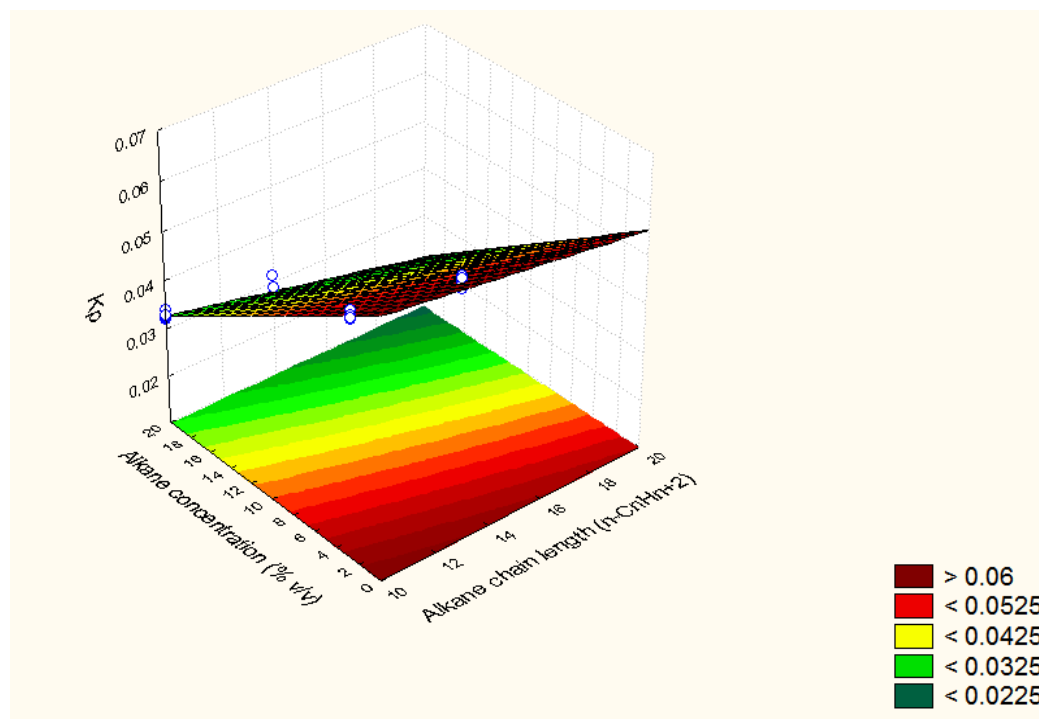


Figure 5.6 Surface response for effect of alkane chain length and alkane concentration on K_p in 2.5-20% (v/v) n -C₁₀₋₁₃ and n -C₁₄₋₂₀-aqueous dispersions at 1000rpm

5.1.1.4 Effect of solids loading, solids particle size and their interaction

Increasing solids loading from 1g/L to 10g/L, solids particle size from 3 μ m to 14 μ m and their interaction did not have statistically significant effects on K_p in 2.5% (v/v) n -C₁₄₋₂₀-solid-aqueous dispersions at 1000rpm at 99% confidence interval. Solids loading depressed K_p with a minor effect of -1.46; solids particle sizes depressed K_p with an effect of -0.46 and their interactive effect was 1.29 which insignificantly enhanced K_p (Figure 5.7) (see Table A7.4).

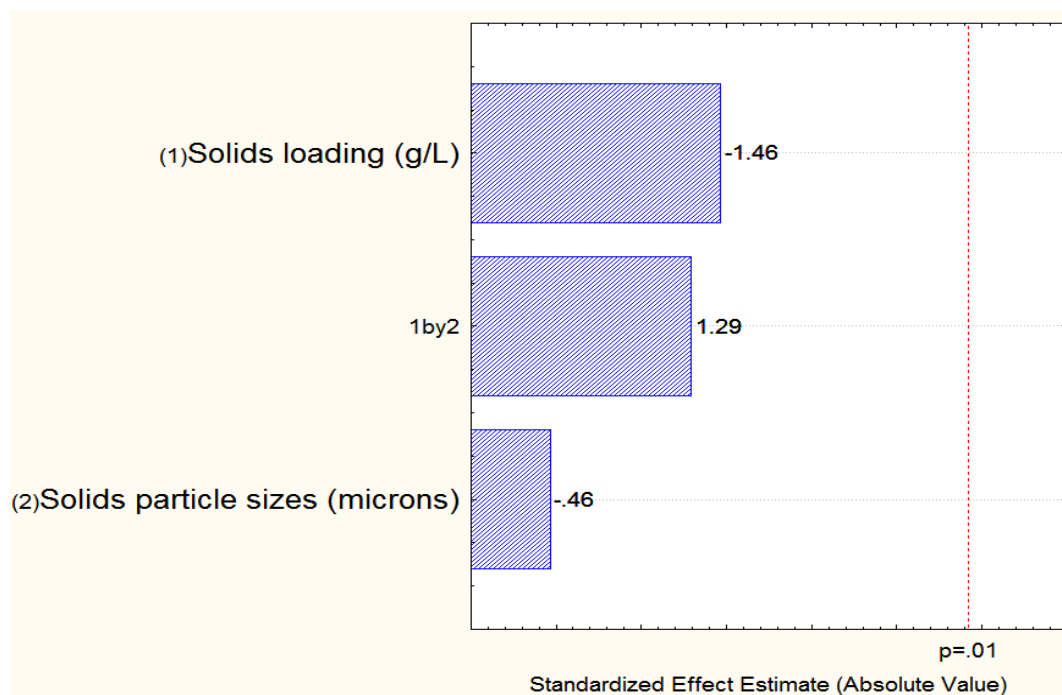


Figure 5.7 Pareto chart for effect of solids loading, solids particle size and their interaction on K_p in 2.5% (v/v) n -C₁₄₋₂₀-solid-aqueous dispersions at 1000rpm

This is also evident in the surface plot where only a slight decrease in K_p occurred with increase on solids addition (Figure 5.8). Maximum K_p of 0.0376s^{-1} was found at a solids particle size of $3\mu\text{m}$ and solids loading of $<2\text{g/L}$. Nevertheless, in a system by Mills *et al.* (1987), it has been suggested that solids loading promoted solids accumulation on the gas-liquid film hindering DO movement through the gas-liquid film to the membrane and solids particles acted as physical barriers to DO transfer through the gas-liquid interface both decreasing K_p . Mills *et al.* (1987) showed that a DO probe in a NaCl aqueous system containing 40wt% of $66\mu\text{m}$ soda lime beads had a probe response time of 25s which was 6s higher as compared to a NaCl aqueous system without solids. This suggests that the effect of solids loading becomes significant at higher levels, possibly at levels higher than would be expected in a bioprocess.

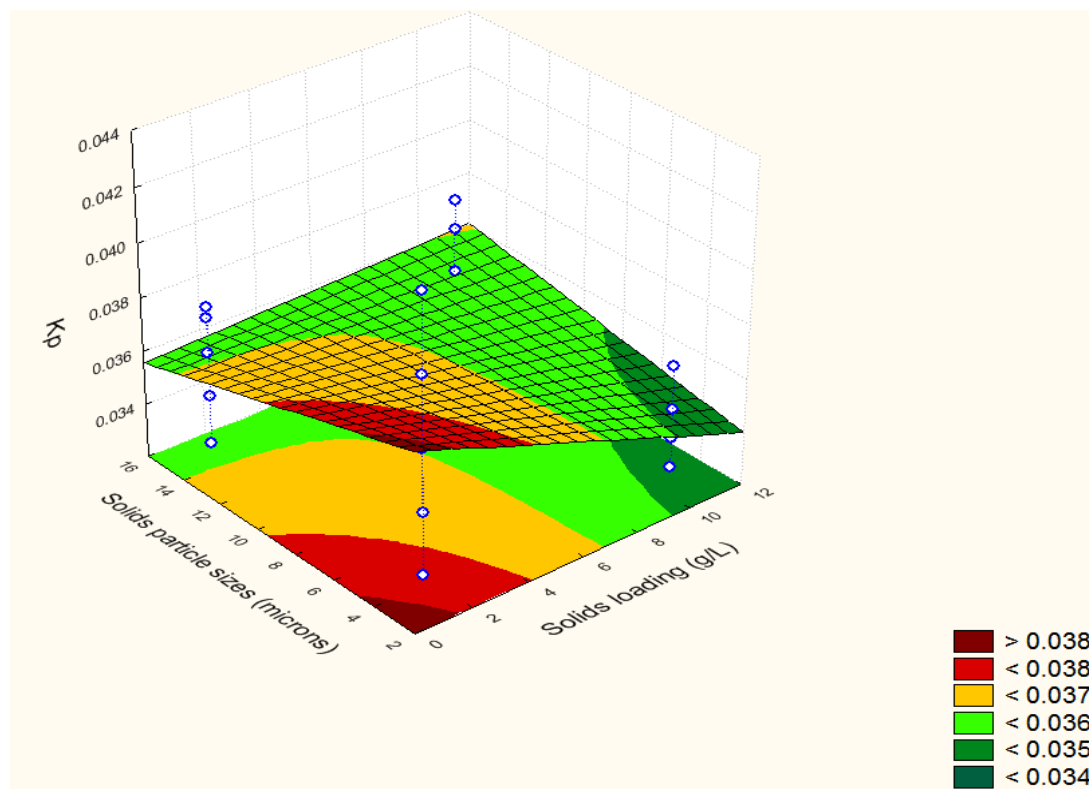


Figure 5.8 Surface response for effect of solids loading and particle size on K_p in 2.5% (v/v) n -C₁₄₋₂₀-solid-aqueous dispersions at 1000rpm

When considering the relative effects of the investigated parameters on K_p , it appears that K_p was predominantly influenced by the increase in the probe electrolyte age and probe membrane age, alkane concentration and alkane chain length which decreased K_p (Figure 5.1; Figure 5.3 and Figure 5.5).

5.1.2 Influence of the probe response lag time on the overall volumetric oxygen transfer coefficient

After an understanding of factors affecting K_p , K_La was determined using both the GOP (lag) second order response model and the GOP (no lag) first order response model in n -C₁₄₋₂₀-aqueous dispersions (see Tables A7.5-A7.7 for results) and n -C₁₀₋₁₃-aqueous dispersions (see Tables A7.8-A7.10 for results). Analysis of the results using a *t*-test whereby equal K_La means were assumed from the two methodologies to test for the differences (see Table A8.1 and Table A8.2 for analysis) showed that the GOP (lag) and the GOP (no lag) did not give the same K_La values under the same process conditions (Figure 5.9 and Figure 5.10). The discrepancy was mainly attributed to the effect of K_p . Overall average K_La values in n -C₁₄₋₂₀-aqueous dispersions were about 50% higher in the GOP (lag) whilst those in n -C₁₀₋₁₃-aqueous dispersions were about 40% higher compared to those from the GOP (no lag) for agitation rates of 600-1200rpm and alkane concentrations of 2.5-20% (v/v). Although

there did not appear to be a definite trend in the difference in $K_{L,a}$ values with changes in alkane concentration, the difference in these values appeared to be damped at the highest alkane concentration for both chain lengths. (Figure 5.11 and Figure 5.12).

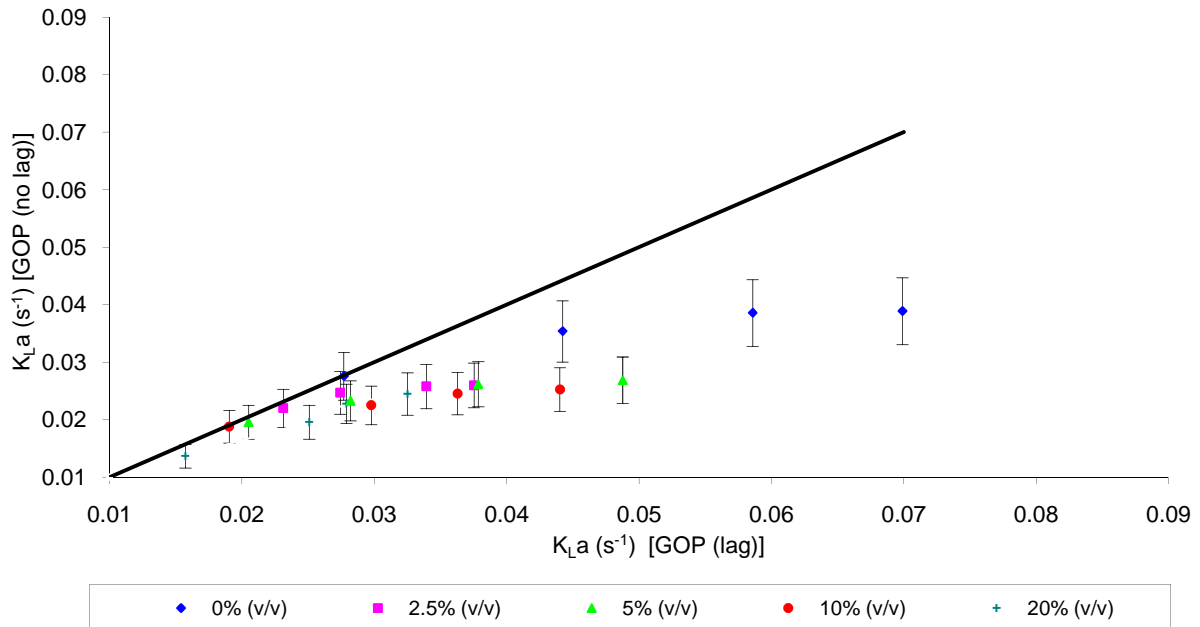


Figure 5.9 Comparison of $K_{L,a}$ results from GOP (no lag) and GOP (lag) in 0-20% (v/v) n -C₁₄₋₂₀-aqueous dispersions for agitation 600-1200rpm

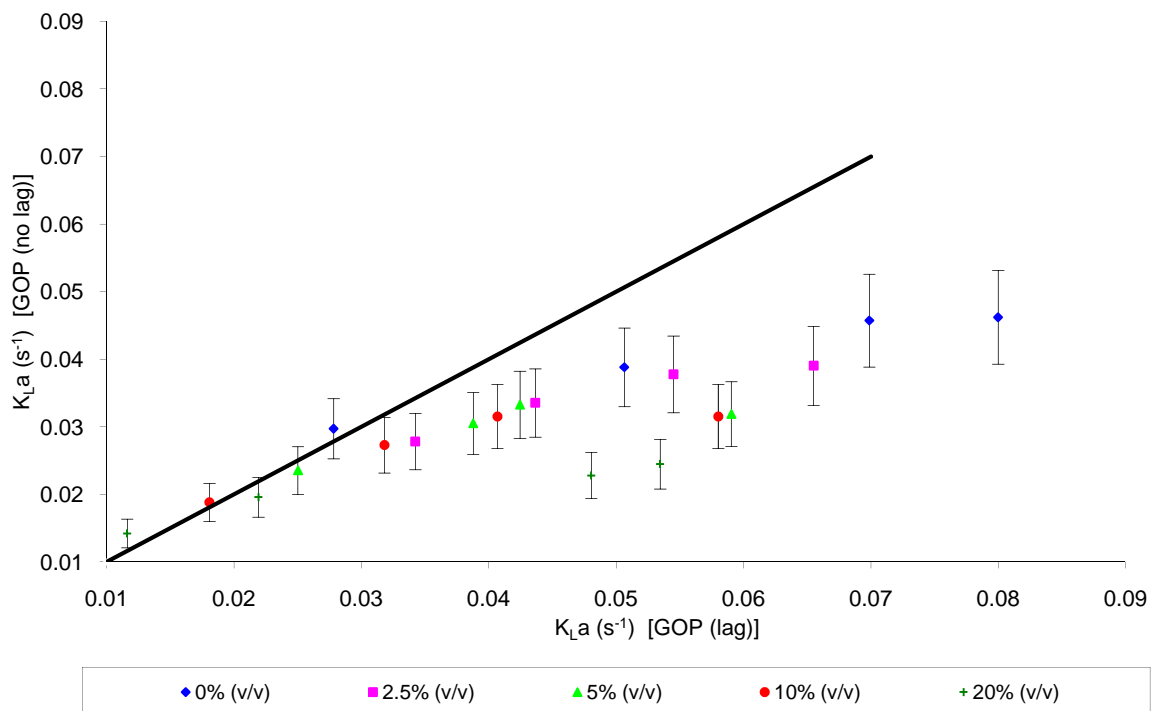


Figure 5.10 Comparison of $K_{L,a}$ results from GOP (no lag) and GOP (lag) in 0-20% (v/v) n -C₁₀₋₁₃-aqueous dispersions for agitation 600-1200rpm

However, as agitation rate increased, the difference between the K_{La} values in the GOP (no lag) and the GOP (lag) increased in both $n\text{-C}_{14-20}$ and $n\text{-C}_{10-13}$ -aqueous dispersions (Figure 5.11 and Figure 5.12). A *t*-test which is based on the analysis of variance quantified the effect of increasing K_{La} error in the GOP (no lag) due to K_p effects with increasing agitation rate as significant since the *F variance ratio* increased as agitation rate increased from 600rpm to 1200rpm (see Table A8.3 and Table A8.4 for analysis).

As agitation rate increased, from 600rpm to 1200rpm the difference for average K_{La} values between the GOP (no lag) and the GOP (lag) increased for all the alkane concentrations and alkane chain lengths, but, is more evident for agitation rates >800rpm (Figure 5.11 and Figure 5.12). In addition, the differences on K_{La} due to K_p effects was more than 1.7 times greater at 1200rpm as compared with 600rpm for all alkane concentrations and alkane chain lengths (see Table A8.3 and Table A8.4's *F variance ratio* at different agitations). Greatest deviations of 45% were observed at 1200rpm in 5% (v/v) $n\text{-C}_{14-20}$ -aqueous dispersions and 46% at 1200rpm and 10% (v/v) in $n\text{-C}_{10-13}$ -aqueous dispersions (Figure 5.11 and Figure 5.12). This is probably due to the fact that as agitation rate increased, K_{La} increased due to enhanced bubble breakage and turbulence on the gas-liquid interface thus promoting DO transfer. Under these conditions, the magnitude of K_{La} and K_p became almost equal i.e. $\tau_p \approx 1/K_p \approx 1/K_{La}$. Van't Riet (1979) and Ruchti *et al.* (1981) have suggested that K_p effects when $\tau_p \approx 1/K_{La}$ could not be neglected.

This result was similar to the work of Nielsen *et al.* (2003) who reported an increase of more than 25% in K_{La} values greater than 0.25s^{-1} if a DO probe response lag time of 11.2s in hexadecane organic phases. Interestingly they obtained the same K_{La} from the GOP (no lag) and the GOP (lag) at low agitations of 400rpm. Gourich *et al.* (2008) also measured K_{La} in propanol and water systems and after incorporating a DO probe response lag time of 7s, their K_{La} increased by more than 40% both in water and propanol at higher gas velocities of 0.087m/s but did not change at low gas velocities of 0.007m/s compared to K_{La} measured by the GOP (no lag).

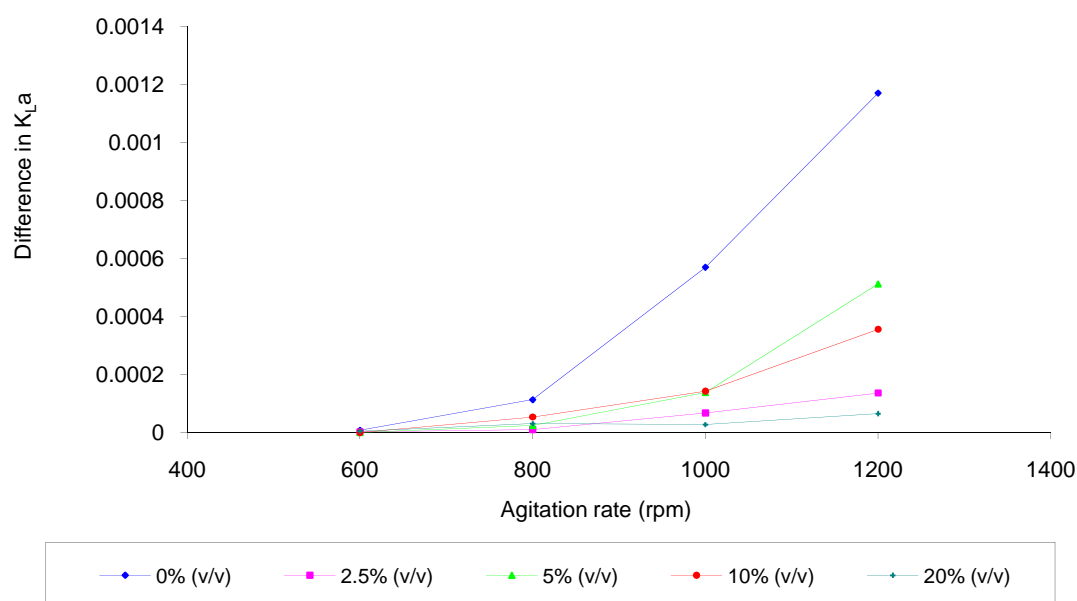


Figure 5.11 Difference in average K_{La} results from the GOP (no lag) and GOP (lag) in 0-20% (v/v) n -C₁₄₋₂₀-aqueous dispersions for agitation 600-1200rpm

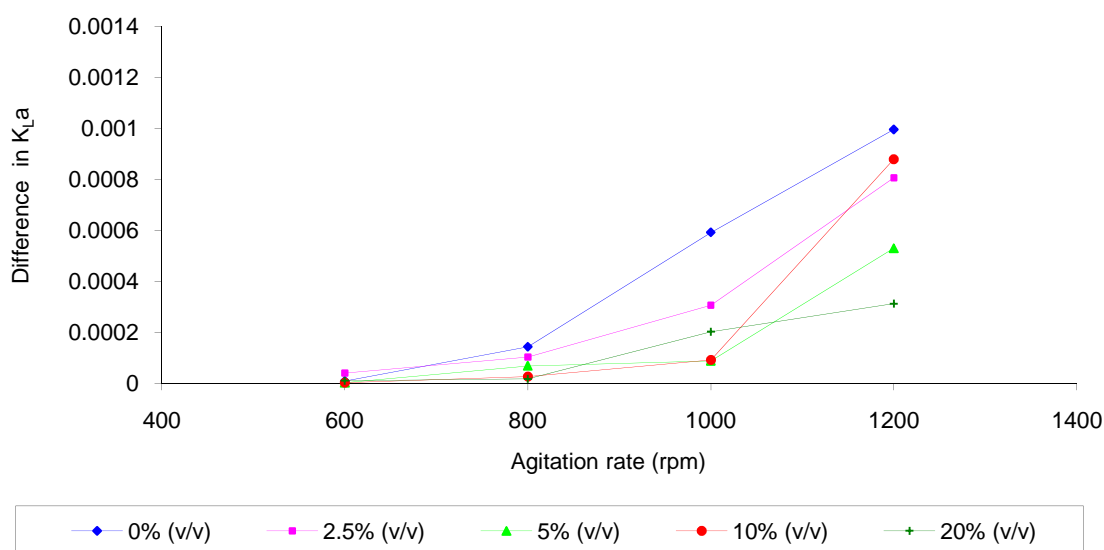


Figure 5.12 Difference in average K_{La} results from the GOP (no lag) and GOP (lag) in 0-20% (v/v) n -C₁₀₋₁₃-aqueous dispersions for agitation 600-1200rpm

K_{La} results for n -C₁₀₋₁₃-aqueous dispersions measured from the GOP (lag) second order response model in this work and those previously measured from the PSP by Correia and Clarke (2009) (see Table A7.11 for results) were compared. K_{La} results from the two methodologies showed no significant difference (Figure 5.13). A *t*-test analysis for the overall average K_{La} values from both the GOP (lag) and the PSP showed only a 1.6% difference which was insignificant (see Table A8.5 for analysis).

Correia and Clarke (2009) also reported the PSP to be superior over the GOP (no lag) as agitation rate increased for all alkane concentrations and a 49% underestimation was observed in 5% (v/v) and 1200rpm (see Figure 2.4). This was mainly attributed to increase in K_p effects on K_{La} as agitation rate and alkane concentration increased resulting in erroneous K_{La} values. This agrees with the trends found in both $n\text{-C}_{14-20}$ -aqueous dispersions with a deviation of 45% at 1200rpm in 5% (v/v) and 46% in $n\text{-C}_{10-13}$ -aqueous dispersions at 1200rpm in 10% (v/v) for this work (Figure 5.11 and Figure 5.12).

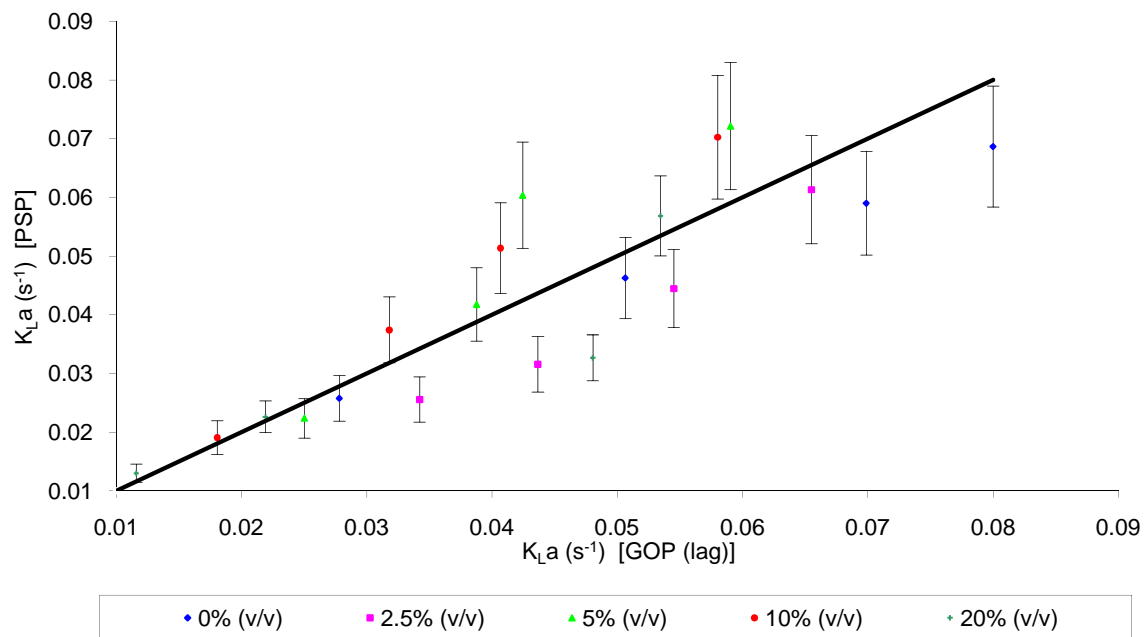


Figure 5.13 Comparison of K_{La} results from the PSP by Correia and Clarke (2009) and GOP (lag) in 0-20% (v/v) $n\text{-C}_{10-13}$ -aqueous dispersions for agitation 600-1200rpm

The GOP (lag) second order response model was therefore, chosen as the accurate K_{La} measurement method in alkane solid-aqueous dispersions over the PSP due to its relative simplicity.

5.2 Quantification of the behavior of the overall volumetric oxygen transfer coefficient in aerated agitated alkane-solid-aqueous dispersions

K_{La} behavior was quantified in aerated agitated alkane-solid-aqueous dispersions using the GOP (lag) second order response model methodology. The effect of agitation rate and the impact of alterations in fluid properties due to changes in solids loading, solids particle sizes, alkane concentration and their interactions on K_{La} , μ and σ were quantified in both alkane-inert solid-aqueous dispersions and alkane-yeast-aqueous dispersions.

5.2.1 Alkane-aqueous dispersions with inert solids

K_{La} behavior was quantified at discrete agitation rates (600-1200rpm), alkane concentrations (2.5-20% (v/v)), inert solids loadings (1-10g/L), solids particle sizes (3-14 μ m) and their interactions in *n*-C₁₄₋₂₀-inert solid-aqueous dispersions (see Table A7.13 and Table A7.14 for results). According to the statistical analysis K_{La} was significantly enhanced by increasing agitation rate by an effect of 19.8 and the interaction between increasing alkane concentration and solids loading by an effect of 4.15 (Figure 5.14). Contrarily increase in alkane concentration significantly decreased K_{La} with an effect of -13.6, increase in solids particle size decreased K_{La} with an effect of -3.33 and also the interaction between increasing agitation rate and solids particle size with an effect of -3.54 (Figure 5.14).

The fluid viscosity was also measured in *n*-C₁₄₋₂₀-inert solid-aqueous dispersions for the same process conditions in which K_{La} was determined to understand K_{La} behavior in terms of fluid properties. The magnitude of the effects and their interactive effects were quantified (see Table A7.15 for results). According to the statistical analysis the fluid viscosity significantly increased with increase in alkane concentration with an effect of 6.12 and solids loading with an effect of 4.37 (Figure 5.15). Contrarily, the fluid viscosity decreased with increase in solids particle size with an effect of -8.24, the interaction between increasing alkane concentration and solids particle size with an effect of -7.55 and the interaction between increasing solids loading and solids particle size with an effect of -3.85 (Figure 5.15).

The fluid surface tension was also measured in *n*-C₁₄₋₂₀-inert solid-aqueous dispersions for the same process conditions at which K_{La} was determined and the size of the effects and their interactive effects were quantified (see Table A7.16 for results). According to the statistical analysis the fluid surface tension significantly

increased with increase in solids loading with an effect of 7.05 (Figure 5.16). Contrarily, increase in solids particle size decreased the fluid surface tension with an effect of -5.50 and the interaction between increasing alkane concentration and solids particle size with an effect of -9.85 (Figure 5.16).

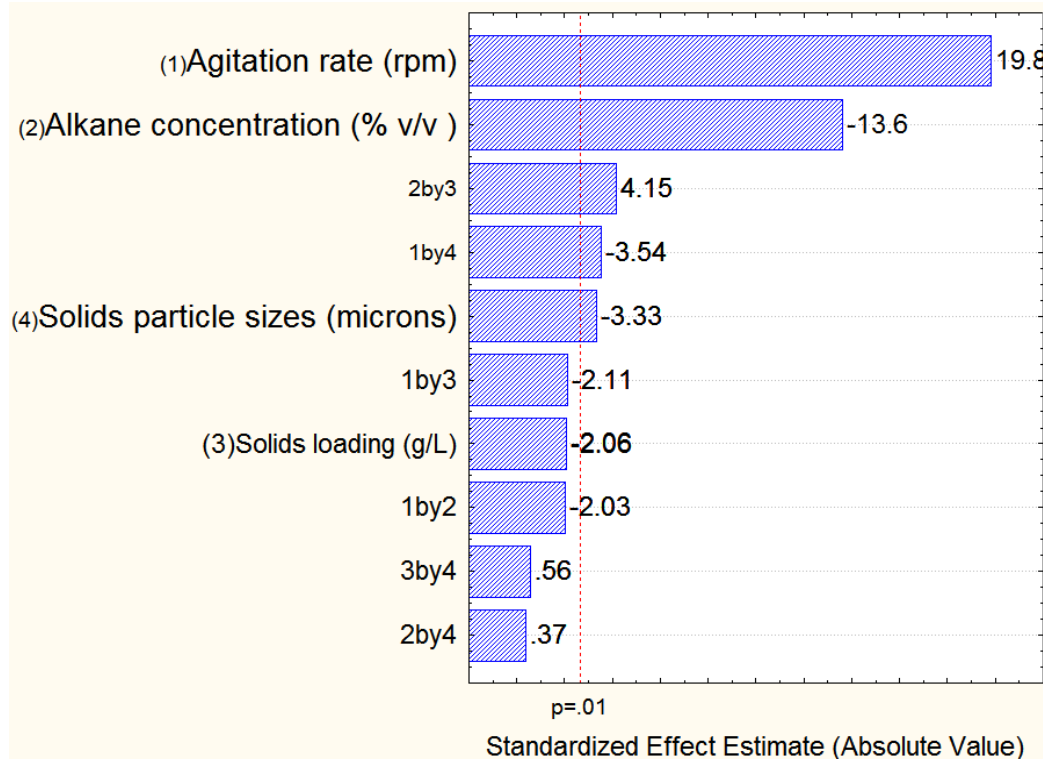


Figure 5.14 Pareto chart for effect of agitation, alkane concentration, inert solids loading, particle size and their interactions on K_La

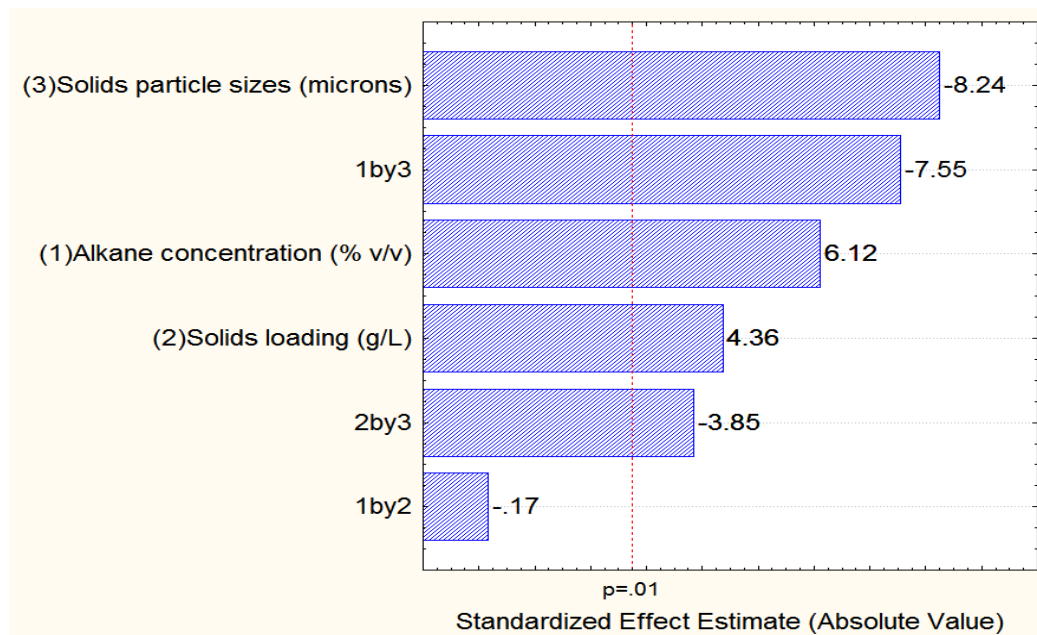


Figure 5.15 Pareto chart for effect of alkane concentration, inert solids loading, particle size and their interactions on fluid viscosity

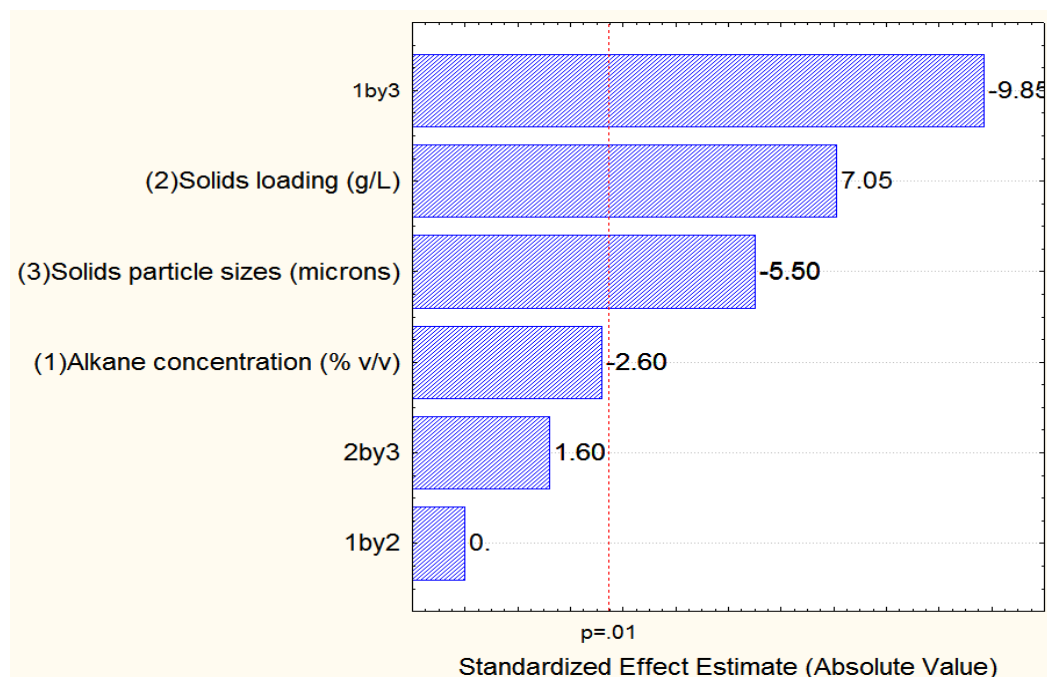


Figure 5.16 Pareto chart for effect of alkane concentration, inert solids loading, particle size and their interactions on fluid surface tension

The effects of the parameters as well as their interactions on $K_{L,a}$ in n -C₁₄₋₂₀-inert solid-aqueous dispersions are discussed in the following sections 5.2.1.1 - 5.2.1.10. The surface response curves in these sections were generated for two varying parameters whilst the other two parameters were assumed constant at median conditions i.e. agitation of 950rpm, alkane concentration of 11.25% (v/v), solids loading of 5.5g/L and solids particle size of 9 μ m.

5.2.1.1 Effect of agitation rate

Increasing agitation rate from 600rpm to 1200rpm significantly enhanced $K_{L,a}$ in n -C₁₄₋₂₀-inert solid-aqueous dispersions (Figure 5.14). Due to the influence of agitation rate, $K_{L,a}$ increased from 0.0275s⁻¹ to 0.060s⁻¹ in 2.5% (v/v) alkane (Figure 5.17) and increased from 0.025s⁻¹ to 0.050s⁻¹ at a solids loading of 1g/L (Figure 5.18) and solids particle size of 3 μ m (Figure 5.19) over the same agitation range. Increases in agitation rate have also been reported to enhance $K_{L,a}$ in hydrocarbon-aqueous dispersions and aqueous systems with solids suspended by several authors (Bartos and Satterfield, 1986; Ju and Sundararajan, 1994, Ozbek and Gayik, 2001; Clarke *et al.*, 2006; Correia and Clarke, 2009).

Increased agitation rate promotes DO bubble breakage resulting in higher gas-liquid interfacial area per unit volume due to reduction in D_{32} and increased ϵ_G (Yoshida and Miura, 1963; van Dierenlonck *et al.*, 1968; Hassan and Robinson, 1977b; Parthasarathy and Ahmed, 1994; Correia *et al.*, 2010). Increased agitation also

caused a reduction in the gas-liquid boundary thickness due to the increased turbulent effects resulting in a higher K_L (Alves *et al.*, 2004). This combined effect caused the higher K_{La} values resulting in increased agitation rate being a major K_{La} enhancement factor.

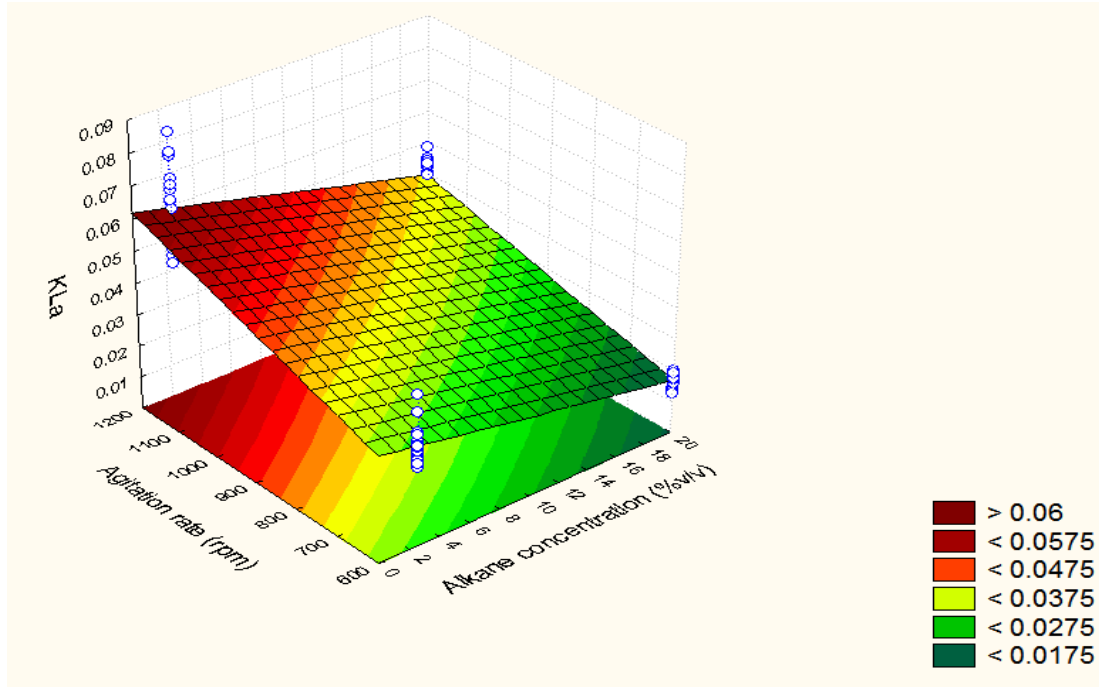


Figure 5.17 Surface response for effect of agitation and alkane concentration on K_{La} at constant inert solids loading of 5.5g/L and particle size of 9 μ m

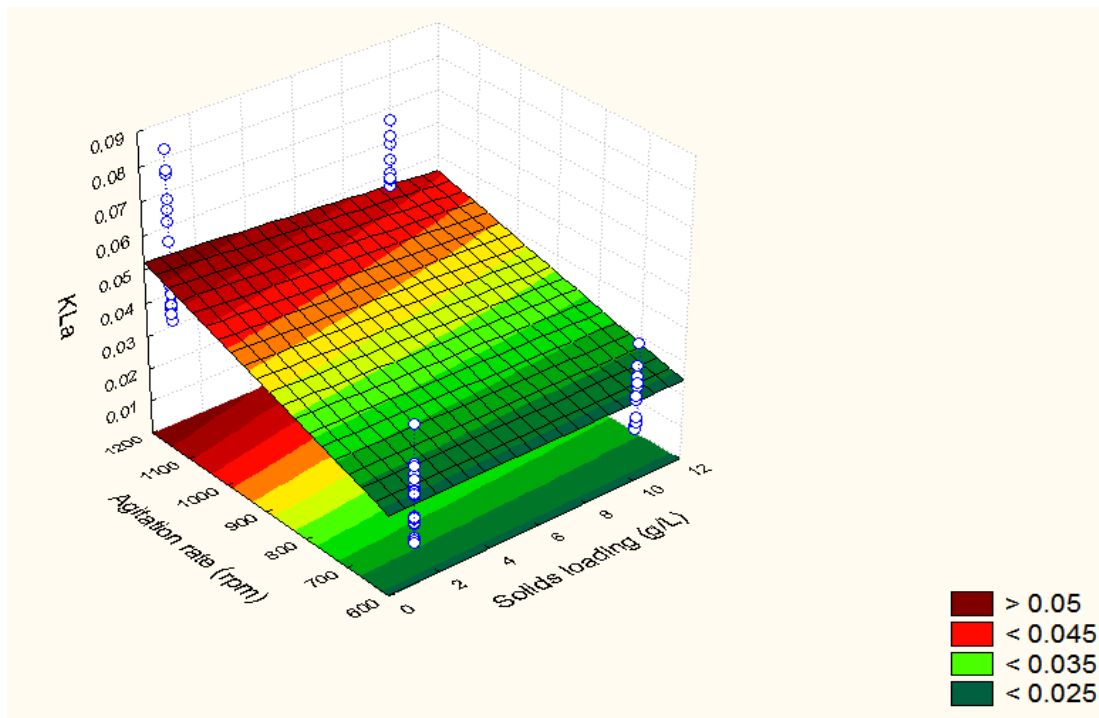


Figure 5.18 Surface response for effect of agitation and inert solids loading on K_{La} at constant 11.25% (v/v) n -C₁₄₋₂₀ alkane and particle size of 9 μ m

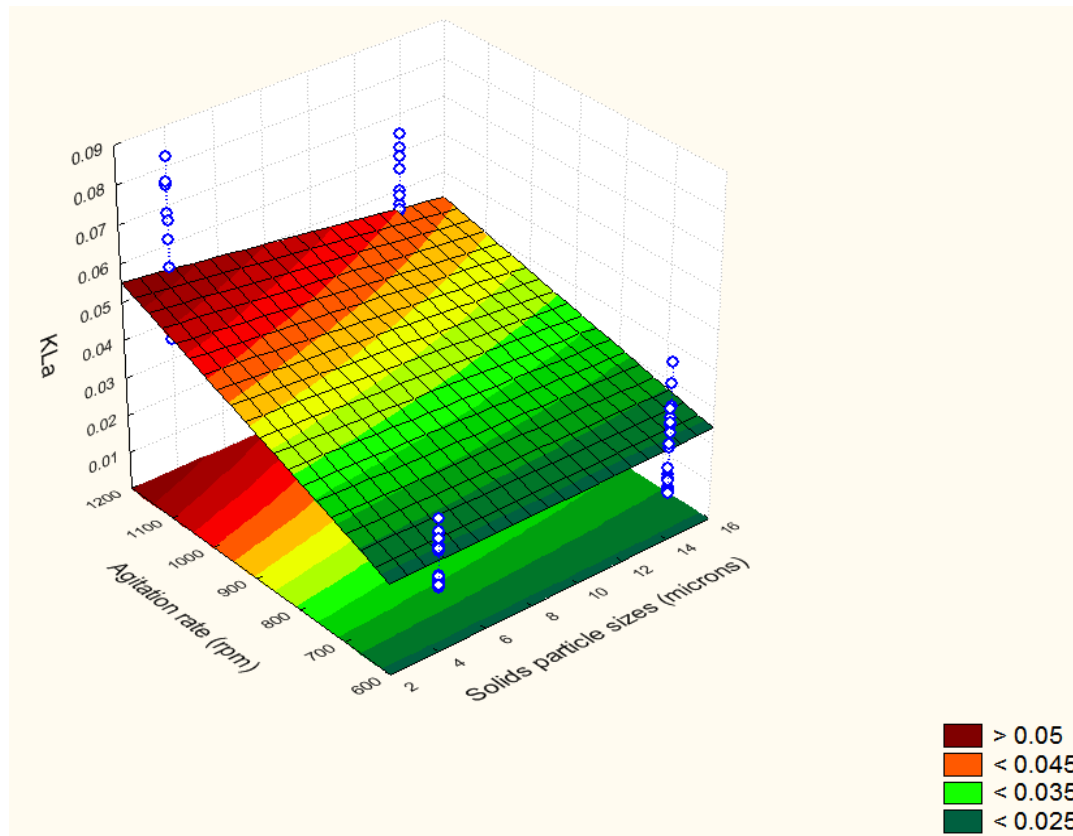


Figure 5.19 Surface response for effect of agitation and particle size on K_{La} at constant 11.25% (v/v) n -C₁₄₋₂₀ alkane and inert solids loading of 5.5g/L

5.2.1.2 Effect of alkane concentration

Increase in alkane concentration from 2.5% (v/v) to 20% (v/v) significantly decreased K_{La} in n -C₁₄₋₂₀-inert solid-aqueous dispersions (Figure 5.14). K_{La} decreased from 0.0275s^{-1} to 0.0175s^{-1} at an agitation of 600rpm (Figure 5.17); decreased from 0.050s^{-1} to 0.0275s^{-1} at a solids loading of 1g/L (Figure 5.20) and decreased from 0.050s^{-1} to 0.0475s^{-1} at solids particle size of $3\mu\text{m}$ (Figure 5.21) over the same alkane concentration range. This is more evident at concentrations $>15\%$ (v/v) due to increase in fluid viscosity with increase in alkane concentration (Figure 5.15) from $1.075\text{mPa}\cdot\text{s}$ to $1.20\text{mPa}\cdot\text{s}$ at a solids loading of 1g/L (Figure 5.22) and increase from $1.15\text{mPa}\cdot\text{s}$ to $1.40\text{mPa}\cdot\text{s}$ at solids particle size of $3\mu\text{m}$ (Figure 5.23). This counteracted the insignificant decrease in fluid surface tension due to increase in alkane concentration from 65mN/m to 63mN/m at a solids loading of 1g/L (Figure 5.16 and Figure 5.24). This overall increase in fluid viscosity promoted bubble coalescence, lowering the gas-liquid interfacial area per unit volume through increased D_{32} and lowered ε_G as indicated by several authors in literature (Schumpe and Deckwer, 1982; Das *et al.*, 1985; Khare and Joshi, 1990; O'Connor *et al.*, 1990;

Schafer *et al.*, 2002; Garcia-Ochoa and Gomez, 2004; Kilonzo and Margaritis, 2004; Hu *et al.*, 2005; Mehria *et al.*, 2005).

The overall increase in fluid viscosity also resulted in lowered DO transport through the gas-liquid film resulting in lower K_L values due to decreased DO diffusivity (Calderbank and Moo-Yang, 1961; Juretzek *et al.*, 2000; Elgozalia *et al.*, 2002; Garcia-Ochoa and Gomez, 2005). This is in agreement to the work of Correia *et al.* (2010) who reported a doubled increase in fluid viscosity over fluid surface tension with increase in alkane concentration in 2.5-20% (v/v) n -C₁₀₋₁₃-aqueous dispersions resulting in K_{La} decrease.

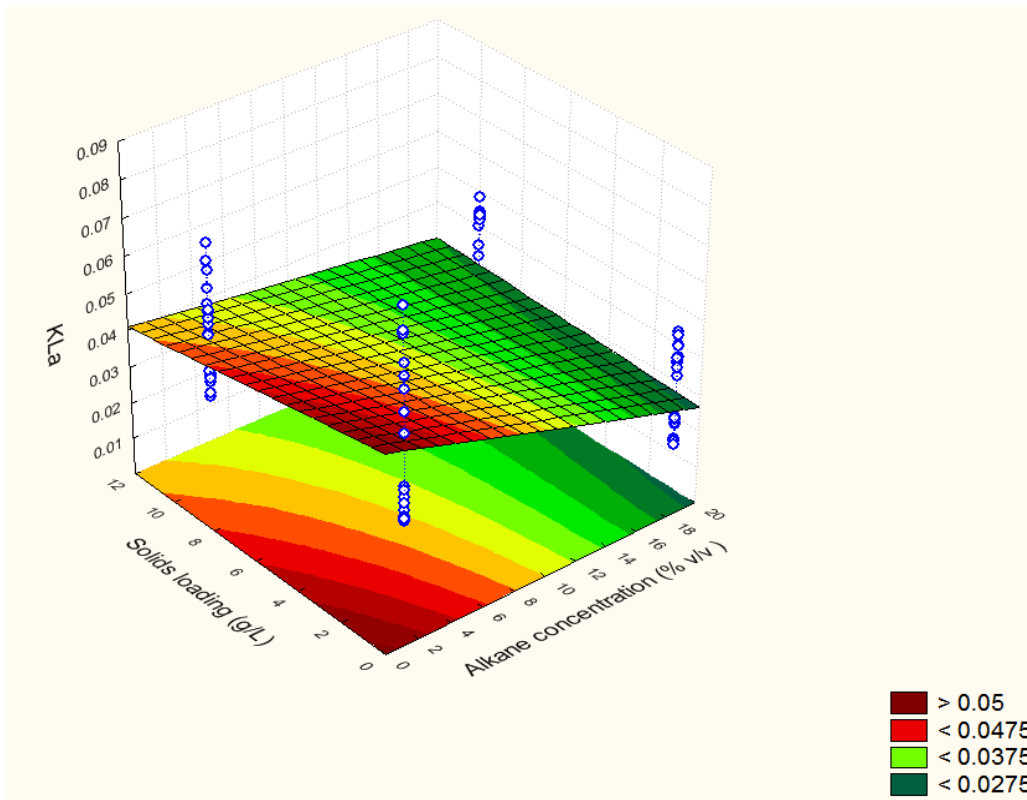


Figure 5.20 Surface response for effect of alkane concentration and inert solids loading on K_{La} at constant agitation of 900rpm and particle size of $9\mu\text{m}$

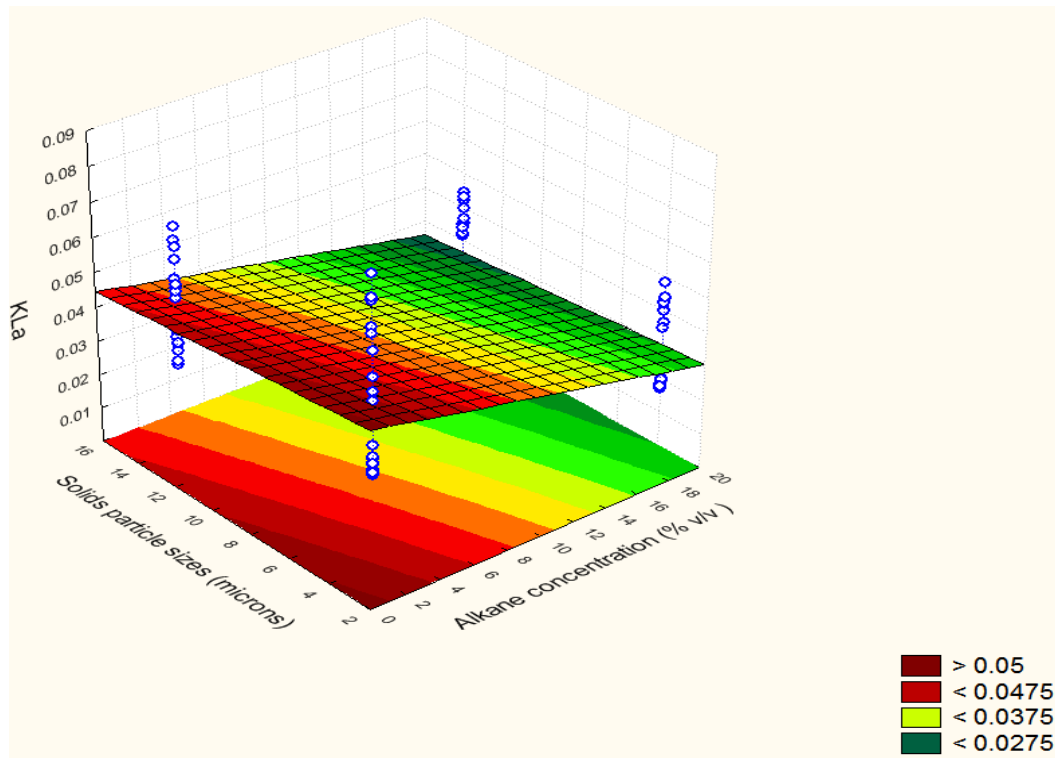


Figure 5.21 Surface response for effect of alkane concentration and particle size on $K_L a$ at constant agitation of 900rpm and inert solids loading of 5.5g/L

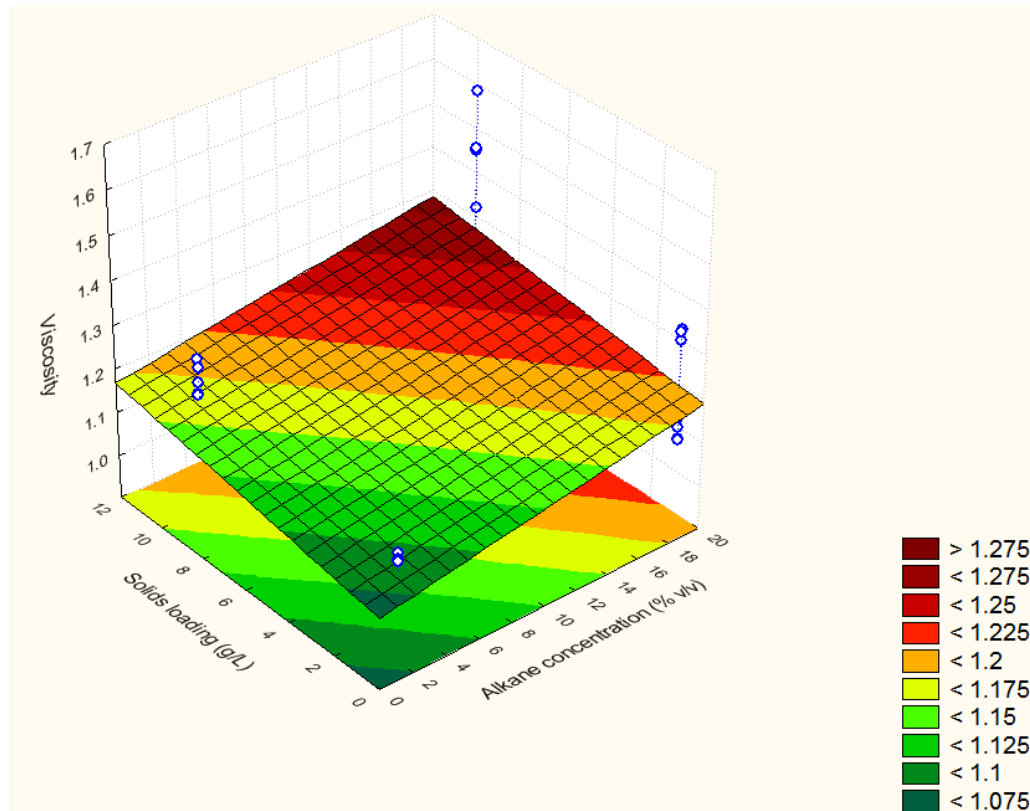


Figure 5.22 Surface response for effect of alkane concentration and inert solids loading on fluid viscosity at constant particle size of 9 μ m

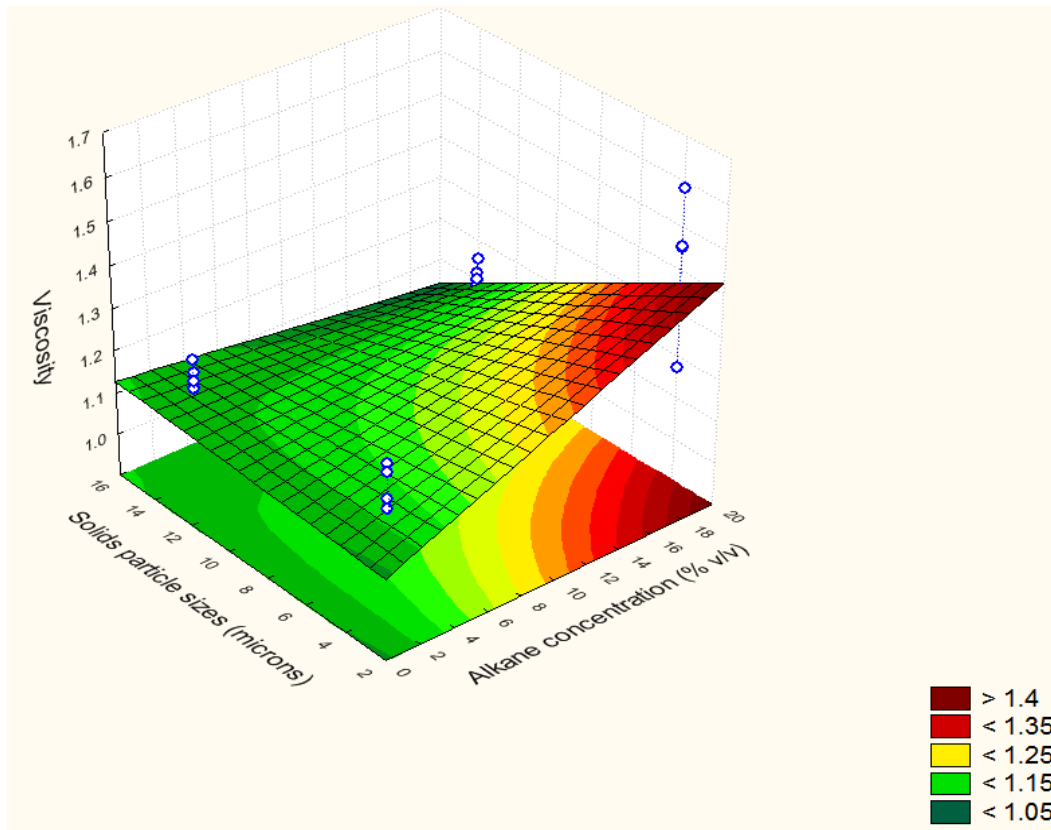


Figure 5.23 Surface response for effect of alkane concentration and particle size on fluid viscosity at constant solids loading of 5.5g/L

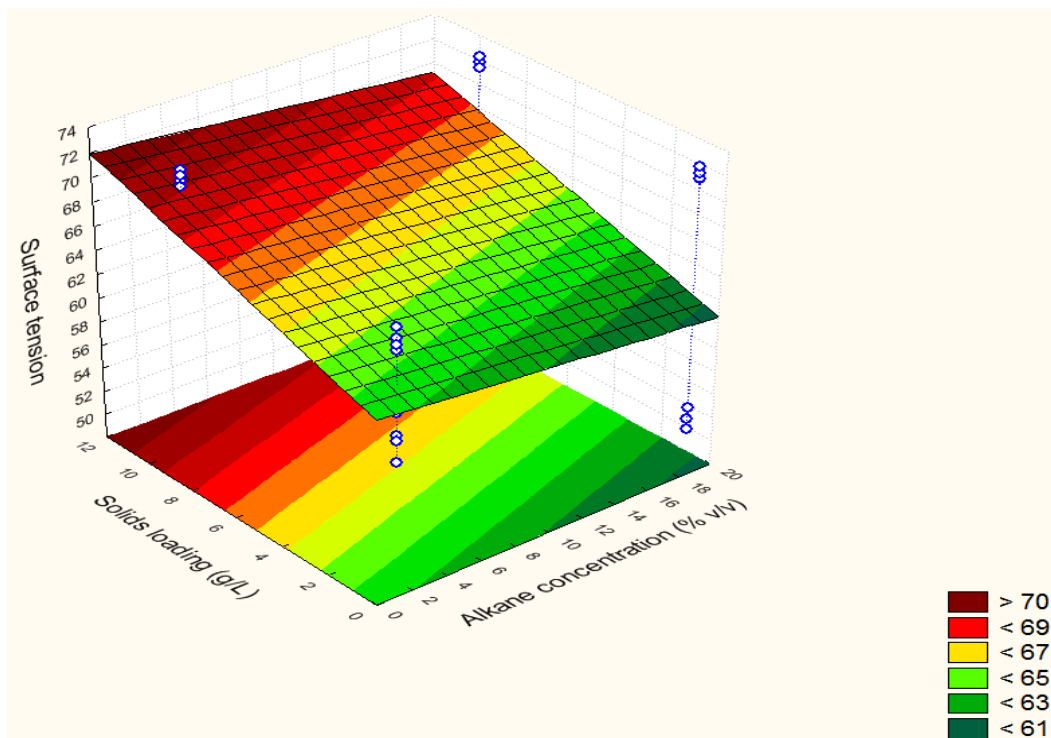


Figure 5.24 Surface response for effect of alkane concentration and inert solids loading on fluid surface tension at constant particle size of 9µm

5.2.1.3 Effect of solids loading

Increase in solids loading from 1g/L to 10g/L decreased K_{La} in $n\text{-C}_{14-20}$ -inert solid-aqueous dispersions but the effect was insignificant (Figure 5.14). K_{La} decreased up to 0.0250s^{-1} at an agitation of 600rpm (Figure 5.18); decreased from 0.050s^{-1} to 0.0375s^{-1} in 2.5% (v/v) $n\text{-C}_{14-20}$ alkane (Figure 5.20) and decreased from 0.050s^{-1} to 0.0375s^{-1} at a particle size of $3\mu\text{m}$ (Figure 5.25) over the same solids loading range. Decreases in K_{La} with increase in solids loading have been widely reported in literature by several authors although the decrease has never been confirmed statistically (Bartoes and Satterfield, 1986; Mills *et al.*, 1987; Chisti and Moo-Yang, 1988; Ju and Sundararajan, 1994; Hwang and Lu, 1997; Kawase *et al.*, 1997; Ozbek and Gayik, 2001; Benchapattarapong *et al.*, 2005; Mena *et al.*, 2005).

A lowering of K_{La} on increased solids loading has been suggested to result due to enhanced coalescence since solids loading increased fluid viscosity. This lowered gas hold up and increasing D_{32} resulting in decreased gas-liquid interfacial area per unit volume (Lee *et al.*, 1982; Gollakotta and Guin, 1984; Fukuma *et al.*, 1987; Mills *et al.*, 1987; Chisti and Moo-Yang, 1988; Sun and Furusaki, 1988; O'Connor *et al.*, 1990; Zahradnik *et al.*, 1992; Yagi and Yoshida, 1994; Van Weert *et al.*, 1999; Krishna *et al.*, 1997; Reese *et al.*, 1996; Nicolella *et al.*, 1998; Freitas and Teixeira, 2001). Solids loading also resulted in blockage of the gas-liquid interface decreasing DO diffusivity and also increased coalescence in the dispersion, both factors effectively lowering K_L (Chisti and Moo-Yang, 1988).

In this work, both fluid viscosity and fluid surface tension increased upon solids addition (Figure 5.15 and Figure 5.16). The fluid viscosity increased from $1.075\text{mPa}\cdot\text{s}$ to $1.175\text{mPa}\cdot\text{s}$ in 2.5% (v/v) $n\text{-C}_{14-20}$ alkane (Figure 5.22) and also from $1.175\text{mPa}\cdot\text{s}$ to $1.40\text{mPa}\cdot\text{s}$ for a particle size of $3\mu\text{m}$ (Figure 5.26). Likewise the fluid surface tension increased from 65mN/m to 70mN/m in 2.5% (v/v) $n\text{-C}_{14-20}$ alkane (Figure 5.24) and also from 67mN/m to 72mN/m for a particle size of $3\mu\text{m}$ (Figure 5.27). This promoted coalescence effects in the dispersion. Albal *et al.* (1983) also reported a fluid viscosity increase upon increased solids loading in glass beads and oil shale particles aqueous systems which resulted in overall decrease of K_{La} .

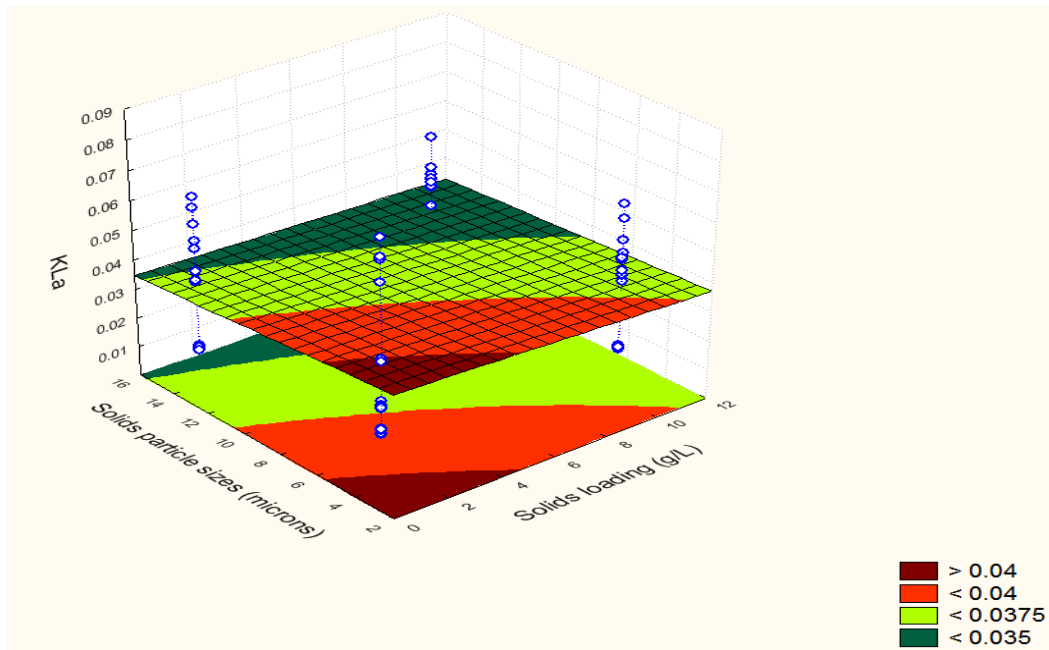


Figure 5.25 Surface response for effect of inert solids loading and particle size on K_{La} at constant agitation of 900rpm and 11.25% (v/v) n -C₁₄₋₂₀ alkane

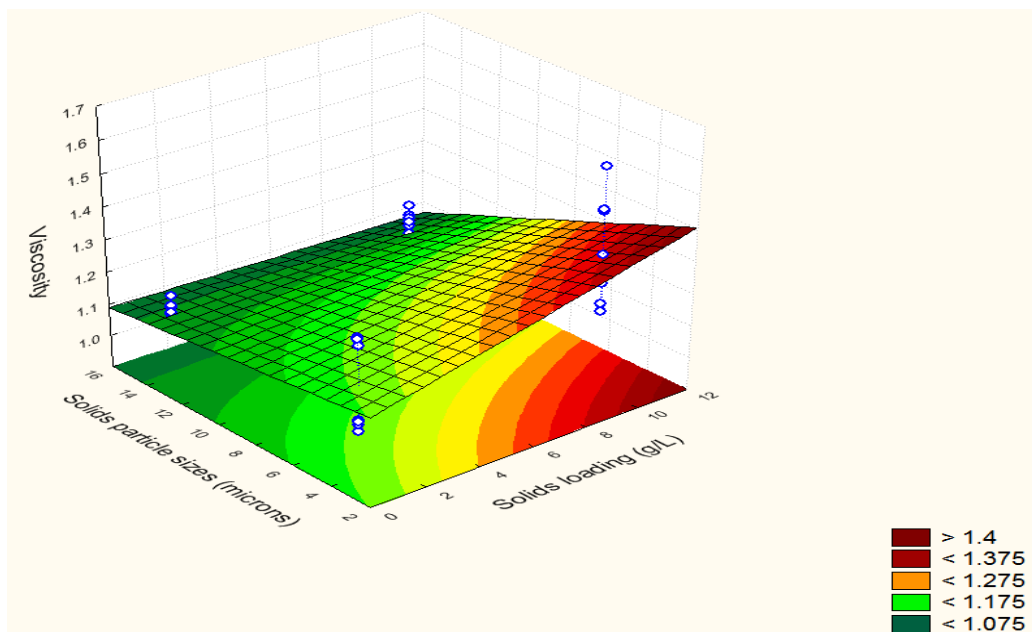


Figure 5.26 Surface response for effect of inert solids loading and particle size on fluid viscosity at constant 11.25% (v/v) n -C₁₄₋₂₀ alkane

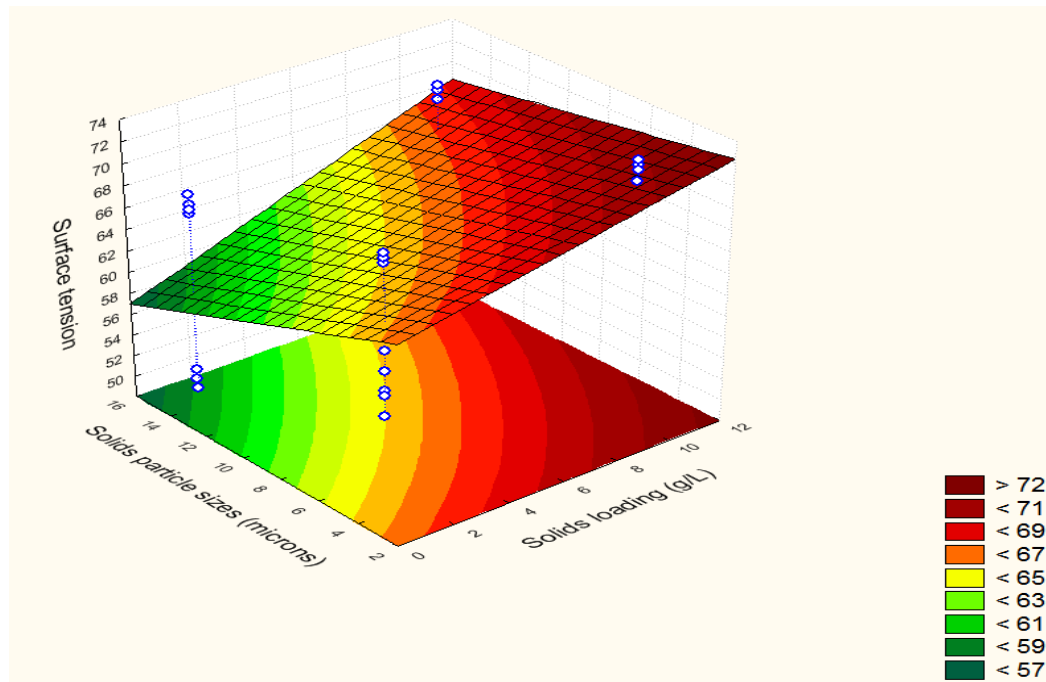


Figure 5.27 Surface response for effect of inert solids loading and particle size on fluid surface tension at constant 11.25% (v/v) n -C₁₄₋₂₀ alkane

5.2.1.4 Effect of solids particle size

$K_L a$ significantly decreased with increase in solids particle size from 3 μ m to 14 μ m in n -C₁₄₋₂₀-inert solid-aqueous dispersions (Figure 5.14). $K_L a$ was less than 0.0250s⁻¹ at an agitation of 600rpm (Figure 5.19), from 0.0500s⁻¹ to 0.0475s⁻¹ in 2.5% (v/v) n -C₁₄₋₂₀ alkane (Figure 5.21) and from 0.0400s⁻¹ to 0.0350s⁻¹ at a solids loading of 1g/L (Figure 5.25) over the same solids particle size range. Large solid particles caused a reduction in gas-liquid interfacial area per unit volume due to the attachment of solid particles on the gas bubble resulting in larger D_{32} and decreased gas hold-up (Miyachi *et al.*, 1981; Sada *et al.*, 1986). Due to this $K_L a$ decreased with increase in solids particle sizes despite the decrease in both fluid viscosity (Figure 5.15; Figure 5.23 and Figure 5.26) and fluid surface tension (Figure 5.16 and Figure 5.27) with increase in solids particle sizes. The same behavior was reported by Nicoletta *et al.* (1998) in aqueous systems with 2.2wt% of 0.34mm basalt particles and 12wt% of 1.95mm biofilm particles. Their ϵ_G decreased with increase in both solids loading and solids particle size and they attributed this to decrease in the number of bubbles present in the system resulting in an overall decreased $K_L a$.

5.2.1.5 Effect of interaction between agitation rate and alkane concentration

The interactive effect between increasing both agitation rate from 600rpm to 1200rpm and alkane concentration from 2.5% (v/v) to 20% (v/v) in n -C₁₄₋₂₀-inert solid-aqueous dispersions was insignificant on $K_L a$ (Figure 5.14). This was because of the viscous

nature of the alkane (Figure 5.15). This reduced the turbulent effect exerted by increase in agitation rate, resulting in both lower gas-liquid interfacial area per unit volume and K_L (Calderbank, 1958; Khare and Joshi, 1990; O'Connor *et al.*, 1990; Schafer *et al.*, 2002). Since the influence of fluid surface tension was negligible in this range, only the effects of turbulence and fluid viscosity were considered.

5.2.1.6 Effect of interaction between agitation rate and solids loading

The interactive effect between increasing agitation rate from 600rpm to 1200rpm and solids loading from 1g/L to 10g/L insignificantly depressed K_La in *n*-C₁₄₋₂₀-inert solid-aqueous dispersions (Figure 5.14). This is possibly because as solids loading increased, the turbulent effects in the fluid were reduced due to the significant increase in both fluid viscosity and fluid surface tension (Figure 5.15 and Figure 5.16). This counteracted the effect of the agitation rate by lowering both gas-liquid interfacial area per unit volume and K_L .

5.2.1.7 Effect of interaction between agitation rate and solids particles size

The interactive effect between increasing agitation rate from 600rpm to 1200rpm and solids particle size from 3 μ m to 14 μ m significantly depressed K_La in the *n*-C₁₄₋₂₀-inert solid-aqueous dispersions (Figure 5.14). This was possibly because of the tendency of the solid particles to attach on the gas-liquid interface as well as on the oxygen bubble especially the large solid particle sizes. This effectively reduced both K_L and the gas-liquid interfacial area per unit volume. This effect counteracted the turbulent effect of the agitation rate, despite a significant decrease in both the fluid viscosity (Figure 5.15) and fluid surface tension (Figure 5.16) on increasing particle size.

5.2.1.8 Effect of interaction between alkane concentration and solids loading

The interactive effect between increase in alkane concentration from 2.5% (v/v) to 20% (v/v) and increase in inert solids loading from 1g/L to 10g/L significantly enhanced K_La in *n*-C₁₄₋₂₀-inert solid-aqueous dispersions (Figure 5.14). This can be explained by a tendency of DO bubble breakage formed by the viscous alkane for concentration of >15% (v/v) by continual solids loading. This was supported by the decrease in both fluid viscosity and surface tension enhancing bubble breakage in the system (Figure 5.15 and Figure 5.16). An alkane-water bubble was found to have a size of 43.97 μ m in 20% (v/v) with 1g/L of CaCO₃ but when 10g/L were introduced, the alkane-water-CaCO₃ bubble was reduced to a size of 39.39 μ m supporting the bubble break up hence enhanced K_La .

5.2.1.9 Effect of interaction between alkane concentration and solids particle size

The interactive effect between increase in alkane concentration from 2.5% (v/v) to 20% (v/v) and solids particle size from 3 μ m to 14 μ m insignificantly enhanced $K_{L}a$ (Figure 5.14). This was possibly due to their interactive effect which caused a significant decrease in both fluid viscosity (Figure 5.15) and fluid surface tension (Figure 5.16). This reduced the dispersion coalescing properties therefore increasing both the gas-liquid interfacial area per unit volume and K_L though in overall it does not enhance $K_{L}a$.

5.2.1.10 Effect of interaction between solids loading and solids particle size

The interactive effect between increase in solids loading from 1g/L to 10g/L and increase in solids particle size from 3 μ m to 14 μ m insignificantly enhanced $K_{L}a$. This is possibly because their interactive effect significantly decreased the fluid viscosity with an effect almost double that of the insignificant increase in fluid surface tension in the *n*-C₁₄₋₂₀-inert solid-aqueous dispersions (Figure 5.14, Figure 5.15 and Figure 5.16).

5.2.2 Alkane-aqueous dispersions with inactive yeast cells

Further work was done under narrowed process conditions to underpin $K_{L}a$ behavior in typical bioprocess conditions with 5 μ m yeast cells as solids (see Table A7.17 and Table A7.18 for results). In the *n*-C₁₄₋₂₀-yeast-aqueous dispersions agitation rate (600-900rpm), alkane concentration (2.5-11.25% (v/v)) and yeast loading (1-5.5g/L) were employed. According to the statistical analysis $K_{L}a$ was enhanced by increase in agitation rate by an effect of 10.78 whilst increasing yeast loading had an almost equal opposing effect on $K_{L}a$ (Figure 5.28). Also the interaction between increasing alkane concentration and yeast loading decreased $K_{L}a$ with an effect of -7.73 (Figure 5.28).

The fluid viscosity was also measured in *n*-C₁₄₋₂₀-yeast-aqueous dispersions (see Table A7.19 for results) to underpin $K_{L}a$ behavior due to alterations in fluid properties. According to the statistical analysis increase in both alkane concentration and yeast loading significantly increased the fluid viscosity with almost equal effects (Figure 5.29).

The fluid surface tension was also measured in *n*-C₁₄₋₂₀-yeast-aqueous dispersions (see Table A7.20 for results) and according to the statistical analysis only increase in

yeast loading significantly increased the fluid surface tension with an effect of 5.71 (Figure 5.30).

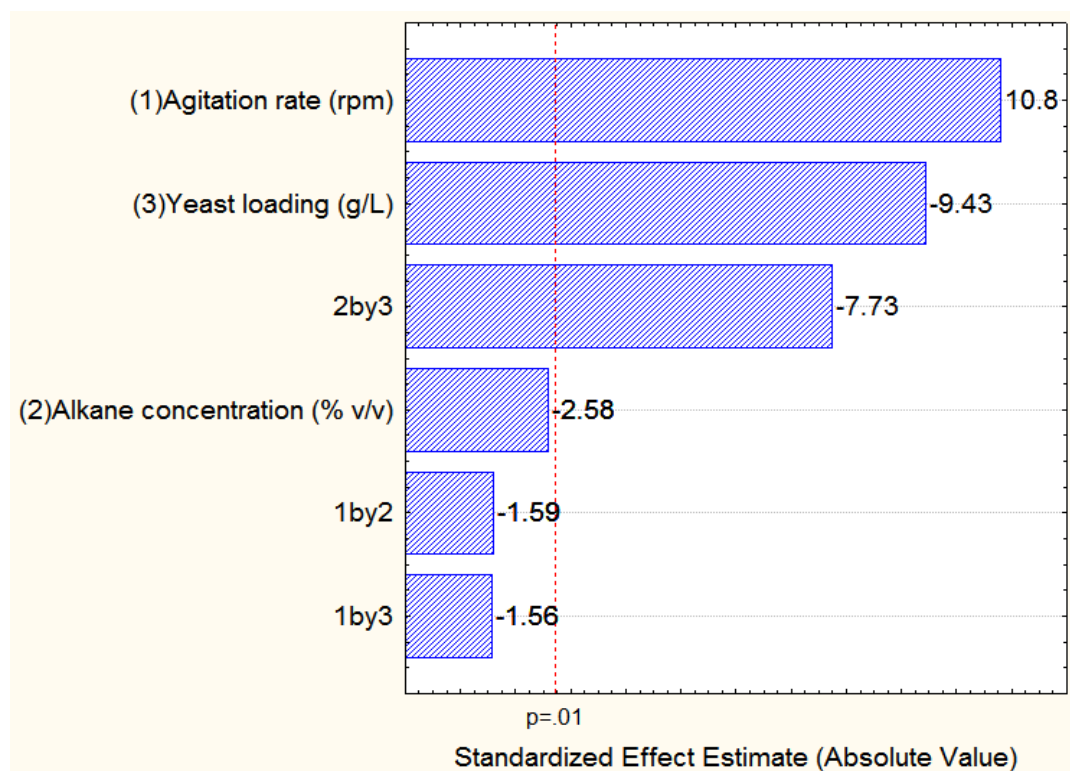


Figure 5.28 Pareto chart for effect of agitation, alkane concentration, yeast loading and their interactions on $K_{L,a}$

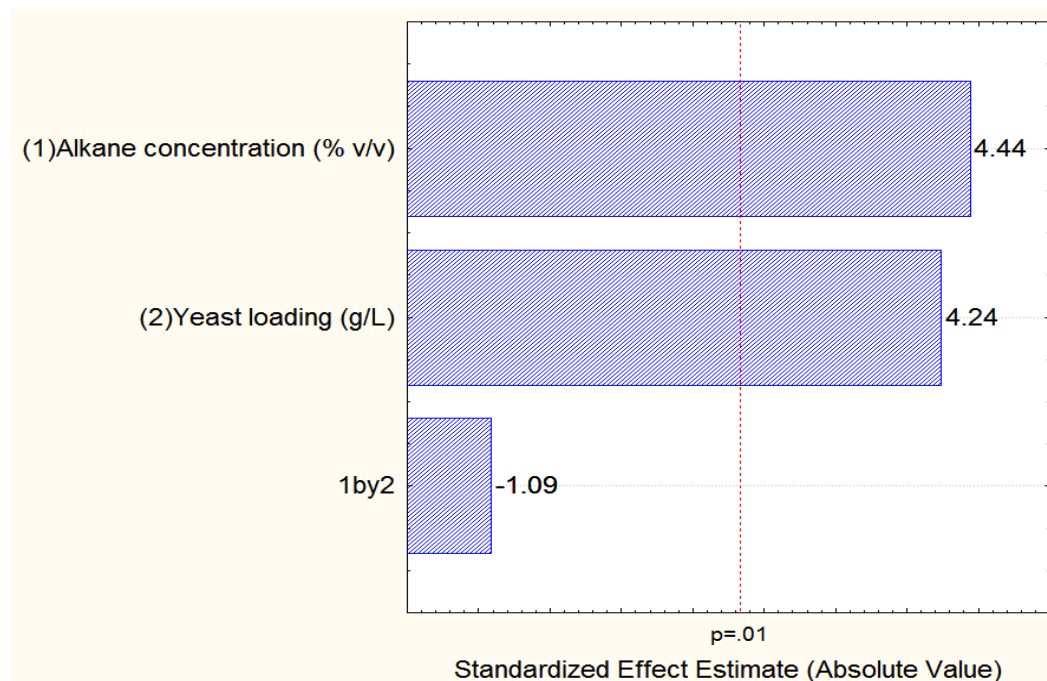


Figure 5.29 Pareto chart for effect of alkane concentration, yeast loading and their interaction on fluid viscosity

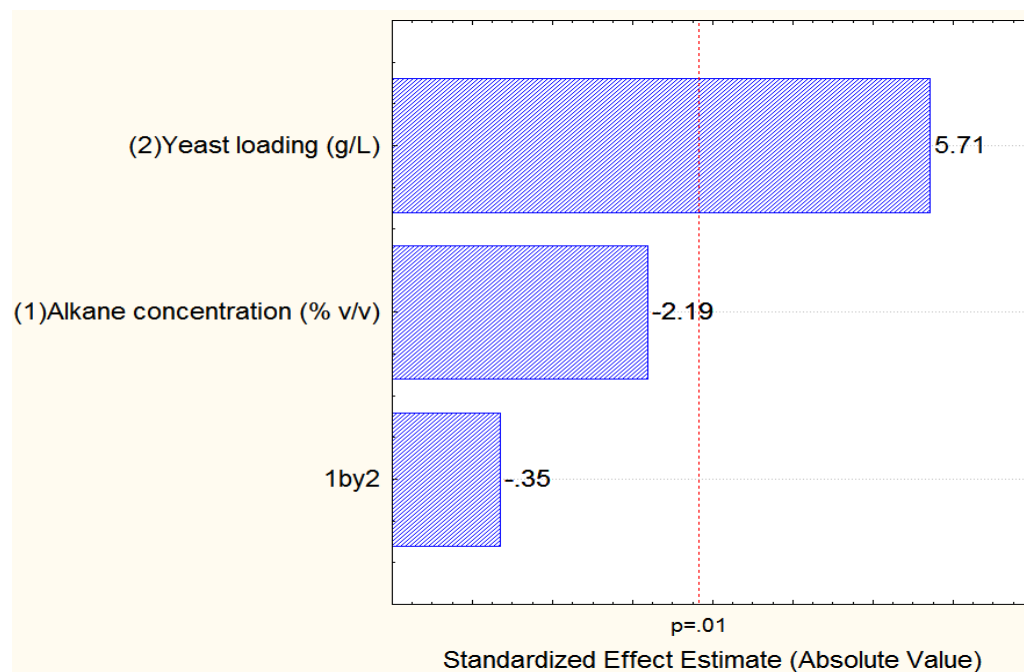


Figure 5.30 Pareto chart for effect of alkane concentration, yeast loading and their interaction on fluid surface tension

The effects of the parameters and their interactions on $K_{L,a}$ in $n\text{-C}_{14-20}$ -yeast-aqueous dispersions are discussed in the following sections, 5.2.2.1 - 5.2.2.6. The surface response curves were generated when two process parameters were varying and one parameter kept constant. A center condition with an agitation of 750rpm, alkane concentration of 6.88% (v/v) and yeast loading of 3.25g/L was investigated to check for any curvature in $K_{L,a}$ behavior.

5.2.2.1 Effect of agitation rate

Increase in agitation rate from 600rpm to 900rpm enhanced $K_{L,a}$ in $n\text{-C}_{14-20}$ -yeast-aqueous dispersions (Figure 5.28). $K_{L,a}$ increased from 0.0230s^{-1} to 0.040s^{-1} in 2.5% (v/v) $n\text{-C}_{14-20}$ alkane (Figure 5.31) and also from 0.0290s^{-1} to 0.0450s^{-1} at a yeast loading of 1g/L (Figure 5.32) over the same agitation rate. Increased agitation rates promoted bubble breakage resulting in lower D_{32} increased both the gas hold-up and the gas-liquid interfacial area per unit volume. High turbulent conditions also reduce the resistance to oxygen transfer through the decreased gas-liquid boundary layer increasing K_L .

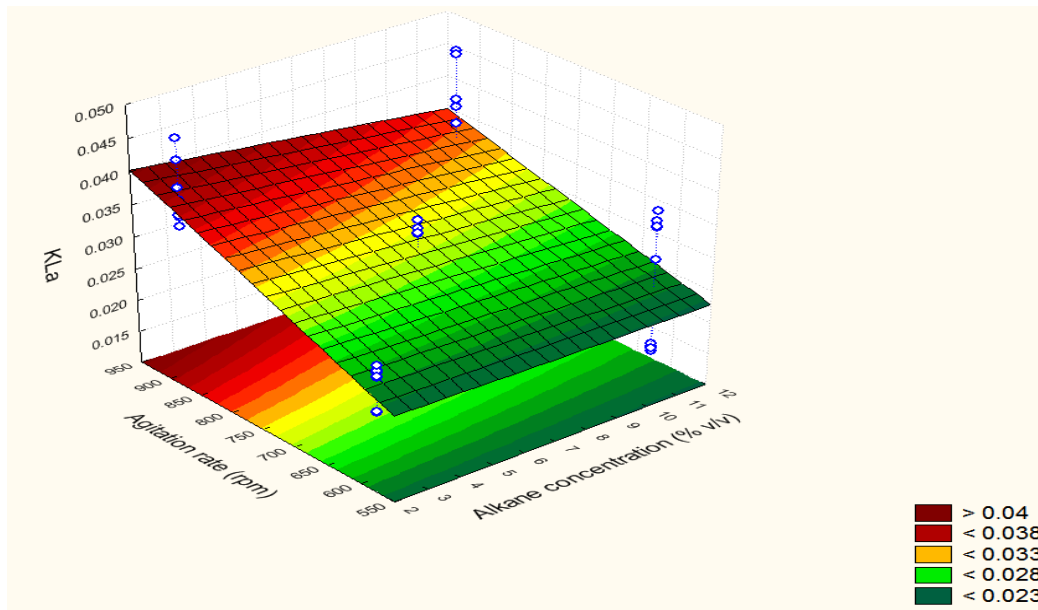


Figure 5.31 Surface response for effect of agitation and alkane concentration on K_{La} at constant yeast loading of 3.25g/L

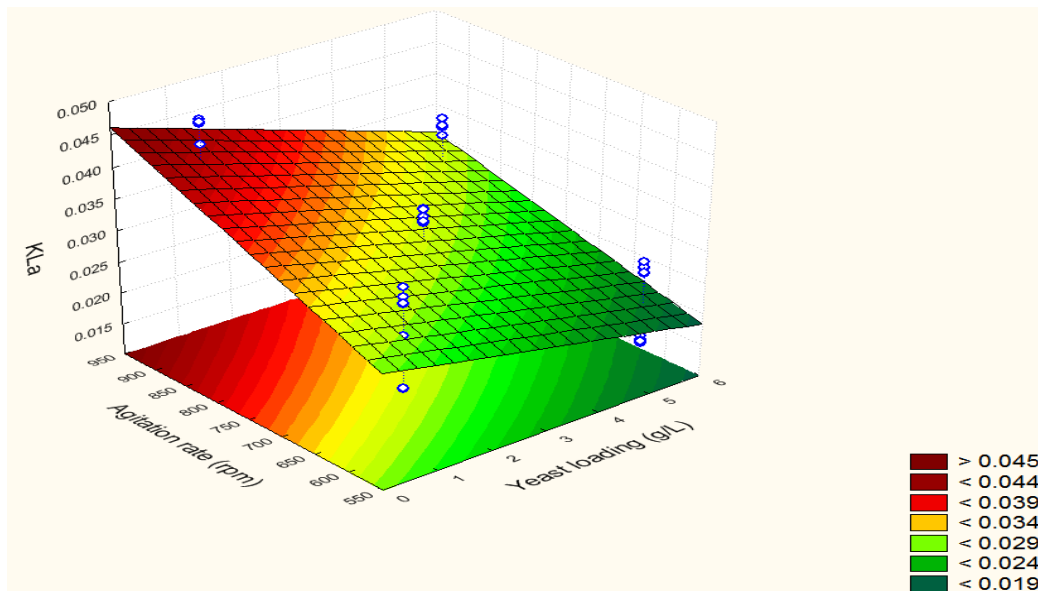


Figure 5.32 Surface response for effect of agitation and yeast loading on K_{La} at constant 6.88% (v/v) $n\text{-C}_{14-20}$ alkane

5.2.2.2 Effect of alkane concentration

The effect of increasing alkane concentration from 2.5% (v/v) to 11.25% (v/v) insignificantly depressed K_{La} in $n\text{-C}_{14-20}$ -yeast-aqueous dispersions (Figure 5.28). However there were exceptions for cases when there were no yeast particles in the $n\text{-C}_{14-20}$ -yeast-aqueous dispersions and for yeast loadings of <2g/L (Figure 5.33). When there were no yeast particles, when alkane concentration increased, K_{La} increased from 2.5% (v/v) to 11.25% (v/v). This was possibly because of the low fluid viscosity and fluid surface tension when there are no yeast cells resulting in less coalescence behavior of the fluid (Kelkar *et al.*, 1983; Hu *et al.*, 2005). This is also in

agreement to the work of van der Meer *et al.* (1992) who indicated that small concentrations of octanol enhanced K_L especially when the octanol drop diameter was sufficiently smaller than the gas-liquid since no adsorption occurred at the gas-liquid interface.

There was also a transition zone for yeast loadings of 1-2g/L which did not affect K_{La} for all the alkane concentrations before K_{La} started to decrease (Figure 5.33). This was in agreement to the work of Albal *et al.* (1983) who indicated that low solids loading of 0.2wt% did not alter K_{La} , but enhanced the surface renewal rate and mobility.

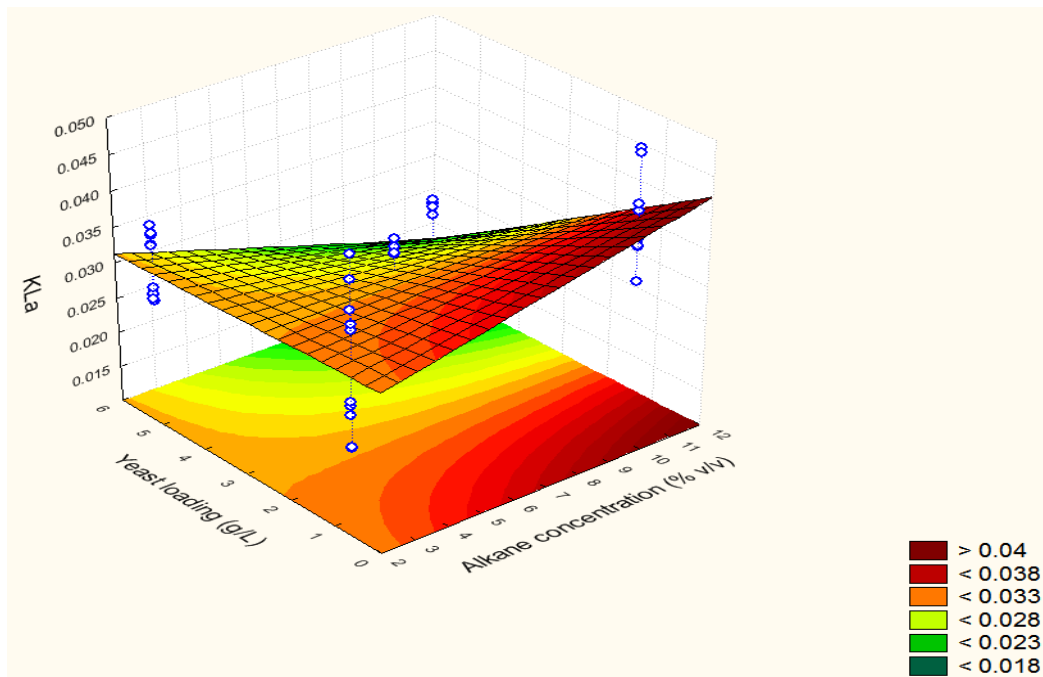


Figure 5.33 Surface response for effect of alkane concentration and yeast loading on K_{La} at constant agitation of 750rpm

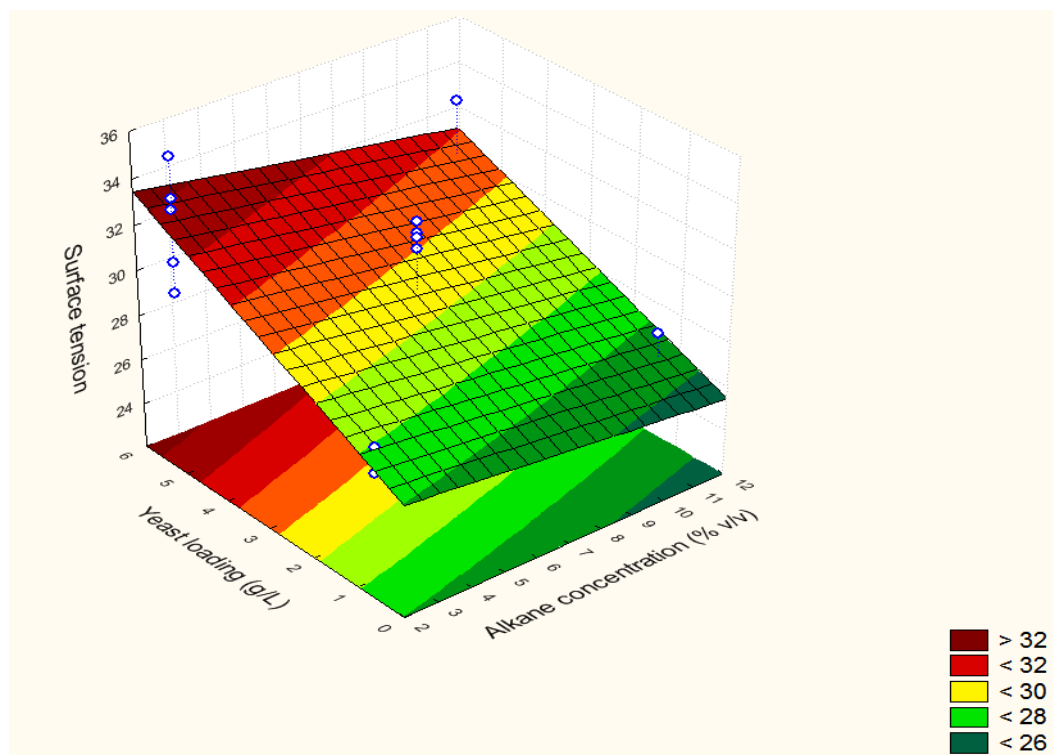


Figure 5.34 Surface response for effect of alkane concentration and yeast loading on fluid surface tension

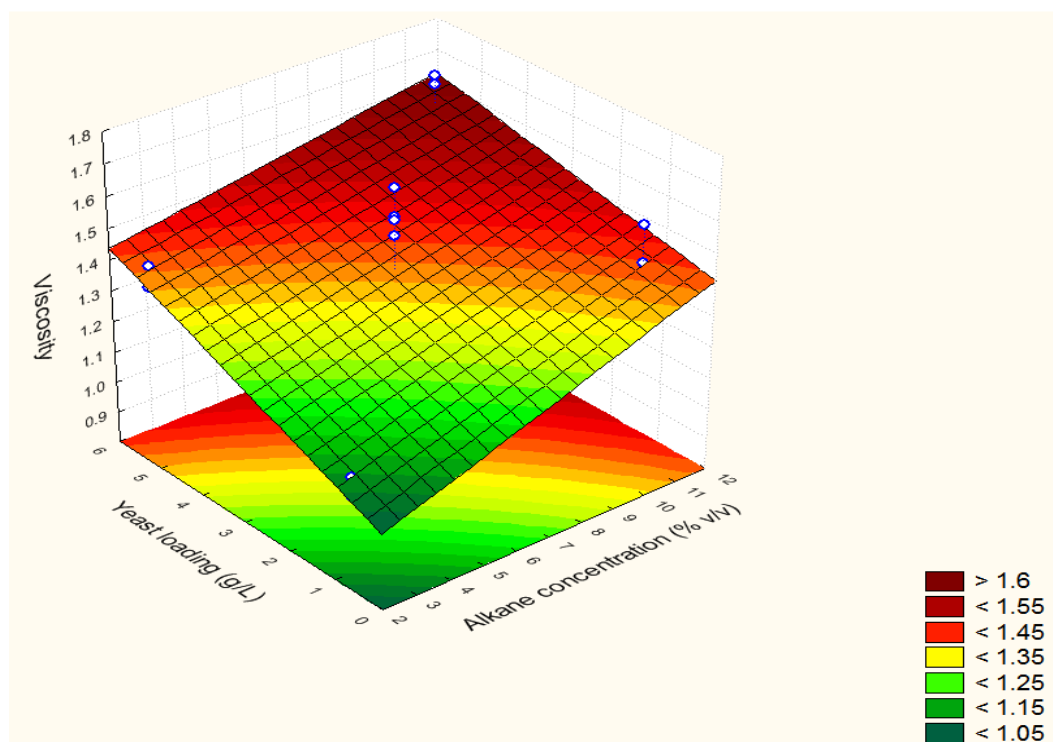


Figure 5.35 Surface response for effect of alkane concentration and yeast loading on fluid viscosity

5.2.2.3 Effect of yeast loading

An increase in yeast loading from 1g/L to 5.5g/L significantly depressed $K_L a$ in n -C₁₄-₂₀-yeast-aqueous dispersions (Figure 5.28 and Figure 5.33). This can be attributed to

increase in coalescence behaviour since increase in yeast loading increased both fluid viscosity (Figure 5.29 and Figure 5.35) and fluid surface tension (Figure 5.30 and Figure 5.34). This resulted in lower specific interfacial areas due to increased D_{32} and lowered gas hold up. K_L also decreased due to decreased DO diffusivity due to the increased coalescence in the media. (See also section 5.2.1.3 for explanation).

5.2.2.4 Effect of interaction between agitation rate and alkane concentration

The interactive effect between increasing both agitation rate from 600rpm to 900rpm and alkane concentration from 2.5% (v/v) to 11.25% (v/v) depressed K_{La} in $n\text{-C}_{14-20}$ -yeast-aqueous dispersions but the effect was insignificant (Figure 5.28). This was because the viscous alkane reduced the turbulent effect exerted by increase in agitation rate.

5.2.2.5 Effect of interaction between agitation rate and yeast loading

The interactive effect between increasing agitation rate from 600rpm to 900rpm and yeast loading from 1g/L to 5.5g/L depressed K_{La} in $n\text{-C}_{14-20}$ -yeast-aqueous dispersions but the effect was insignificant (Figure 5.28). This was possibly because as yeast loading increased, the turbulent effects in the fluid were reduced due to increase in both fluid viscosity and fluid surface tension (Figure 5.29 and Figure 5.30). This counter acted the effect of the agitation rate lowering both the gas-liquid interfacial area per unit volume and K_L .

5.2.2.6 Effect of interaction between alkane concentration and yeast loading

The interactive effect between increase in alkane concentration from 2.5% (v/v) to 11.25% (v/v) and increase in yeast loading from 1g/L to 5.5g/L significantly decreased K_{La} (Figure 5.28). This was despite their interactive effects insignificantly decreasing both the fluid viscosity and (Figure 5.29) and the fluid surface tension (Figure 5.30). This was possibly due to the diminishment of the gas-liquid flux area by the denser yeast particles in the viscous alkane media; this resulted in the decrease of the interfacial area per unit volume.

5.2.3 Comparison of trends in systems with inert solids to those with inactive yeast

An increase in agitation rate increased K_{La} in systems with both inert solids and inactive yeast i.e. from 600rpm to 1200rpm in $n\text{-C}_{14-20}$ -inert solid-aqueous dispersions and increase from 600rpm to 900rpm in $n\text{-C}_{14-20}$ -yeast-aqueous dispersions (Figure 5.14 and Figure 5.28).

An increase in alkane concentration decreased K_{La} in both systems, but was significant only in $n\text{-C}_{14-20}$ -inert solid-aqueous dispersions since high alkane concentrations of 2.5-20% (v/v) were used unlike in the $n\text{-C}_{14-20}$ -yeast-aqueous dispersions where low alkane concentrations of 2.5-11.25% (v/v) were used (Figure 5.14 and Figure 5.28).

An increase in solids loading decreased K_{La} in both systems, but was only significant in systems with inactive yeast compared to that with inert solids loading (Figure 5.14 and Figure 5.28). This was possibly because the yeast particle was denser than the corn flour and CaCO_3 particles. The increased density likely increased coalescence thereby diminishing of the oxygen flux area resulting in lower K_{La} . This is shown by the large differences in K_{La} values between the $3\mu\text{m}$ CaCO_3 particle with density of 700kg/m^3 and the $5\mu\text{m}$ yeast with density of 900kg/m^3 irrespective of agitation rate employed (Table 5.1).

Higher solid particle densities were also found to cause a more pronounced K_{La} decrease in aqueous systems with glycerol, glycol, barium chloride and sodium sulfate solutions when comparing in the effect of bronze spheres (density 8770kg/m^3) with glass spheres (density of 2500kg/m^3) Koide *et al.* (1984). Freitas and Teixeira (2001) confirmed this behavior with solids loading of up to 30% (v/v) in aqueous solutions containing a 2.151mm particle with density of 1048kg/m^3 compared to 2.131mm calcium alginate beads with density of 1023kg/m^3 . They indicated that denser particles had lower K_{La} due to increased coalescence due a diminished flux area as reflected by a smaller gas-liquid interfacial area per unit volume.

Table 5.1: K_{La} behavior due to density differences in 2.5% (v/v) $n\text{-C}_{14-20}$ -solid aqueous dispersions

K_{La} in 1g/L solids loading			
Agitation	Yeast	CaCO_3	% Diff in K_{La}
600rpm	0.0237	0.0278	15
1200rpm	0.0350	0.0762	54
K_{La} in 10g/L solids loading			
Agitation	Yeast	CaCO_3	% Diff in K_{La}
600rpm	0.0153	0.0315	51
1200rpm	0.0341	0.0559	39

The interaction of increasing alkane concentration and solids loading enhanced K_{La} in systems with inert solids but depressed K_{La} in systems with inactive yeast (Figure

5.14 and Figure 5.28). This was possibly because the reduction of the gas-liquid flux area by the denser yeast particles in the viscous alkane media outweighed the bubble breakage tendency that was observed in lower density solids systems (corn flour and CaCO_3). This interaction was the only difference between the two systems.

Lastly the interactions of increasing agitation rate and alkane concentration as well as increasing agitation rate and solids loading insignificantly depressed K_La in both systems with the inert solids and inactive yeast.

6 CONCLUSIONS

Conclusions from this work are based on two major parts which are firstly, the evaluation of an accurate and less K_{La} measurement method which incorporates the K_p effects. Secondly, the quantification of K_{La} behavior in aerated agitated alkane-solid-aqueous dispersions with inert solids and inactive yeast using the GOP (lag) methodology is addressed. Quantification of K_{La} behavior was based on effects of agitation rate as well as alterations in fluid properties due to alkane concentration, solids loading, solids particle sizes and their interactions.

6.1 Evaluation of measurement methodology

In evaluation of an accurate and less complex K_{La} methodology, the GOP (lag) with K_p effects incorporated, the second order response model was found to be superior over the GOP (no lag) first order response model. K_p was found to significantly affect K_{La} measurement in the GOP in viscous alkane multiphase systems.

K_p was found to be a varying parameter depending on the DO probe dynamics, alkane concentration and alkane chain length. K_p decreased with increases in both the probe membrane and probe electrolyte age with membrane age causing the major decrease about double the effect. Increase in membrane usage promoted stretching of the membrane whilst continual usage of the electrolyte decreased its conductivity. High K_p values of 0.0559s^{-1} were obtained when both membrane and electrolyte were new but decreased to 0.0329s^{-1} after 5 days in use.

K_p also decreased with increase in alkane concentration from 2.5% (v/v) to 20% (v/v) but was independent of agitation rates of 600rpm to 1200rpm and the interaction between these two factors. Increase in alkane concentration increased the thickness of the liquid film due to the alkanes' viscous nature which decreased the transfer of DO through the film thereby increasing the DO probe response lag time. The agitation rate in this work provided sufficient mixing such that K_p was not influenced by the range of agitation used in this work. Consequently, a maximum K_p of 0.0434s^{-1} was therefore found in 2.5% (v/v) at 1200rpm.

Further increase in alkane chain lengths from $n\text{-C}_{10-13}$ to $n\text{-C}_{14-20}$ and alkane concentration from 2.5% (v/v) to 20% (v/v) both decreased K_p . Alkane concentration had an effect 7 times greater as compared to that of alkane chain length. Both factors increased the fluid viscosity hence thickening of the liquid film resulting in longer probe response lag times. High K_p values of 0.0589s^{-1} were therefore obtained in

2.5% (v/v) *n*-C₁₀₋₁₃-aqueous dispersions as compared with relatively lower K_p of 0.0280s⁻¹ obtained in 20% (v/v) *n*-C₁₄₋₂₀-aqueous dispersions.

Lastly, increased solids loading from 1g/L to 10g/L and increased solids particle size from 3 μ m to 14 μ m did not significantly affect K_p in alkane-solid-aqueous dispersions. It's possible that such solids loadings and particle sizes do not exert any significant resistance at the fluid film since they were in suspension. All the interactive effects investigated on K_p were negligible.

These results demonstrate that K_p is not a constant value but is determined by the alkane chain length and alkane concentration in alkane multiphase systems. This means that K_p needs to be determined before measuring K_{La} in alkane multiphase systems to achieve the accurate K_{La} value.

Comparison of K_{La} values measured by the gassing out procedure incorporating the actual K_p (GOP (lag)) with those measured by the gassing out procedure assuming zero K_p (GOP (no lag)) demonstrated conclusively that K_{La} values from the former were more accurate. Differences of over 40% were observed for agitations of 600-1200rpm and alkane concentrations of 2.5-20% (v/v). The differences were attributed to the influence of K_p . Additionally, the differences on K_{La} due to K_p effects increased with increase in agitation rate and was more than 1.7 times higher at 1200rpm as compared to those at 600rpm for all alkane concentrations and alkane chain lengths. Specifically, the highest deviation of 45% was observed at 1200rpm in 5% (v/v) *n*-C₁₄₋₂₀-aqueous dispersions and 46% in *n*-C₁₀₋₁₃-aqueous dispersions at 1200rpm and 10% (v/v). This was attributed to the magnitude of K_p being almost equal to K_{La} i.e. $K_p \approx K_{La}$ at higher agitation rates, when the effect of K_p became more pronounced. Lastly K_{La} values measured by the GOP (lag) and the more complex PSP were the same for all agitations and alkane concentrations, with differences as low as 1.6% which was very insignificant at 99% confidence interval. This confirmed the accuracy of the GOP (lag) methodology.

Consequently, the GOP (lag) second order response model was then chosen as the accurate K_{La} measurement method over the relatively more complex PSP methodology. For the first time, the GOP (lag) with the actual K_p value incorporated per each process condition was applied in quantification of K_{La} in the alkane-solid-aqueous dispersions.

6.2 Quantification of the behavior of the overall volumetric oxygen transfer coefficient in alkane-solid-aqueous dispersions

Conclusions will be based only on the significant effects affecting $K_{L,a}$ in the multiphase systems with either inert solids or inactive yeast. Furthermore, conclusions based will be based in similarities or different between these two systems.

6.2.1 Alkane-aqueous dispersions with inert solids

In the $n\text{-C}_{14-20}$ -inert solid-aqueous dispersions $K_{L,a}$ was enhanced by increased agitation rate with an effect 5 times higher that of enhancement due to interaction of increased alkane concentration and solids loading. An increase in agitation rate increased $K_{L,a}$, most likely through increasing both the gas-liquid interfacial area per unit volume due to increased ε_G and decreased D_{32} and increased K_L due to increased turbulence reducing the gas-film thickness. In addition, interaction between increase in alkane concentration and inert solids loading enhanced $K_{L,a}$ due to breakage of the alkane-DO bubble by continual solids loading decreasing D_{32} and increasing the gas-liquid interfacial area per unit volume. This was however, only observed for alkane concentrations greater than 15% (v/v). Also their interactive effect between these two parameters decreased the fluid viscosity reducing the bubble coalescence in the system.

In the $n\text{-C}_{14-20}$ -inert solid-aqueous dispersions $K_{L,a}$ was depressed by increased alkane concentration with an effect 4 times higher that of depression due to increased solids particle sizes and the interaction of increased agitation rate and solids particle sizes. An increase in alkane concentration decreased $K_{L,a}$ due to an overall increased fluid viscosity. The increase in fluid viscosity had a 2.35 higher effect compared to decrease in fluid surface tension promoting an overall effect of increased coalescence in the dispersion. This lead to increased D_{32} , lowering both the gas-liquid interfacial area per unit volume, ε_G and in also reducing DO transport through the film with resultant lower K_L . Additionally, increasing solids particle sizes decreased $K_{L,a}$ since solids particles via their attachment to the DO bubble increasing D_{32} , possibly lowered the gas-liquid interfacial area per unit volume. The decrease on $K_{L,a}$ upon increased solids particle sizes suggest that the negative effect of attachment to the oxygen bubble predominate over the positive effect of the decrease in fluid viscosity and surface tension by almost equal magnitudes.

Furthermore, interaction between increase in agitation rate and solids particle size significantly depressed $K_{L,a}$, possibly due to the presence of solid particles as physical barriers to DO transfer counteracting the turbulent effects of agitation.

Due to the different impact the type of solids, alkane concentration and agitation rate have on $K_{L,a}$, maximum $K_{L,a}$ of 0.0762s^{-1} was obtained in 2.5% (v/v)- $3\mu\text{m}$ - $n\text{-C}_{14-20}$ -inert solid-aqueous systems with the inert solids at a solids loading of 1g/L and agitation of 1200rpm.

6.2.2 Alkane-aqueous dispersions with inactive yeast

In the $n\text{-C}_{14-20}$ -yeast-aqueous dispersions $K_{L,a}$ was enhanced on increased agitation rate with an effect of 10.78. An increase in agitation rate increased $K_{L,a}$, most likely through increasing both the gas-liquid interfacial area per unit volume due to increased ε_G and decreased D_{32} and increased K_L due to increased turbulence reducing the gas-film thickness.

In the $n\text{-C}_{14-20}$ -yeast-aqueous dispersions $K_{L,a}$ was depressed by increased yeast loading with an effect 1.2 times higher than that of depression due to interaction of increased yeast loading and alkane concentration. Increase in yeast loading decreased $K_{L,a}$ since yeast loading significantly increased both fluid viscosity and fluid surface tension by equal effects, thereby promoting coalescence and thickening of the gas-liquid interface. This caused a decrease in the gas-liquid interfacial area per unit volume through increasing the D_{32} , lowering the ε_G and also decreasing K_L . Yeast particles had a significant effect on $K_{L,a}$ decrease due to their high density. In addition the interaction of increase in alkane concentration and yeast loading depressed $K_{L,a}$ also due to the diminishment of the gas-liquid flux by the high density yeast particles in the viscous alkane media resulting in lower gas-liquid interfacial areas per unit volume.

In $n\text{-C}_{14-20}$ -yeast-aqueous dispersions $K_{L,a}$ had a maximum value of 0.0415s^{-1} in 11.25% (v/v) and yeast loadings of 1g/L and agitation of 900rpm. A typical bioprocess using yeast as cells in alkane multiphase systems is advisable at 1g/L, 11.25% (v/v) and 900rpm from an oxygen supply perspective since the oxygen transfer rate will be at maximum at these conditions.

6.2.3 Comparison of trends in systems with inert solids to those with inactive yeast

An increase in agitation rates enhanced K_{La} in both systems whilst increasing alkane concentration and solids loading depressed K_{La} in both systems as well. However there was a contradiction between the interaction of increasing alkane concentration and solids loading. In systems with inert solids, the interaction promoted bubble breakage resulting in enhanced K_{La} whilst in systems with inactive yeast, the interaction depressed K_{La} due to diminishment of the gas-liquid flux resulting in lower K_{La} values.

In conclusion K_{La} is enhanced by increased agitation rates and depressed by increased alkane concentration, solids loading, solids particles sizes and solids density in alkane based bioprocesses.

7 RECOMMENDATIONS

After a rigorous quantification of K_La behavior in alkane multiphase systems using an accurate, reliable measurement method, the following recommendations are useful for future work. Firstly there is need to experimentally quantify the individual contributions of the volumetric oxygen transfer coefficient (K_L) and the gas-liquid interfacial area per unit volume (a) to K_La behavior in alkane-solid-aqueous dispersions. Since K_La is affected by both parameters there is need to know the actual contribution of each parameter so that we can fully underpin K_La behavior in alkane multiphase systems in terms of each parameter.

Secondly there is need to simulate and model the experimental results obtained for K_La in the multiphase systems and apply the model to a range of aeration rate, agitation rate, alkane concentration, solids loading and solids particle size in alkane-solid-aqueous dispersions. Since K_La is a critical parameter for oxygen transfer, developing a predictive model will be valuable for designing and operating of hydrocarbon based bioprocesses.

8 REFERENCES

1. Aiba, S. and Huang, S. Y. (1969). "Oxygen permeability and diffusivity in polymer membranes immersed in liquids", *Chem. Eng. Sci.*, 24, p 1149 - 1159.
2. Albal, R. S., Shah, Y.T. and Schumpe, A. (1983). "Mass transfer in multiphase agitated contactors", *Chem. Eng. J.*, 27, p 61 - 80.
3. Alper, E., Wichtendahl, B. and Deckwer, W. D. (1980). "Gas absorption mechanism in catalytic slurry reactors", *Chem. Eng. Sci.*, 35, p 217 - 222.
4. Al Taweel, A.M. and Cheng, Y.H, (1995). "Effect of surface tension on gas/liquid contacting in a mechanically agitated tank with stator", *Chem. Eng Res. Des.*, 73, p 654 - 660.
5. Alves, S.S., Maia, C.I. and Vasconcelos, J.M.T. (2004). "Gas-liquid mass transfer coefficient in stirred tanks interpreted through bubble contamination kinetics", *Chem. Eng. Process.*, 43(7), p 823 - 830.
6. Bailey, J.E. and Ollis, D.F. (1986). *Biochemical Engineering Fundamentals*. Verma, K. and Martin, C.C., editors. 2nd Ed. New York, McGraw-Hill. p 459 - 460.
7. Bandyopadhyay, B., Humphrey, A.E. and Taguchi, H. (1967). "Dynamic measurement of the volumetric oxygen transfer coefficient in fermentation systems", *Biotechnol. Bioeng.*, 9(4), p 533 – 544.
8. Bartos, T.M and Satterfield, C.N (1986). "Effects of finely divided solids on mass transfer between a gas and an organic liquid", *AIChE J.*, 32(5), p 773 - 781.
9. Benedek, A.A. and Heideger, W.J. (1970). "Polagraphic oxygen analyzer: The effect of instrument lag in non-steady state re-aeration test", *Water. Research.*, 4, p 627 - 640.
10. Benchapattarapong, N., Anderson, W. A., Bai, F. and Moo-Yang, M. (2005). "Rheology and hydrodynamic properties of *Tolypocladium inflatum* broth and its simulation", *Bioprocess. Biosyts. Eng.*, 27, p 239 - 247.
11. Bi, Y., Hill, G.A. and Sumner, R.J. (2001). "Enhancement of the overall volumetric oxygen transfer coefficient in a stirred tank bioreactor using ethanol", *Can. J. Chem. Eng.*, 79(3), p 463 - 467.

12. Calderbank, P.H. (1958). "Physical rate processes in industrial fermentation. Part I: The interfacial area in gas-liquid contacting with mechanical agitation", *Trans. I. Chem. E.*, 36(A), p 443 - 459.
13. Chan, E.C. and Kuo, J. (1997). "Biotransformation of dicarboxylic acid by immobilized *Cryptococcus* cells", *Enzyme. Microb. Tech.*, 20 (8), p 585 – 589.
14. Chandrasekaran, K. and Sharma, M.M. (1977). "Absorption of oxygen in aqueous solutions of sodium sulfite in the presence of activated carbon as catalyst", *Chem. Eng. Sci.*, 32, p 669.
15. Chapman, C.M., Nienow, A. W., Cooke, M. and Middleton, J.C. (1983). "Particle-gas-liquid mixing in stirred vessels. Part IV: Mass transfer and final conclusions", *Chem. Eng. Res. Des.*, 61, p 182 - 185.
16. Chisti, M.Y. and Moo-Yang, M (1988). "Hydrodynamics and oxygen transfer in pneumatic bioreactor devices", *Biotech. Bioeng.*, 31, p 487 - 494.
17. Clarke, K.G. and Correia, L.D.C. (2008). "Oxygen transfer in hydrocarbon-aqueous dispersions and its applicability in alkane bioprocesses: A review," *Biochem. Eng. J.*, 39(3), p 405 - 429.
18. Clarke, K.G, Williams, P.C, Smit, M.S. and Harrison, S.T.L. (2006). "Enhancement and repression of the volumetric oxygen transfer coefficient through hydrocarbon addition and its influence on oxygen transfer rate in stirred tank bioreactors", *Biochem. Eng. J.*, 28(3), p 237 - 242.
19. Correia, L.D.C., Aldrich, C. and Clarke, K.G. (2010). "Interfacial gas-liquid transfer area in alkane-aqueous dispersions and its impact on the overall volumetric transfer coefficient", *Biochem. Eng. J.*, 49(1), p 133 - 137.
20. Correia, L.D.C. and Clarke, K.G. (2009). "Measurement of the overall volumetric oxygen transfer coefficient in alkane-aqueous dispersions", *J.Chem. Technol. Biotechnol.*, 84(12), p 1793 - 1797.
21. Correia, L.D.C. (2007). Oxygen transfer in hydrocarbon-aqueous dispersions and its applicability to alkane-based bioprocesses. Master's Thesis: Department of Process Engineering. Stellenbosch University. p 81.
22. Dang, N.D.P., Karrer, D.A. and Dunn, I.J. (1977). "Oxygen transfer coefficients by dynamic model moment analysis", *Biotechnol. Bioeng.*, 19(6), p 853 – 865.

23. Das, T.R., Bandyopadhyay, A., Parthasarathy, R. and Kumar, R. (1985). "Gas-liquid interfacial area in stirred vessels: The effect of an immiscible liquid phase", *Chem. Eng. Sci.*, 40(2), p 209 - 214.
24. Doran, P.M. (1995). *Bioprocess Engineering Principles*. 1st ed. Elsevier, Academic Press. 190 - 201 p.
25. Elgozalia, A., Linek, V., Fialova, M., Wein, O. and Zahradnik, J. (2002). "Influence of viscosity and surface tension on performance of gas-liquid contactors with ejector type gas distributor", *Chem. Eng. Sci.*, 57, p 2987 - 2994.
26. Freitas, C. and Teixeira, J. A. (2001). "Oxygen mass transfer in a high solids loading three phase internal loop airlift reactor", *Chem. Eng. J.*, 84, p 57 - 61.
27. Frijlink, J.J. and Smith, J.M. (1986). "Coalescence in three phase systems", Paper 23. International Conference Bioreactor fluid dynamics, Cambridge England, BHRA.
28. Fuchs, R., Ryu, D.D.W. and Humphrey, A.E. (1971). "Effect of surface aeration on scale up procedures for fermentation processes", *Ind. Eng. Chem. Proc. Des. Dev.*, 10(2), p 190 - 195.
29. Fukui, S. and Tanaka, A. (1980). Production of useful compounds from alkane media in Japan. In: *Advances in Biochemical Engineering*. Berlin, Springer, Vol. 17, p 1 - 35.
30. Fukuma, M., Muroyama, K. and Yasunishi, A. (1987). "Properties of bubble swarm in a slurry bubble column", *Japan. Chem. Eng. J.*, 20(1), p 28 - 32.
31. Garcia-Ochoa, F. and Gomez, E. (2004). "Theoretical prediction of gas-liquid mass transfer coefficient, specific area and hold up in sparged stirred tanks", *Chem. Eng. Sci.*, 59, p 2489 - 2501.
32. Garcia-Ochoa, F. and Gomez, E. (2005). "Prediction of gas-liquid mass transfer coefficient in sparged stirred tank bioreactors", *Biotechnol. Bioeng.*, 92(6), p 761 - 772.
33. Garcia-Ochoa, F. and Gomez, E. (2009). "Bioreactor scale up and oxygen transfer rate in microbial processes: An overview", *Biotechnology Advances.*, 27, p 153 - 176.
34. Godbole, S.P., Schumpe, A. and Shah, Y.T. (1984). "Hydrodynamics and mass transfer in non-Newtonian solutions in a bubble column", *AIChE J.*, 30(2), p 213 - 219.

35. Gollakota, S.V. and Guin, J.A. (1984). "Comparative study of gas-liquid mass transfer coefficients in stirred autoclaves, tubing bomb micro reactors and bubble columns", *Ind. Eng. Chem. Pro. Des. Dev.*, 23, p 52 - 59.
36. Gourich, B., Vial, Ch., Azher, E.I., Belhaj Soulami, M. and Ziyad, M. (2008). "Influence of hydrodynamics and probe response on oxygen mass transfer measurements in a high aspect ratio bubble column reactor: Effect of the coalescence behavior of the liquid phase", *Biochem. Eng. J.*, 39, p 1 - 14.
37. Gous, K. (2003). Continuous processing of Vesiculated Beads. Master's Thesis: Department of Process Engineering. Stellenbosch University. p 1 - 171.
38. Hassan, I.T.M. and Robinson, C.W. (1977a). "Oxygen transfer in mechanically agitated aqueous systems containing dispersed hydrocarbon", *Biotechnol. Bioeng.*, 19(5), p 661 - 682.
39. Hassan, I.T.M. and Robinson, C.W. (1977b). "Stirred-tank mechanical power requirement and gas hold up in aerated aqueous phases", *AIChE J.*, 23(1), p 48 - 56.
40. <http://www.powderandbulk.com>
41. <http://www.tutorvista.com/ks/defination-of-surface-tension>
42. Hu, B., Pacek, A.W., Stitt, E.H. and Nienow, A.W. (2005). "Bubble sizes in agitated air-alcohol systems with and without particles: Turbulent and transitional flow", *Chem. Eng. Sci.*, 60(22), p 6371 - 6377.
43. Hwang, S. and Lu, W. (1997). "Gas-liquid mass transfer in an internal loop airlift reactor with low density particles", *Chem. Eng. Sci.*, 52(5), p 853-857.
44. Joosten, G.E.H., Schindler, J.G.M. and Jansen, J.J. (1977). "The influence of suspended solid materials on the gas-liquid mass transfer in stirred gas liquid contactors", *Chem. Eng. Sci.*, 32, p 563 - 566.
45. Ju, L. and Sundararajan, A. (1994). "The effects of cells on oxygen transfer in bioreactors: physical presence of cells as solid particles", *Chem. Eng. Biochem.*, 56(1), p B15 - B24.
46. Juarez, P. and Oreans, J. (2001). "Oxygen transfer in a stirred reactor in laboratory scale", *Latin. American. Applied. Res.*, 31, p 433 - 439.
47. Juretzek, T., Wang, H.J., Nicaud, J.M., Mauersberger, S. and Barth, G. (2000). "Comparison of promoter suitable for regulated over expression of β -

- galactosidase in the alkane-utilizing yeast *Yarrowia lipolytica*", *Biotechnol. Bioprocess. Eng.*, 5(5), p 320 - 326.
48. Kawase, Y. Araki, T., Shimizu, K. and Miura, H. (1997). "Gas-liquid mass transfer in three phase stirred tank reactors: Newtonian and Non-Newtonian fluids", *Canadian. Chem. Eng. J.*, 75, p 1159 - 1164.
 49. Keitel, G. and Onken, U. (1981). "Errors in the determination of mass transfer in gas-liquid dispersions", *Chem. Eng. Sci.*, 36(12), p 1927 - 1932.
 50. Kelkar, B.G., Godbole, S.P., Honath, M.F., Shah, Y.T., Carr, N.L. and Deckwer, W.D. (1983). "Effect of addition of alcohols on gas hold-up and back mixing in bubble columns", *AIChE J.*, 29(3), p 361 - 369.
 51. Khare, A.S. and Joshi, J.B. (1990). "Effect of fine particles on gas hold-up in three-phase sparged reactors", *Chem. Eng. J.*, 44(1), p 11 - 25.
 52. Kilonzo, P.M. and Margaritis, A. (2004). "The effects of non-Newtonian fermentation broth viscosity and small bubble segregation on oxygen mass transfer in gas-lift bioreactors: a critical review", *Biochem. Eng. J.*, 17, p 27 - 40.
 53. Kim, J.O. and Kim, S.D. (1990). "Gas-liquid mass transfer in a three phase fluidized bed with floating bubble breakers", *Canadian. Chem. Eng. J.*, 68, p 368 - 375.
 54. Kirk-Othmer. (1978). *Chemical Encyclopedia of Chemical Technology*, Volume 8, Third Edition. p 921 - 923.
 55. Koide, K., Hayashi, T., Sumino, K. and Iwamoto, S. (1976). "Mass transfer from single bubbles in aqueous solutions of surfactants", *Chem. Eng. Sci.*, 31, p 963 - 967.
 56. Koide, K., Takazawa, A., Komura, M. and Matsunaga, H. (1984). "Gas hold-up and volumetric liquid phase mass transfer coefficient in solid suspended bubble columns", *Japan. Chem. Eng. J.*, 17(5), p 459 - 466.
 57. Koide, K., Yamazoe, S. and Harada, S. (1985). "Effects of surface active substances on gas hold up and gas liquid mass transfer in bubble column", *Japan. Chem. Eng. J.*, 18(4), p 287 - 292.
 58. Kosaric, N. (1996). Biosurfactants. *Biotechnology: Products of primary metabolism*. Roehr, M., editor. 2nd ed. Weinheim, VCH.

59. Krishna, R., de Swartz, J.W., Ellenberger, J., Martina, G.B. and Maretto, C. (1997). "Gas hold-up in slurry bubble columns: Effect of column diameter and slurry concentrations", *AIChE J.*, 43(2), p 311 - 316.
60. Lee, J.C. Ali, S.S. and Tasakor, P. (1982). "Influence of suspended solids on gas-liquid mass transfer in an agitated tank", 4th Euro Conference Mixing BHRA, Cranfield.
61. Letzel, H.M., Schouten, J.C., Krishna, R. and Van den Bleek, C.M. (1999). "Gas hold up in bubble column reactors operated at elevated pressure", *Chem. Eng. Sci.*, 54, p 2237 - 2246.
62. Lewis, W.K. (1916). "The principles of countercurrent extraction", *J. Ind. Eng. Chem.*, 8(7), p 825 - 833.
63. Linek, V., Benes, P. and Vacek, V. (1984). "An experimental study of oxygen probe linearity and transient characteristics in the high oxygen concentration range," *J. Electro anal. Chem.*, 169(1/2), p 233 - 257.
64. Linek, V., Benes, P. and Vacek, V. (1989). "Dynamic pressure method for $k_L a$ measurement in large-scale bioreactors", *Biotechnol. Bioeng.*, 33(11), p 1406 - 1412.
65. Linek, V., Benes, P., Sinkule, J. and Moucha, T. (1993). "Non-ideal pressure step method for $k_L a$ measurement", *Chem. Eng. Sci.*, 48(9), p 1593 - 1599.
66. Linek, V., Moucha, T., Dousova, M. and Sinkule, J. (1994). "Measurement of $K_L a$ by dynamic pressure method in pilot-plant fermenters," *Biotechnol. Bioeng.*, 43(6), p 477 - 482.
67. Linek, V., Kordac, M. and Moucha, T. (2005). "Mechanism of mass transfer from bubbles in dispersions. Part II: Mass transfer coefficients in stirred gas-liquid reactor and bubble column", *Chem. Eng. Process.*, 44(1), p 121 - 130.
68. Luyben, W.L. and Luyben, M.L. (1997). *Essentials of Process Control*. McGraw Hill. Chemical Engineering Series. p 41.
69. Marlin, T.E. (1992). *Process Control. Designing processes and control systems for dynamic performance*. McGraw-Hill, Inc. p 107 - 152.
70. Mandersloot, W.G.B. and Scott, K.J. (1990). "Rheology of particle suspension", *SA. Chem. Eng.*, 2(2), p 53 - 69.

71. Mena, P.C., Pons, M.N., Teixeira, J.A and Rocha, F.A. (2005). "Using image analysis in the study of multiphase gas absorption", *Chem. Eng. Sci.*, 60, p 5144 - 5150.
72. Mehrnia, M. R., Towfighi, J., Bonakdarpour, C. and Akbarnejad, M.M. (2005). "Gas hold-up and oxygen transfer in a draft tube airlift bioreactor with petroleum based liquids", *Biochem. Eng. J.*, 22(2), p 105 - 110.
73. Merchuk, J.C., Yona, S., Siegel, M.H. and Ben Zvi, A. (1990). "On the first-order approximation to the response of dissolved oxygen electrodes for dynamic $K_L a$ estimation", *Biotechnol. Bioeng.*, 35(11), p 1161 – 1163.
74. Mettler Toledo Instrument Manual (2005), InPro[®] 6800 Series O₂ sensors instruction manual. 1 - 100p.
75. Mezger, T. G. (2002). *The Rheology Handbook: For users of rotational and oscillary rheometers*, 1st edition, Vincentz Verlag, Hannover, p 55 - 68.
76. Mills, D. B., Bar, R. and Kirwan, D. J. (1987). "Effects of solids on oxygen transfer in agitated three phase systems," *AIChE J.*, 33(9), p 1542 - 1549.
77. Mimura, A., Sugeno, M., Ooka, T. and Takeda, I. (1971). "Biochemical engineering analysis of hydrocarbon fermentation", *J. Ferment. Technol.*, 49(3), p 245 - 254.
78. Mimura, A., Takeda, I. and Wakasa, R. (1973). "Some characteristic phenomena of oxygen transfer in hydrocarbon fermentation", *Biotechnol. Bioeng.*, 4(1), p 467 - 484.
79. Miyachi, M., Iguchi, A., Uchida, S. and Koide, K. (1981). "Effect of solid particles in liquid phase on liquid side mass transfer coefficient", *Canadian. Chem. Eng. J.*, 59, p 640 - 641.
80. Moo-Young, M. (1975). "Microbial reactor design for synthetic protein production", *Can. J. Chem. Eng.*, 53(2), p 113 - 118.
81. Mukherjee, Das, P. and Sen, A. (2006). "Towards commercial production of microbial surfactants". *Trends in Biotechnol.*, 24(11), p 509 - 515.
82. Nakanoh, M. and Yoshida, F. (1980). "Gas absorption by Newtonian and non-Newtonian liquids in a bubble column", *Ind. Eng. Chem. Proc. Des. Dev.*, 19(1), p 190 – 195.
83. New Brunswick Scientific (2005). *Guide to operations: Bioflo 110 modular bench top fermentor*. No. M1273-0054. Revision G, Edison, New Jersey.

84. Nicoletta, C., van Loosdrecht, M.C.M., van der Lans, R.G.J.M. and Heijnen, J.J. (1998). "Hydrodynamic characteristics and gas liquid mass transfer in a biofilm airlift suspension reactor", *Biotechnol. Bioeng.*, 60, p 627 - 635.
85. Nielsen, J., Villadsen, J. and Lidén, G. (2002). *Bioreaction Engineering Principles*. 2nd Ed. New York, Kluwer Academic / Plenum Publishers. p 540.
86. Nielsen, D.R., Daugulis, A.J. and McLellan, P.J. (2003). "A novel method of simulating oxygen mass transfer in two-phase partitioning bioreactors", *Biotechnol. Bioeng.*, 83(6), p 735 - 742.
87. Nikolov, V., Farag, I. and Nikolov, I. (2000). "Gas-liquid mass transfer in bioreactor with three phase inverse fluidized bed", *Bioprocess. Eng.*, 23, p 427 - 429.
88. O'Connor, C.T., Randall, E.W. and Goodall, C.M. (1990). "Measurement of the effects of physical and chemical variables on bubble size", *Int. J. Miner. Process.*, 28(1/2), p 139 - 149.
89. Oguz, H., Brehm, A. and Deckwer, W.D. (1987). "Gas-liquid mass transfer in sparged agitated slurries", *Chem. Eng. Sci.*, 42(7), p 1815 - 1822.
90. Ozbek, B. and Gayik, S. (2001). "The studies on the oxygen mass transfer coefficient in a bioreactor", *Process. Biochemistry.*, 36, p 729 - 741.
91. Ozturk, S. and Schumpe, A. (1987). "The influence of suspended solids on oxygen transfer to organic liquids in a bubble column," *Chem. Eng. Sci.*, 42, p, 1781-1785.
92. Parthasarathy, R., Jameson, G.J. and Ahmed, N. (1991). "Bubble breakup in stirred vessels: Predicting the Sauter mean diameter", *Trans. I. Chem. E.*, 69(A), p 295 - 301.
93. Parthasarathy, R. and Ahmed, N. (1994). "Sauter mean and maximum bubble diameters in aerated stirred vessels", *Trans. I. Chem. E.*, 72(A), p 565 - 572.
94. Pelofsky, A.H.J. (1966). "Surface tension-viscosity relation for liquids", *J. Chem. Eng. Data.*, 11(3), p 394 - 397.
95. Pennels, D. (2008). Influence of solids on the overall volumetric oxygen transfer coefficient in aerated alkane-aqueous dispersions. Final Year Laboratory Project: Department of Process Engineering. Stellenbosch University. p 30.
96. Preusting, H., Kingma, J., Huisman, G., Steinbüchel, A. and Witholt, B. (1993). "Formation of polyester blends by a recombinant strain of

- Pseudomonas oleovorans*: different poly(3-hydroxyalkanoates) are stored in separate granules," *J. Polym. Environ.*, 1(1), p 11 - 21.
97. Queimada, A. J., Marrucho, I. M., Stenby, E.H. and Coutinho, J.A.P. (2004). "Generalized relation between surface tension and viscosity: a study of pure and mixed *n*-alkanes", *Fluid. Phase. Equilibria.*, 222-223, p 161 - 168.
98. Quicker, G., Schumpe, A. and Deckwer, W.D. (1984). "Gas-liquid interfacial areas in a bubble column with suspended solids", *Chem. Eng. Sci.*, 39(1), p 183 - 185.
99. Reese, J., Jiang, P. and Fan, L.S. (1996). "Bubble characteristics in three-phase systems used for pulp and paper processing", *Chem. Eng. Sci.*, 51(10), p 2501 - 2510.
100. Ruchti, G., Dunn, I.J. and Bourne, J.R. (1981). "Comparison of dynamic oxygen electrode methods for measurement of K_La ", *Biotechnol. Bioeng.*, 23, p 277 - 290.
101. Sada, E., Kumazawa, H. and Lee, C.H. (1986). "Influences of suspended fine particles on gas hold-up and mass transfer characteristics in a slurry bubble column", *AIChE J.*, 32(5), p 853 - 855.
102. Salvacion, J.L., Murayama, M., Ohtaguchi, K. and Koide, K. (1995). "Effects of alcohols on gas hold-up and volumetric liquid phase mass transfer coefficient in gel suspended bubble column", *Japan. Chem. Eng.*, 28(4), p 434 - 441.
103. Seborg, D.E., Edgar, T.F. and Mellichamp, D.A. (1989). Process dynamics and control. Wiley Series in Chemical Engineering. 43-48; 101 - 117 p.
104. Schäfer, R., Merten, C. and Eigenberger, G. (2002). "Bubble size distributions in a bubble column reactor under industrial conditions", *Exp. Therm. Fluid Sci.*, 26(6/7), p 595 - 604.
105. Schumpe, A. and Deckwer, W.D. (1982). "Gas hold ups, specific interfacial areas and mass transfer coefficients of aerated carboxymethyl cellulose solutions in a bubble column", *Ind. Eng. Chem. Eng. Res. Des.*, 21, p 706 - 711.
106. Shennan, J.L. and Levi, J.D. (1974). The growth and yeasts on hydrocarbons. In: *Progress in Industrial Microbiology*. Hockenhull, D.J.D., editor. Edinburgh, Churchill Livingstone, Vol. 13, p 1 - 57.

107. Shuler, M.L. and Kargi, F. (2002). Bioprocess engineering: Basic concepts. *Physical and Chemical Engineering Sciences*. Amundson, N.R., editor. 2nd Ed. Upper Saddle River, Prentice-Hall, Inc. p 1 - 553.
108. Singer, M.E. and Finnerty, W.R. (1984). Microbial metabolism of straight-chain and branched alkanes. In: *Petroleum Microbiology*. Atlas, R.M., editor. New York, MacMillan. p 1 - 59.
109. Sridhar, T. and Potter, O.E. (1980). "Gas holdup and bubble diameters in pressurized gas-liquid stirred vessels", *Ind. Eng. Chem. Fund.*, 19(1), p 21 - 26.
110. Stellenbosch University Physical Chemistry 324 (2009). Practical manual guide. p 1 - 3.
111. Sun, Y. and Furusaki, S. (1988). "Mean bubble diameter and oxygen transfer coefficient in a three-phase fluidized bed bioreactor", *Japan. Chem. Eng. J.*, 21(1), p 20 - 24.
112. Tribe, L.A., Briens, C.L. and Margaritis, A. (1995). "Determination of the volumetric mass transfer coefficient using the dynamic gassing out method: Analysis of errors caused by dissolved oxygen probes", *Biotechnol. Bioeng.*, 46, p 388 - 392.
113. van der Meer, A.B., Beenackers, A. A. C. M., Burghard, R., Mulder, N.H. and Fok, J. H. (1992). "Gas/liquid mass transfer in a four phase stirred fermenters: Effects of organic phase hold up and surfactant concentration", *Chem. Eng. Sci.*, 47(9-11), p 2369 - 2374.
114. van Dierendonck, L.L., Fortuin, J.M.F. and Vanderbos, D. (1968). Proceedings on the 4th European Symposium on Chemical Reactor Engineering, Brussels, 9 September.
115. van Weert, G., van der Werff, D. and Derksen, J.J. (1995). "Transfer of oxygen from air to mineral slurries in a Rushton turbine agitated tank", *Minerals. Eng.*, 8(10), p 1109 - 1124.
116. Vandu, C.O. and Krishna, R. (2003). "Gas hold-up and volumetric mass transfer coefficient in a slurry bubble column", *Chem. Eng. Technol.*, 26, p 779 - 782.
117. Vandu, C.O. and Krishna, R. (2004). "Volumetric mass transfer coefficients in slurry bubble columns operating in the churn-turbulent flow regime", *Chem. Eng. Pro.*, 43, p 987 - 995.

118. Van't Riet, K. (1979). "Review of measuring methods and results in no viscous gas-liquid mass transfer in stirred vessels", *Ind. Eng. Chem. Proc. Des. Dev.*, 18(3), p 357 - 364.
119. Vining, G.G. (1998). *Statistical methods for Engineers*. Brooks/Cole Publishing Co. p 353 - 450.
120. Westerterp, K.R., van Dierendonck, L.L. and de Kraa, J.A. (1963). "Interfacial areas in agitated gas-liquid contactors", *Chem. Eng. Sci.*, 18(3), p 157 - 176.
121. Whitman, W.G. (1923). "Preliminary experimental confirmation of the two-film theory of gas absorption", *Chem. Metall. Eng.*, 29, p 146 - 148.
122. Yagi, H. and Yoshida, F. (1974). "Oxygen absorption in fermenters-Effects of surfactants, antifoaming agents and sterilized cells", *J. Ferment. Technol.*, 52(12), p 905 - 916.
123. Yoshida, F. and Miura, Y. (1963). "Gas absorption in agitated gas-liquid contactors", *Ind. Eng. Chem. Proc. Des. Dev.*, 2(4), p 263 - 268.
124. Zahradnik, J., Drapal, L. and Kstanek, F. (1992). "Hydrodynamics and mass transfer characteristics of sectionalized aerated slurry reactors", *Chem. Eng. and. Pro.*, 31, p 263 - 272.
125. Zahradnik, J., Fialova, M. and Linek, V. (1999). "The effect of surface active substances on bubble coalescence in aqueous media", *Chem. Eng. Sci.*, 54, p 4757 - 4766.

APPENDICES

A.1: Derivation of first order response model used for measurement of the overall volumetric oxygen transfer coefficient

According to the two film theory Fick's law can be applied to the oxygen transfer between the gas phase (equation A1.1) and liquid phase (equation A1.2) if it is assumed that the rate of DO transfer is directly proportional to the concentration gradient and the area available for transport.

$$N_{O_2G} = k_G a (C_G - C_{Gi}) \quad [A1.1]$$

$$N_{O_2L} = k_L a (C_{Li} - C_L) \quad [A1.2]$$

If oxygen transfer occurs at steady state, there will be no DO accumulation in the liquid or at the interface i.e. any oxygen transported through the gas phase will be transported to the liquid phase hence $N_{O_2G} = N_{O_2L}$. Therefore the OTR will be referred as N_{O_2} only. The equilibrium concentration of the gas phase will be directly proportional to the liquid phase concentration when equilibrium exists at the interface (equation A1.3) (Doran, 1995).

$$C_{Gi} = m C_{Li} \quad [A1.3]$$

Where m is the oxygen distribution coefficient

Or alternatively this gas phase concentration at equilibrium, which is proportional to the liquid phase concentration at equilibrium (equation A1.3), can be written in the form represented by equation A1.4;

$$C_{Li} = \frac{C_{Gi}}{m} \quad [A1.4]$$

Equations A1.3 and A1.4 are then used to eliminate the interfacial concentrations (C_{Gi} and C_{Li}) in equations A1.1 and A1.2. On substitution of equation A1.3 into equations A1.1, equation A1.5 is obtained for the gas phase transfer. Likewise, substitution of equation A1.4 into equation A1.2, equation A1.6 is obtained for the liquid phase transfer:

$$\frac{N_{O_2}}{k_G a} = C_G - m C_{Li} \quad [A1.5]$$

$$\frac{N_{O_2}}{k_L a} = \frac{C_{Gi}}{m} - C_L \quad [A1.6]$$

Upon re-arranging equation A1.2 and multiplying the result by m , the oxygen distribution factor equation A1.7 is obtained. On substitution of equation A1.3 into A1.7, equation A1.8 is obtained.

$$\frac{mN_{O_2}}{k_L a} = mC_{Li} - mC_L \quad [A1.7]$$

$$\frac{mN_{O_2}}{k_L a} = C_{Gi} - mC_L \quad [A1.8]$$

Likewise, re-arranging equation A1.1 and dividing the result by m equation A1.9 is obtained. On substitution of equation A1.4 into A1.9, equation A1.10 is obtained.

$$\frac{N_{O_2}}{mk_G a} = \frac{C_G}{m} - \frac{C_{Gi}}{m} \quad [A1.9]$$

$$\frac{N_{O_2}}{mk_G a} = \frac{C_G}{m} - C_{Li} \quad [A1.10]$$

The interfacial term for the gas phase (C_{Gi}) can now be eliminated by adding equations A1.5 and A1.8 together to yield equation A1.11. Likewise, the interfacial term for the liquid phase (C_{Li}) can be eliminated by adding equations A1.6 and A1.10 together to yield equation A1.12. This is done under the condition that there is no accumulation at the gas-liquid interface i.e. $C_{Gi} = mC_{Li}$.

$$N_{O_2} \left(\frac{1}{k_G a} + \frac{m}{k_L a} \right) = C_G - mC_L \quad [A1.11]$$

$$N_{O_2} \left(\frac{1}{mk_G a} + \frac{1}{k_L a} \right) = \frac{C_G}{m} - C_L \quad [A1.12]$$

The oxygen transfer coefficient for the gaseous phase resistance can be defined as K_G (equation A1.13). Likewise the DO transfer coefficient liquid phase resistance can then be defined as K_L (equation A1.14).

$$\frac{1}{K_G a} = \frac{1}{k_G a} + \frac{m}{k_L a} \quad [A1.13]$$

$$\frac{1}{K_L a} = \frac{1}{mk_G a} + \frac{1}{k_L a} \quad [A1.14]$$

When equation A1.13 is substituted into equation A1.11, equation A1.15 according to the gas phase resistance is obtained. If equation A1.14 is substituted into equation A1.12, equation A1.16 according to the liquid phase resistance is obtained. Equations A1.15 and A1.16 represent the oxygen transfer rate in the gas-liquid system.

$$N_{O_2} = K_G a (C_G - mC_L) \quad [A1.15]$$

$$N_{O_2} = K_L a \left(\frac{C_G}{m} - C_L \right) \quad [A1.16]$$

Equations A1.15 and A1.16 are usually expressed using equilibrium concentrations for the gaseous phase (equation A1.17) and for the liquid phase (equation A1.18) (Doran, 1995).

$$mC_L = C_G^* \quad [A1.17]$$

$$\frac{C_G}{m} = C_L^* \quad [A1.18]$$

Substitution of equation A1.17 into equation A1.15 results in equation A1.19 which defines OTR according to the gas phase resistance. Likewise, substitution of equation A1.18 into equation A1.16 results in equation A1.20 which defines OTR according to the liquid phase resistance (Doran, 1995).

$$N_{O_2} = K_G a (C_G - C_G^*) \quad [A1.19]$$

$$N_{O_2} = K_L a (C_L^* - C_L) \quad [A1.20]$$

If resistance to oxygen transfer is predominantly controlled by the gas phase resistance, i.e. $k_G \gg k_L$, the oxygen transfer coefficient for the gas phase is defined as K_G . The OTR according to the gas phase resistance (equation A1.19) is used to predict the oxygen transfer rate and equation A1.13 will reduce to $1/K_G a \gg \gg 1/k_G a$.

Likewise if resistance to DO transfer is predominantly controlled by the liquid phase resistance, i.e. $k_G \ll k_L$, the overall DO transfer coefficient in the liquid phase is defined as K_L . The DO transfer rate according to the liquid phase resistance (equation A1.20) is used to predict the DO transfer rate and equation A1.14 will reduce to $1/K_L a \gg \gg 1/k_L a$.

Since the liquid phase DO transfer resistance will dominate due to oxygen poor solubility (Doran, 1995), the DO transfer rate in the fluid is defined by equation A1.21.

This is the first order response model used for $K_L a$ measurement in the gassing out procedure (Mimura *et al.*, 1973; Hassan and Robinson, 1977a; Clarke *et al.*, 2006; Correia and Clarke, 2009).

$$N_{O_2} = OTR = \frac{dC}{dt} = K_L a (C^* - C) \quad [A1.21]$$

A.2: Laplace transforms solution for second order response model used for measurement of the overall volumetric oxygen transfer coefficient

A Laplace transform is an integral transform that is denoted by $\mathfrak{L}[f(t)]$ as the linear operator of an original function $f(t)$ with $t \geq 0$ that transforms into an image function $F(s)$ with a complex argument s (equation A2.1) (Seborg *et al.*, 1989; Marlin, 1995).

$$F(s) = \mathfrak{L}[f(t)] = \int_0^{\infty} f(t) e^{-st} dt \quad [\text{A2.1}]$$

A general first order response model has a transfer function with an output variable, $Y(s)$ and an input variable; $X(s)$ (equation A2.2) (Seborg *et al.*, 1989; Marlin, 1995).

$$\frac{Y(s)}{X(s)} = \frac{K}{\tau s + 1} \quad [\text{A2.2}]$$

Where K is the process gain (-) and τ is the time constant (s^{-1}).

For a step input as applied in cases when measuring the DO probe response and $K_L a$, the step input is denoted with magnitude M . The input variable, $X(s)$ will then equal to the step input magnitude divided by the complex argument (equation A2.3).

$$X(s) = \frac{M}{s} \quad [\text{A2.3}]$$

The output variable, $Y(s)$ from equation A2.2 can therefore be represented by equation A2.4 after incorporating equation A2.3.

$$Y(s) = \frac{KM}{s(\tau s + 1)} \quad [\text{A2.4}]$$

Where KM is a lumped constant for the process gain and the step input magnitude that represent the final steady state value after a step change i.e. the DO saturation in this case.

Using the Laplace transform for the first order response model with a step change time domain function (Table A2.1), the output variable after a step change (equation A2.4), the time domain (equation A2.5) is obtained (Seborg *et al.*, 1989; Marlin, 1995).

$$y(t) = KM \left(1 - e^{-t/\tau} \right) \quad [\text{A2.5}]$$

Table A2.1: Laplace transforms for 1st and 2nd order models (Seborg *et al.* 1989)

Model	f(t)	F(s)
1 st order model due to a step change	$\left(1 - e^{-t/\tau}\right)$	$\frac{1}{s(\tau s + 1)}$
2 nd order model	$\frac{1}{\tau_1 - \tau_2} \left(e^{-t/\tau_1} - e^{-t/\tau_2} \right)$	$\frac{1}{(\tau_1 s + 1)(\tau_2 s + 1)}$

If the output variable for the transfer function after a step change (equation A2.5) is applied to both the first order response model for the DO transfer rate (equation A2.6) and the first order response model for the DO probe response (equation A2.7), equations A2.8 and A2.9 are obtained respectively with $K_M = C^* = C_p^*$ at saturation conditions and $t_0 = 0$ and $C(t)$ and $C_p(t)$ as the output variables.

$$\frac{dC}{dt} = K_L a (C^* - C) \quad [A2.6]$$

$$\frac{dC_p}{dt} = K_p (C_p^* - C_p) \quad [A2.7]$$

$$C(t) = C^* \left(1 - e^{-K_L a t}\right) \quad [A2.8]$$

$$C_p(t) = C_p^* \left(1 - e^{-K_p t}\right) \quad [A2.9]$$

A second order transfer function (equation A2.10) results whenever two first order processes are connected in series (Figure A2.1). In our case this applies to the DO probe first order response model (equation A2.7) which is used to measure $K_L a$ and the first order response model for DO transfer rate (equation A2.6).

$$\frac{Y(s)}{X(s)} = \frac{K_1 K_2}{(\tau_1 s + 1)(\tau_2 s + 1)} = \frac{K}{(\tau_1 s + 1)(\tau_2 s + 1)} \quad [A2.10]$$

Where K_1 and K_2 are process gain constant for both first order models.

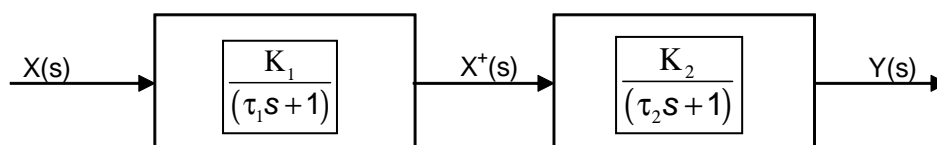


Figure A2.1 Two first order models in series which yield an overall second order model (Seborg *et al.*, 1989)

Using the Laplace transform for a second order response time domain functions, the transfer function for a 2nd order model (equation A2.10), the time domain (equation A2.11) is obtained (Table A2.1) (Seborg *et al.*, 1989; Marlin, 1995).

$$y(t) = \frac{1}{\tau_1 - \tau_2} \left(e^{-t/\tau_1} - e^{-t/\tau_2} \right) \quad [\text{A2.11}]$$

The time domain (equation A2.11) implies that τ_1 is $1/K_L a$ and τ_2 is $1/K_p$ since the DO probe, which has a first order response model is being introduced in series with the oxygen transfer rate first order response model in the alkane multiphase system. This also implies that $K_1 = 1/K_L a$ and $K_2 = 1/K_p$.

The time domain (equation A2.11) will therefore be represented by equation A2.12 and can be reduced in the form represented by equation A2.13.

$$y(t) = \frac{1}{\frac{1}{K_L a} - \frac{1}{K_p}} \left(K_1 e^{-t/\frac{1}{K_L a}} - K_2 e^{-t/\frac{1}{K_p}} \right) \quad [\text{A2.12}]$$

$$y(t) = \frac{K_L a K_p}{K_p - K_L a} \left(K_1 e^{-K_L a t} - K_2 e^{-K_p t} \right) \quad [\text{A2.13}]$$

Equation A2.13 reduces to equation A2.14 after substituting the process gain constants K_1 and K_2 .

$$y(t) = \frac{1}{K_p - K_L a} \left(K_p e^{-K_L a t} - K_L a e^{-K_p t} \right) \quad [\text{A2.14}]$$

The time domain for DO concentration change indicated by the DO probe, C_p , is represented by equation A2.14 at any given time which then takes the form of equation A2.15 since the response is a second order form for both the DO probe and the DO transfer.

$$y(t) = \left(\frac{C_p^* - C_p}{C_p^* - C_{p0}} \right) \quad [\text{A2.15}]$$

This implies that equation A2.14 = equation A2.15, and an equation represented by A2.16 is obtained.

$$\left(\frac{C_p^* - C_p}{C_p^* - C_{p0}} \right) = \frac{1}{K_p - K_L a} \left[K_p e^{-K_L a t} - K_L a e^{-K_p t} \right] \quad [\text{A2.16}]$$

If initial conditions are considered; $C_{p0} = 0$ at $t_0 = 0$; equation A2.16 reduces to equation A2.17 and A2.18 (Fuchs *et al.*, 1971; Nakanoh and Yoshida, 1980; Keitel and Onken, 1981; Letzel *et al.*, 1999; Vandu and Krishna, 2004).

$$\left(1 - \frac{C_p}{C_p^*}\right) = \frac{1}{K_p - K_L a} \left[K_p e^{-K_L a t} - K_L a e^{-K_p t} \right] \quad [\text{A2.17}]$$

$$\frac{C_p}{C_p^*} = 1 - \frac{1}{K_p - K_L a} \left[K_p e^{-K_L a t} - K_L a e^{-K_p t} \right] \quad [\text{A2.18}]$$

This, equation A2.18 is the second order response model used to measure $K_L a$ accurately in the hydrocarbon multiphase systems.

A.3: Analytical derivation of second order response model used for measurement of the overall volumetric oxygen transfer coefficient

The rate of DO transfer in hydrocarbon multiphase phase systems has a first order response model (equation A3.1) (Mimura *et al.*, 1973; Hassan and Robinson, 1977a; Clarke *et al.*, 2006).

$$\frac{dC}{dt} = K_L a (C^* - C) \quad [A3.1]$$

The DO probe used to measure the DO change also has a first order response model (equation A3.2) (Aiba and Huang, 1969; Van't Riet 1979; Ruchti *et al.*, 1981; Godbole *et al.*, 1984; Tribe *et al.*, 1994; Luyben and Luyben, 1997; Nikolov *et al.*, 2000; Juarez and Orens, 2001).

$$\frac{dC_p}{dt} = K_p (C_p^* - C_p) \quad [A3.2]$$

Dimensionless quantities are introduced (equations A3.3 and A3.4) for both the DO transfer rate (equation A3.1) and the DO probe response (equation A3.2) respectively (Fuchs *et al.*, 1971):

$$Y = \left(\frac{C^* - C}{C^* - C_o} \right) \quad [A3.3]$$

$$Y_p = \left(\frac{C_p^* - C_p}{C_p^* - C_{p0}} \right) \quad [A3.4]$$

In these expressions (equations A3.3 and A3.4), C_{p0} and C_o represent the DO concentration at initial conditions and C_p^* and C^* represent the DO concentration at saturation conditions.

DO concentration outputs cannot be used to represent the actual DO concentration due to K_p effects. In actual fact, the DO concentration indicated by the oxygen probe, C_p , as a function of time, t , is related to the actual concentration by equation A3.5. This equation A3.5 represents the DO change as a function of time with the K_p effects incorporated (Fuchs *et al.*, 1971; Nielsen *et al.*, 2003; Vandu and Krishna, 2004).

$$\frac{dC_p}{dt} = K_p (C - C_p) \quad [A3.5]$$

The dimensionless quantity for oxygen transfer (equations A3.3) was substituted into the oxygen transfer rate (equation A3.1) resulting in equation A3.6. Likewise the dimensionless quantity for the DO probe (equation A3.4) was substituted into the actual DO change that is taking place with the DO probe lag time incorporated (equation A3.5) resulting in equation A3.7.

$$\frac{dY}{dt} = -K_L a Y \quad [A3.6]$$

$$\frac{dY_p}{dt} = K_p (Y - Y_p) \quad [A3.7]$$

Re-arranging and integrating the oxygen transfer rate equation with its dimensionless constant substituted (equation A3.6) obtained equations A3.8-A3.10:

$$\int \frac{dY}{Y} = -\int K_L a dt \quad [A3.8]$$

$$\ln Y = e^{-K_L a t} + C \quad [A3.9]$$

$$Y = C e^{-K_L a t} \quad [A3.10]$$

Expanding and separating variables in the actual DO change taking place with its dimensionless constant substituted (equation A3.7) yields equation A3.11.

$$\frac{dY_p}{dt} = K_p Y - K_p Y_p \quad [A3.11]$$

Upon substitution of equation A3.10 into A3.11, equation A3.12 is obtained.

$$\frac{dY_p}{dt} = K_p C e^{-K_L a t} - K_p Y_p \quad [A3.12]$$

Equation A3.12 is then solved using the linear non-homogeneous differential equations concept by separating variables and integrating to yield equations A3.13-A3.32.

$$\frac{dY_p}{dt} + K_p Y_p = 0 \quad [A3.13]$$

$$\int \frac{dY_p}{Y_p} = -\int K_p dt \quad [A3.14]$$

$$\ln Y_p = e^{-K_p t} + D \quad [A3.15]$$

$$Y_p = De^{-K_p t} \quad [A3.16]$$

The function from equation A3.16 is in the form represented by equation A3.17 and the complimentary function represented by equation A3.18.

$$f = B' e^{-A' t} \quad [A3.17]$$

Such that the complimentary function is represented by equation A3.18.

$$Y_c = B' e^{-A' t} \quad [A3.18]$$

The complimentary form for equation A3.12 is represented by equation A3.19 which upon re-arranging equation A3.20 is obtained.

$$\frac{dY_c}{dt} + K_p Y_c = K_p B' e^{-A' t} - B' A' e^{-A' t} \quad [A3.19]$$

$$\frac{dY_c}{dt} + K_p Y_c = (K_p B' - B' A') e^{-A' t} \quad [A3.20]$$

Equation A3.20 can also be written in the form represented by equation A3.21 since it is a complimentary form of equation A3.12.

$$\frac{dY_c}{dt} + K_p Y_c = K_p C e^{-K_L a t} \quad [A3.21]$$

Equating equation A3.20 and A3.21 implies that:

$$A' = K_L a \quad [A3.22]$$

And

$$(K_p B' - B' A') = K_p C \quad [A3.23]$$

$$B' (K_p - A') = K_p C \quad [A3.24]$$

$$B' = \frac{K_p C}{K_p - A'} = \frac{K_p C}{K_p - K_L a} \quad [A3.25]$$

But the complimentary form (Y') is a combination of both the DO change in the multiphase systems and the DO probe response i.e.

$$Y' = Y_p + Y_c \quad [A3.26]$$

Equation A3.26 represents our function and the complimentary form for the DO change with the DO probe response dynamics incorporated.

Substitution of equations A3.16 and A3.18 into equation A3.26 results into equation A3.27 with substitution of B' from equation A3.25.

$$Y' = De^{-K_p t} + \frac{K_p C}{K_p - K_L a} e^{-K_L a t} \quad [A3.27]$$

Upon re-arranging and expanding of equation A3.27 yields equation A3.28.

$$Y' = \frac{1}{K_p - K_L a} \left[D(K_p - K_L a) e^{-K_p t} + K_p C e^{-K_L a t} \right] \quad [A3.28]$$

Equation A3.28 implies that:

$$D(K_p - K_L a) = -K_L a; C = 1 \quad [A3.29]$$

Or upon further simplification equation A3.29 can be represented by equation A3.30.

$$D = \frac{-K_L a}{K_p - K_L a}; C = 1 \quad [A3.30]$$

Equation A3.28 can therefore be written as equation A3.31 after substituting equation A3.30.

$$Y' = \frac{1}{K_p - K_L a} \left[-K_L a e^{-K_p t} + K_p e^{-K_L a t} \right] \quad [A3.31]$$

If Y' from equation A3.26 is equal to the actual change in DO with probe characteristics incorporated, equation A3.32 is obtained.

$$Y' = \left(\frac{C_p^* - C_p}{C_p^* - C_{p0}} \right) \quad [A3.32]$$

Equating equation A3.31 and equation A3.32 yields the second order response model used for $K_L a$ measurement in the hydrocarbon multiphase systems (equation A3.33).

$$\left(\frac{C_p^* - C_p}{C_p^* - C_{p0}} \right) = \frac{1}{K_p - K_L a} \left[K_p e^{-K_L a t} - K_L a e^{-K_p t} \right] \quad [A3.33]$$

This 2nd order response model (equation A3.33) reduces to equations A3.34-A3.37 upon further simplification considering initial conditions when $C_{p0} = 0$ and $t_0 = 0$ (Fuchs *et al.*, 1971; Nakanoh and Yoshida, 1980; Keitel and Onken, 1981; Letzel *et al.*, 1999; Vandu and Krishna, 2004). These equations are in the form represented by equation A2.18.

$$\left(1 - \frac{C_p}{C_p^*}\right) = \frac{1}{K_p - K_L a} \left[K_p e^{-K_L a t} - K_L a e^{-K_p t} \right] \quad [\text{A3.34}]$$

$$\frac{C_p}{C_p^*} = 1 - \frac{1}{K_p - K_L a} \left[K_p e^{-K_L a t} - K_L a e^{-K_p t} \right] \quad [\text{A3.35}]$$

The DO probe response lag time (τ_p) can also be expressed as the inverse of the DO probe response lag time (K_p) i.e. $\tau_p = 1/K_p$ (Merchuk *et al.*, 1990), substitution of τ_p into equation A3.35 results in equation A3.36 (Garcia-Ochoa and Gomez, 2009).

$$\frac{C_p}{C_p^*} = 1 + \frac{1}{1 - \tau_p K_L a} \left[\tau_p K_L a e^{-t/\tau_p} - e^{-K_L a t} \right] \quad [\text{A3.36}]$$

A.4: Characteristics of the probe and derivation of the probe response lag time

A4.1: Probe characteristics

The DO probe used in this work for DO measurements was a 12mm Mettler Toledo membrane type which was used for DO transfer from the fluid film to the electrolyte and KCl was used as the electrolyte. This electrolyte provided a full circuit for the electrolytic reactions to occur between the anode and cathode. Redox equations occur at the probe silver anode and the platinum cathode during DO change measurements (equations A4.1-A4.3) (Mettler Toledo instrument manual, 2005).

Cathode reaction:



Anode reaction:



Overall reaction:

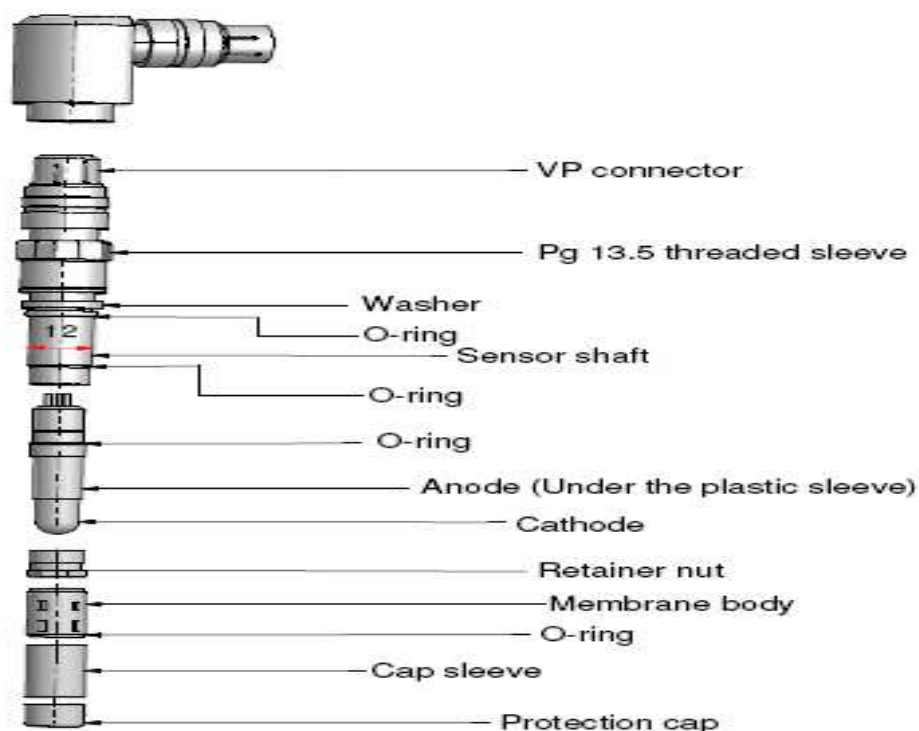


Figure A4.1 Mettler Toledo InPro® 6800 DO probe used for %DO change measurements (Redrawn from Mettler Toledo Instrument manual)

The DO probe was first polarized for 6 hours before calibration. K_{La} , τ_p and K_p were then determined after the calibration procedure.

A4.2: Derivation of the probe response lag time

The DO probe used to measure the DO has a first order response model (equation A4.4) (Aiba and Huang, 1969). The DO probe response lag time (τ_p) is defined as the time for the DO to reach 63.2% of DO saturation after an experimental step change in the sparged gas (Van't Riet, 1979; Ruchti *et al.*, 1981; Tribe *et al.*, 1994; Luyben and Luyben, 1997; Nikolov *et al.*, 2000; Juarez and Oreans, 2001).

$$\tau_p \frac{dC_p}{dt} = C_p^* - C_p \quad [A4.4]$$

Where the DO probe response lag time can also be written as the inverse of the DO probe lag time (K_p) (equation A4.5) (Merchuk *et al.*, 1990).

$$\tau_p = 1/K_p \quad [A4.5]$$

Upon re-arranging the DO probe first order response model (equation A4.4), equations A4.6 and A4.7 are obtained.

$$\frac{dC_p}{dt} = \frac{C_p^* - C_p}{\tau_p} \quad [A4.6]$$

$$\frac{dC_p}{C_p^* - C_p} = \frac{1}{\tau_p} dt \quad [A4.7]$$

Upon integrating when $C_{p0} = 0$ and $t_0 = 0$ at initial conditions equation A4.7 and re-arranging, equations A4.8-A4.12 are obtained.

$$\ln\left(\frac{C_p^* - C_{p0}}{C_p^* - C_p}\right) = \frac{1}{\tau_p}(t - t_0) \quad [A4.8]$$

$$\ln\left(\frac{C_p^* - C_p}{C_p^* - C_{p0}}\right) = -\frac{1}{\tau_p}(t - t_0) \quad [A4.9]$$

At initial conditions for a non-respiring system; as in the alkane-solid-aqueous dispersions during DO absorption, $C_{p0} = 0$ and $t_0 = 0$, equation A4.9 can therefore be represented as equations A4.10.

$$\ln\left(\frac{C_p^* - C_p}{C_p^*}\right) = -\frac{1}{\tau_p} t \quad [A4.10]$$

Upon linearization of equation A4.10 and re-arranging, equations A4.11-A4.12 are obtained.

$$1 - \frac{C_p}{C_p^*} = e^{-\frac{t}{\tau_p}} \quad [A4.11]$$

$$\frac{C_p}{C_p^*} = 1 - e^{-\frac{t}{\tau_p}} \quad [A4.12]$$

The DO probe response lag time is then determined when the time of experiment is equal to the DO response lag time i.e. $t = \tau_p$ (Luyben and Luyben, 1997). The DO probe response (equation A4.12) at this condition can be represented by equation A4.13 which upon further simplification results in equation A4.14 which shows the fraction of C_p over C_p^* at that particular time as 0.632. The time at which this fraction is 63.2% of the final steady state value corresponds to the DO response lag time.

$$\frac{C_p}{C_p^*} = 1 - e^{-\frac{\tau_p}{\tau_p}} = 1 - e^{-1} \quad [A4.13]$$

$$\frac{C_p}{C_p^*} = 0.632 \quad [A4.14]$$

A.5: Sample calculation of the overall volumetric oxygen transfer coefficient using the second order response model

Equation solver was used to minimize the sum of errors between the GOP (lag) second order response model and the GOP (no lag) first order response model by changing K_{La} in the target cell. K_{La} from the first order response model was used as the initial K_{La} and changed depending on the K_p value. The actual K_{La} was obtained when the sum of errors between the %DO from the first order response model and the %DO second order response model was minimal per finite time. Table A5.1 shows a sample K_{La} calculation in Excel. The initial K_{La} from the first order response model was 0.0453s^{-1} and when a K_p of 0.0440s^{-1} was incorporated to the %DO change in the second order response model, K_{La} increased to 0.0823 s^{-1} with a minimal sum of errors of 152.7.

Table A5.1: Sample K_{La} calculation using the second order response model in Excel

Time	%DO (1 st order model)	%DO (2 nd order model)	Σ Errors
0	0.0	0.0	0.00
10	4.0	12.1	65.08
20	27.3	33.1	33.08
30	51.7	52.4	0.44
40	69.8	67.3	6.06
50	81.6	78.1	12.26
60	88.8	85.5	10.78
70	93.3	90.5	7.80
80	95.9	93.8	4.35
90	97.6	96.0	2.61
100	98.8	97.4	1.96
110	99.6	98.3	1.64
120	100.1	98.9	1.40
130	100.5	99.3	1.44
140	100.7	99.5	1.32
150	100.8	99.7	1.19
160	100.9	99.8	1.18
Final	101.0		$\Sigma 152.57$

A.6: Theory on fluid viscosity and surface tension measurement

The $n\text{-C}_{14-20}$ -aqueous dispersions with solids particles were first homogenized before viscosity and surface tension measurements. This was done to ensure uniformity of the dispersion for accurate measurements.

A.6.1 The homogenization process

A lab bench model homogenizer was used for homogenization (Figure A6.1). Homogenization is the breaking down of the dispersed particles under pressure which is created when the dispersion is passed through a small orifice causing changes in physical properties of dispersion such that a uniform emulsion is obtained (Gous, 2003). The alkane-solid-aqueous dispersion was passed through a 4mm diameter non-return ball type valve by downward movement into the homogenizer cylinder. The dispersion was trapped within the cylinder by the plunger and spring which were tightly fitted inside the homogenizer cylinder. The plunger was divided into two sections; section 1 with a diameter of 4.5mm and section 2 with a diameter of 8mm, both with 0.25mm deep grooves (Figure A6.1). This was done to increase the homogenized surface area of fluid as it flowed down the cylinder. Pressure was created inside the cylinder due to the trapping of fluid forcing the 6mm diameter spring to compress. This forced the fluid to flow through the plunger grooves causing a shearing action to be exerted on the particles resulting in a uniformly distributed emulsion (Kirk-Othmer, 1978). The emulsion was then expelled from the cylinder to a 100ml beaker through a 4mm nozzle where it was subjected to a sudden pressure drop enhancing the uniformity of the alkane-solid-aqueous dispersion (Figure A6.1).

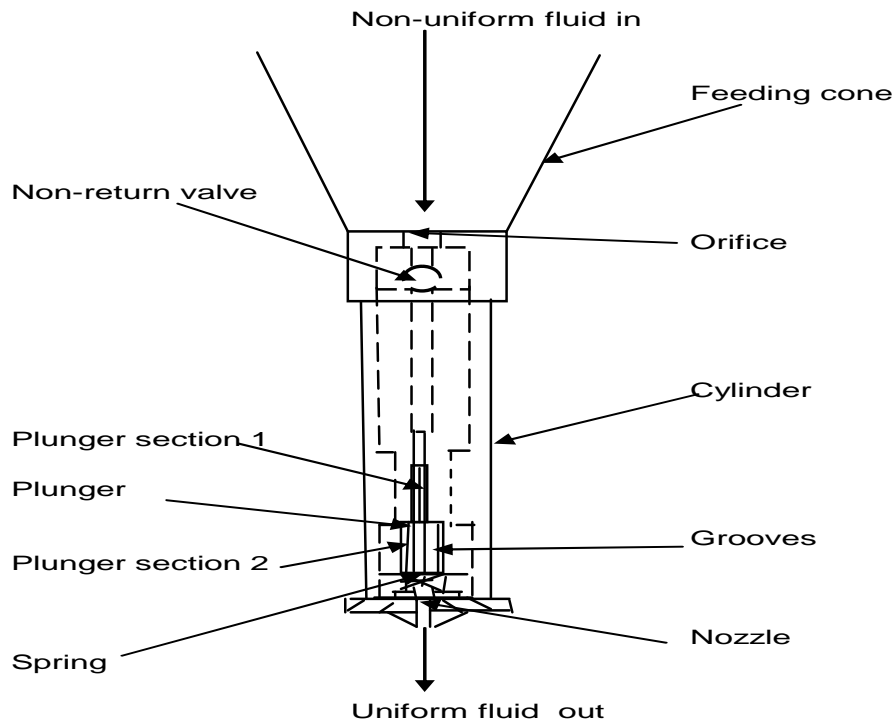


Figure A6.1 Homogenizer components (Gous, 2003)

A.6.2 Theory on fluid viscosity and surface tension

The dynamic viscosity of a fluid is related to the fluid's resistance to flow (Doran, 1995) and is determined through directly relating the velocity gradient of the fluid to its shear force (F) (equation A6.1).

$$\frac{dv}{dy} \propto F \quad [\text{A6.1}]$$

Where v is the fluid velocity (ms^{-1}) and y is the distance of fluid layer from the bottom plate (m).

If flow between two plates is considered with the top plate being stationary whilst the bottom plate is moved by a shear force, F , then a thin film of the fluid attaches itself to both plates. The fluid attached at the stationary plate will have a zero velocity whilst the bottom plate moves with the fluid. The fluid attached to the plates has the greatest velocity which decreases as the distance towards the stationary plate decreases (Doran 1995). The shear stress (τ) can therefore be said to be equal to the force per unit area of the fluid within the plates (equation A6.2).

$$\tau = \frac{F}{A} \quad [\text{A6.2}]$$

If the relationship of the fluid velocity gradient to the shear force (equation A6.1) and the fluid shear stress (equation A6.2) is combined, a proportionality relationship (equation A6.3) is obtained which reduces to Newton's Law of Viscosity (equation A6.4) with the dynamic viscosity (μ) as the constant of proportionality (Doran 1995).

$$\tau \propto \frac{dv}{dy} \quad [\text{A6.3}]$$

$$\tau = -\mu \frac{dv}{dy} \quad [\text{A6.4}]$$

The shear rate (γ) can therefore be described as $-dv/dy$ such that Newton's law of viscosity (equation A6.4) can also be represented by the ratio between the shear stress (τ) and the shear rate (γ) which is constant for Newtonian fluids (equation A6.5)

$$\frac{\tau}{\gamma} = \mu = \text{constant} \quad [\text{A6.5}]$$

The fluid surface tension is a property of a fluid that makes it behave as if its surface is enclosed in an elastic skin due to the effect of intermolecular forces surrounding each molecule in the fluid (<http://www.tutorvista.com/ks/defination-of-surface-tension>).

A.7: Reproducibility of raw data in the alkane multiphase systems

Experimental results for K_p , K_{La} , fluid viscosity and fluid surface tension were repeated 5 times in the alkane-aqueous dispersions and alkane-solid-aqueous dispersions for improved accuracy and an average result was used. All experiments were reproducible and a very small standard deviation was observed (see Figures A7.1-A7.4 and Tables A7.1-A7.20). Furthermore K_{La} results from n -C₁₀₋₁₃-aqueous-dispersions GOP (no lag) first order response model were reproducible to those of Correia (2007) under the same conditions with deviations as low as 2.2% according to a *t*-test analysis (see Figure A7.5 and Tables A7.8 and A7.12). The slight differences observed may be due to K_p effects since different membrane age and electrolyte ages were used.

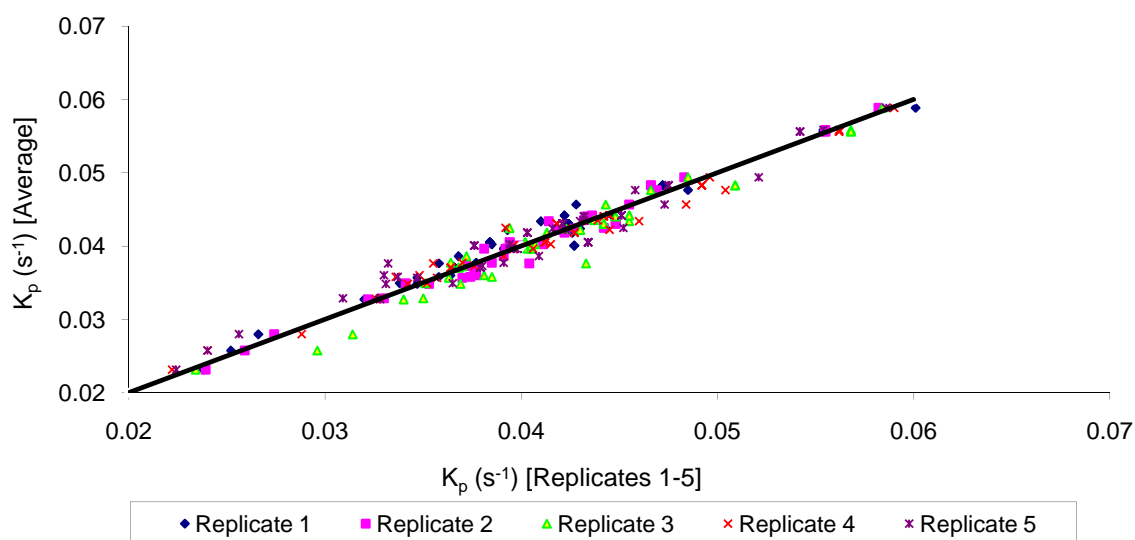


Figure A7.1 K_p reproducibility in the alkane multiphase systems

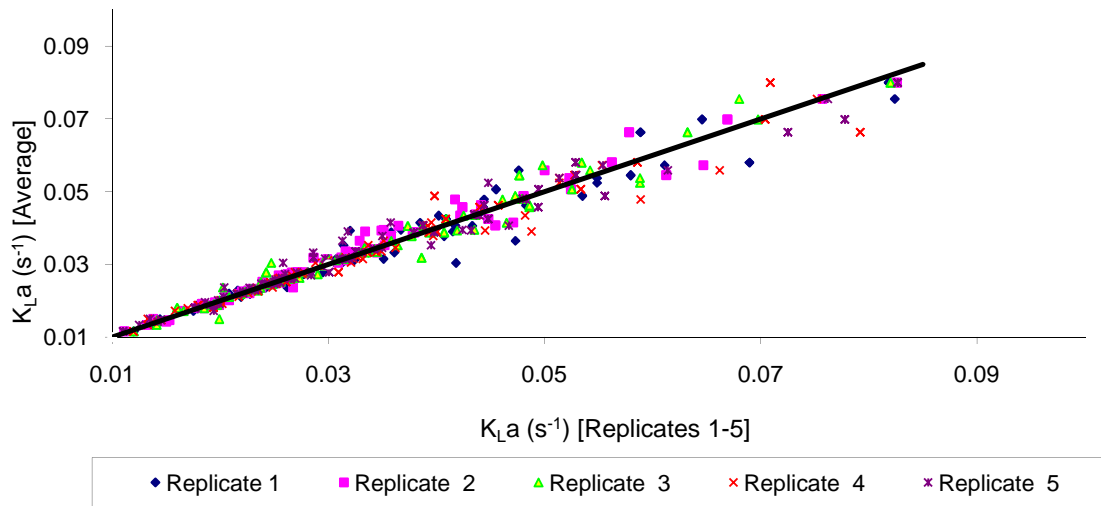


Figure A7.2 K_{La} reproducibility in the alkane multiphase systems

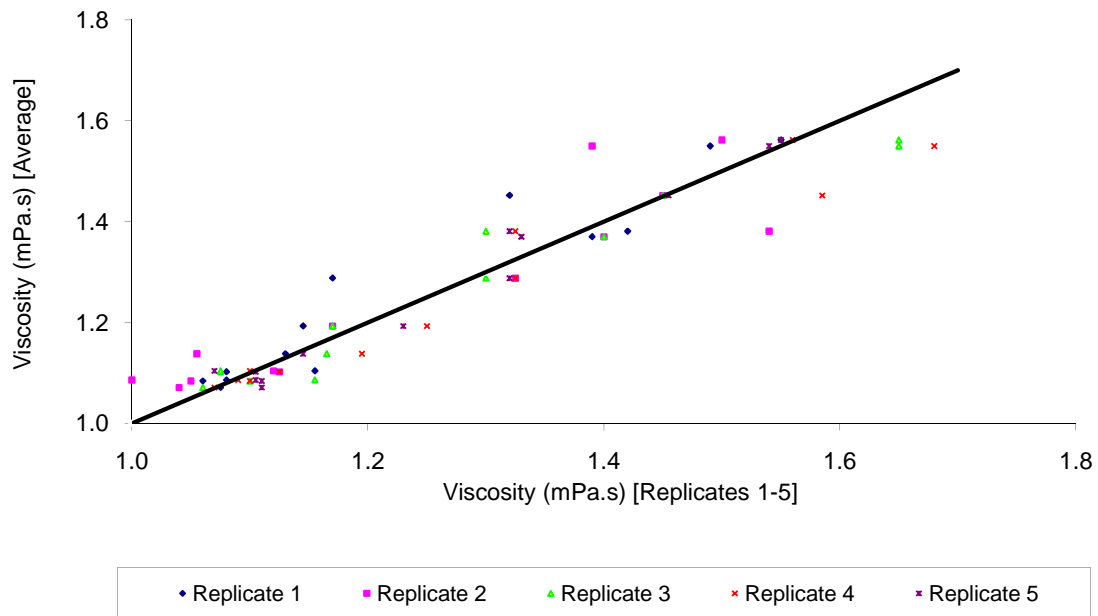


Figure A7.3 Fluid viscosity reproducibility in the alkane multiphase systems

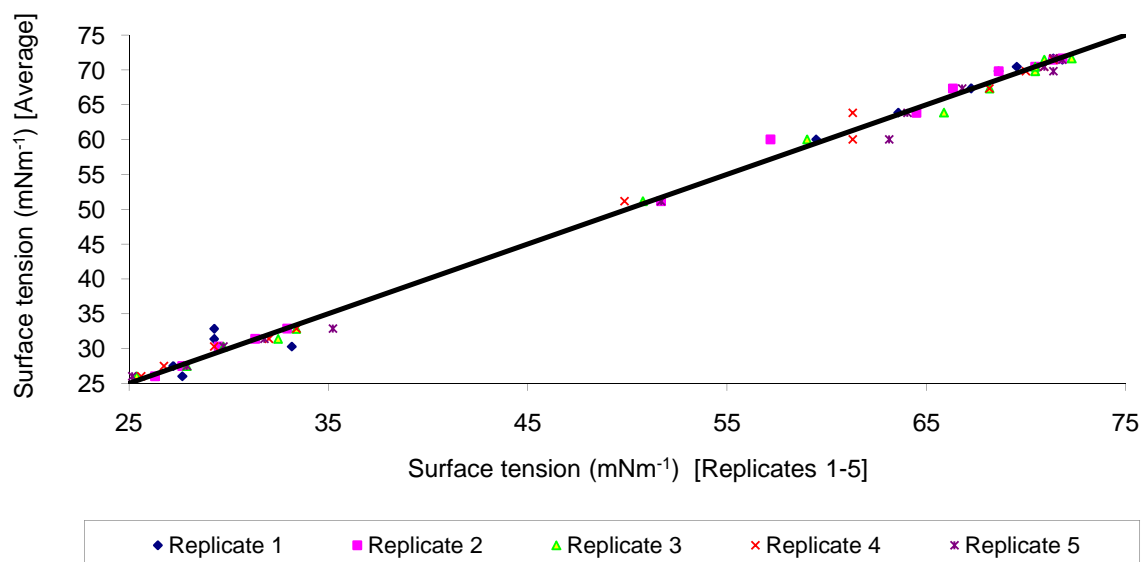


Figure A7.4 Fluid surface tension reproducibility in the alkane multiphase systems

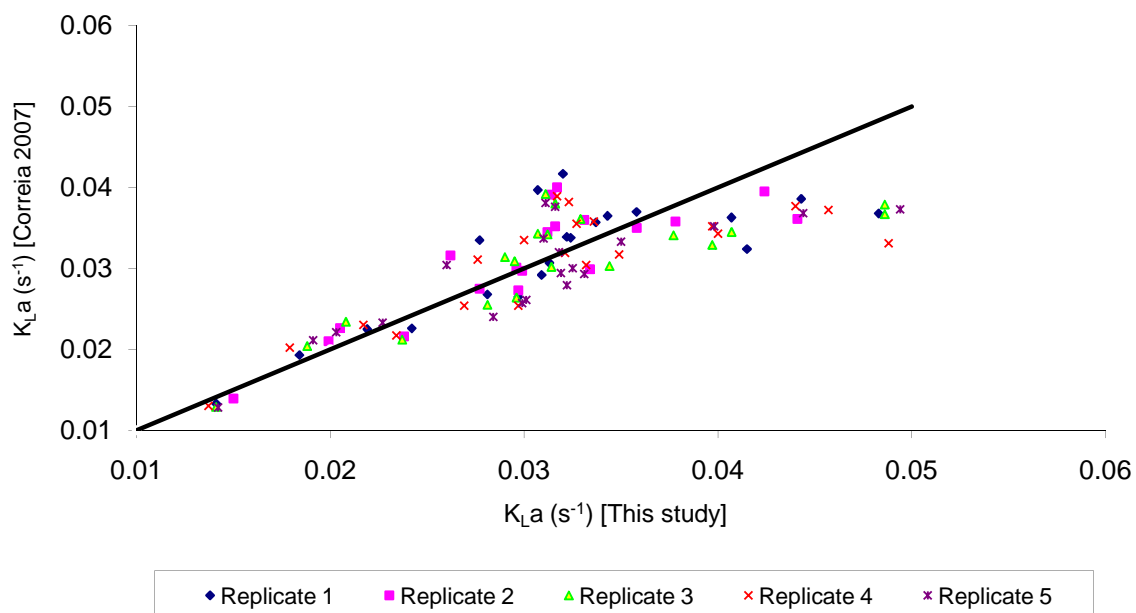


Figure A7.5 $K_{L,a}$ reproducibility in *n*-C₁₀₋₁₃-aqueous dispersions using the GOP (no lag) with same process conditions as Correia (2007)

Table A7.1: K_p data for influence of membrane age, electrolyte age and their interaction in 2.5% (v/v) n -C₁₄₋₂₀-aqueous dispersions

n -C ₁₄₋₂₀ (% v/v)	Agitation rate (rpm)	Membrane age (days)	Electrolyte age (days)	Replicates (K_p ; s ⁻¹)					Average	Standard deviation
				1	2	3	4	5		
2.5	1000	1	1	0.0554	0.0555	0.0568	0.0562	0.0554	0.0559	0.0006
2.5	1000	1	5	0.0398	0.0381	0.0403	0.0406	0.0394	0.0396	0.0010
2.5	1000	5	1	0.0428	0.0455	0.0443	0.0484	0.0473	0.0457	0.0023
2.5	1000	5	5	0.0327	0.0330	0.0350	0.0328	0.0309	0.0329	0.0015

Table A7.2: K_p data for influence of agitation rate, alkane concentration and their interaction in n -C₁₄₋₂₀-aqueous dispersions

n -C ₁₄₋₂₀ (% v/v)	Agitation rate (rpm)	Replicates (K_p ; s ⁻¹)					Average	Standard deviation
		1	2	3	4	5		
2.5	600	0.0430	0.0427	0.0423	0.0423	0.0416	0.0424	0.0005
2.5	1200	0.0410	0.0414	0.0455	0.0460	0.0430	0.0434	0.0023
20	600	0.0365	0.0372	0.0370	0.0376	0.0380	0.0373	0.0006
20	1200	0.0377	0.0385	0.0364	0.0370	0.0391	0.0377	0.0011

Table A7.3: K_p data for influence of alkane chain length, alkane concentration and their interaction in alkane-aqueous dispersions

Alkane conc. (% v/v)	Chain length	Agitation rate (rpm)	Replicates ($K_p; s^{-1}$)					Average	Standard deviation
			1	2	3	4	5		
2.5	C ₁₀₋₁₃	1000	0.0601	0.0582	0.0584	0.0590	0.0586	0.0589	0.0008
20	C ₁₀₋₁₃	1000	0.0320	0.0322	0.0340	0.0326	0.0328	0.0327	0.0008
2.5	C ₁₄₋₂₀	1000	0.0554	0.0555	0.0568	0.0562	0.0542	0.0556	0.0010
20	C ₁₄₋₂₀	1000	0.0266	0.0274	0.0314	0.0288	0.0256	0.0280	0.0023

Table A7. 4: K_p data for influence of solids loading, solids particle size and their interaction in 2.5% (v/v) *n*-C₁₄₋₂₀-solid-aqueous dispersions

<i>n</i> -C ₁₄₋₂₀ (% v/v)	Agitation rate (rpm)	Solids loading (g/L)	Solids particle size (μm)	Replicates ($K_p; s^{-1}$)					Average	Standard deviation
				1	2	3	4	5		
2.5	1000	1	3	0.0358	0.0404	0.0433	0.0355	0.0332	0.0376	0.0041
2.5	1000	1	14	0.0347	0.0353	0.0369	0.0342	0.0331	0.0348	0.0014
2.5	1000	10	3	0.0364	0.0377	0.0381	0.0348	0.0330	0.0360	0.0021
2.5	1000	10	14	0.0358	0.0374	0.0385	0.0336	0.0337	0.0358	0.0022

Table A7.5: $K_L a$ data obtained from the GOP (no lag) in n -C₁₄₋₂₀-aqueous dispersions

n -C ₁₄₋₂₀ conc. (% v/v)	Agitation rate (rpm)	Replicates ($K_L a$; s ⁻¹)					Average	Standard deviation
		1	2	3	4	5		
0%	600	0.0297	0.0297	0.0296	0.0297	0.0299	0.0297	0.0001
	800	0.0358	0.0378	0.0407	0.0400	0.0398	0.0388	0.0020
	1000	0.0443	0.0424	0.0486	0.0440	0.0494	0.0457	0.0031
	1200	0.0483	0.0441	0.0486	0.0457	0.0444	0.0462	0.0021
2.5%	600	0.0208	0.0227	0.0219	0.0226	0.0221	0.0220	0.0008
	800	0.0264	0.0241	0.0246	0.0246	0.0238	0.0247	0.0010
	1000	0.0265	0.0255	0.0256	0.0265	0.0251	0.0258	0.0006
	1200	0.0262	0.0257	0.0265	0.0253	0.0265	0.0260	0.0005
5%	600	0.0201	0.0208	0.0199	0.0200	0.0198	0.0201	0.0004
	800	0.0237	0.0229	0.0228	0.0234	0.0235	0.0233	0.0004
	1000	0.0262	0.0256	0.0262	0.0260	0.0269	0.0262	0.0005
	1200	0.0273	0.0254	0.0270	0.0266	0.0284	0.0269	0.0011
10%	600	0.0181	0.0189	0.0197	0.0180	0.0194	0.0188	0.0008
	800	0.0228	0.0220	0.0223	0.0235	0.0221	0.0225	0.0006
	1000	0.0247	0.0239	0.0248	0.0252	0.0242	0.0246	0.0005
	1200	0.0255	0.0239	0.0256	0.0261	0.0252	0.0253	0.0008
20%	600	0.0144	0.0138	0.0199	0.0133	0.0135	0.0150	0.0028
	800	0.0201	0.0195	0.0199	0.0200	0.0186	0.0196	0.0006
	1000	0.0216	0.0226	0.0235	0.0232	0.0232	0.0228	0.0008
	1200	0.0242	0.0244	0.0245	0.0245	0.0250	0.0245	0.0003

Table A7.6: $K_L a$ data obtained from the GOP (lag) in $n\text{-C}_{14-20}$ -aqueous dispersions

$n\text{-C}_{14-20}$ conc. (% v/v)	Agitation rate (rpm)	Replicates ($K_L a$; s^{-1})					Average	Standard deviation
		1	2	3	4	5		
0%	600	0.0268	0.0271	0.0242	0.0309	0.0301	0.0278	0.0027
	800	0.0455	0.0524	0.0525	0.0533	0.0494	0.0506	0.0032
	1000	0.0646	0.0669	0.0697	0.0704	0.0778	0.0699	0.0050
	1200	0.0818	0.0826	0.0820	0.0709	0.0827	0.0800	0.0051
2.5%	600	0.0222	0.0233	0.0211	0.0244	0.0246	0.0231	0.0015
	800	0.0277	0.0247	0.0270	0.0300	0.0277	0.0274	0.0019
	1000	0.0321	0.0326	0.0344	0.0364	0.0341	0.0339	0.0017
	1200	0.0342	0.0367	0.0375	0.0384	0.0408	0.0375	0.0024
5%	600	0.0201	0.0202	0.0209	0.0207	0.0206	0.0205	0.0003
	800	0.0278	0.0284	0.0273	0.0288	0.0287	0.0282	0.0006
	1000	0.0353	0.0372	0.0374	0.0394	0.0399	0.0378	0.0019
	1200	0.0458	0.0441	0.0490	0.0432	0.0617	0.0488	0.0076
10%	600	0.0175	0.0195	0.0197	0.0185	0.0200	0.0190	0.0010
	800	0.0283	0.0290	0.0292	0.0309	0.0314	0.0298	0.0013
	1000	0.0351	0.0356	0.0404	0.0338	0.0365	0.0363	0.0025
	1200	0.0438	0.0433	0.0467	0.0413	0.0450	0.0440	0.0020
20%	600	0.0151	0.0151	0.0157	0.0158	0.0169	0.0157	0.0008
	800	0.0247	0.0245	0.0256	0.0273	0.0234	0.0251	0.0015
	1000	0.0271	0.0275	0.0306	0.0262	0.0280	0.0279	0.0017
	1200	0.0323	0.0321	0.0343	0.0308	0.0331	0.0325	0.0013

Table A7.7: K_p values used for $K_L a$ determination from the GOP (lag) in n -C₁₄₋₂₀-aqueous dispersions

n -C ₁₄₋₂₀	Agitation	Replicates (K_p ; s ⁻¹)					Average	Standard
		1	2	3	4	5		
conc. (% v/v)	rate (rpm)							deviation
0	1000	0.0393	0.0418	0.043	0.0445	0.0424	0.0422	0.0019
2.5	1000	0.0554	0.0555	0.0568	0.0562	0.0542	0.0556	0.0010
5	1000	0.0443	0.0442	0.0394	0.0392	0.0452	0.0425	0.0029
10	1000	0.0338	0.0341	0.0351	0.0352	0.0365	0.0349	0.0011
20	1000	0.0484	0.0483	0.0485	0.0496	0.0521	0.0494	0.0016

Table A7.8: K_{La} data obtained from the GOP (no lag) in n -C₁₀₋₁₃-aqueous dispersions

n -C ₁₀₋₁₃ conc. (% v/v)	Agitation rate (rpm)	Replicates (K_{La} ; s ⁻¹)					Average	Standard deviation
		1	2	3	4	5		
0%	600	0.0297	0.0297	0.0296	0.0297	0.0299	0.0297	0.0001
	800	0.0358	0.0378	0.0407	0.0400	0.0398	0.0388	0.0020
	1000	0.0443	0.0424	0.0486	0.0440	0.0494	0.0457	0.0031
	1200	0.0483	0.0441	0.0486	0.0457	0.0444	0.0462	0.0021
2.5%	600	0.0281	0.0277	0.0281	0.0269	0.0284	0.0278	0.0006
	800	0.0343	0.0316	0.0344	0.0349	0.0325	0.0335	0.0014
	1000	0.0407	0.0358	0.0377	0.0397	0.0350	0.0378	0.0024
	1200	0.0415	0.0334	0.0397	0.0488	0.0318	0.0390	0.0068
5%	600	0.0242	0.0238	0.0237	0.0234	0.0227	0.0236	0.0006
	800	0.0313	0.0296	0.0295	0.0321	0.0301	0.0305	0.0011
	1000	0.0337	0.0331	0.0329	0.0336	0.0331	0.0333	0.0003
	1200	0.0322	0.0312	0.0312	0.0327	0.0322	0.0319	0.0007
10%	600	0.0184	0.0199	0.0188	0.0179	0.0191	0.0188	0.0008
	800	0.0277	0.0262	0.0290	0.0276	0.0260	0.0273	0.0012
	1000	0.0307	0.0314	0.0316	0.0323	0.0316	0.0315	0.0006
	1200	0.0320	0.0317	0.0311	0.0317	0.0311	0.0315	0.0004
20%	600	0.0141	0.0150	0.0141	0.0137	0.0142	0.0142	0.0005
	800	0.0219	0.0205	0.0208	0.0217	0.0203	0.0210	0.0007
	1000	0.0309	0.0299	0.0314	0.0332	0.0319	0.0315	0.0012
	1200	0.0324	0.0317	0.0307	0.0300	0.0310	0.0312	0.0009

Table A7.9: $K_L a$ data obtained from the GOP (lag) in n -C₁₀₋₁₃-aqueous dispersions

n -C ₁₀₋₁₃ conc. (% v/v)	Agitation rate (rpm)	Replicates ($K_L a$; s ⁻¹)					Average	Standard deviation
		1	2	3	4	5		
0%	600	0.0268	0.0271	0.0242	0.0309	0.0301	0.0278	0.0027
	800	0.0455	0.0524	0.0525	0.0533	0.0494	0.0506	0.0032
	1000	0.0646	0.0669	0.0697	0.0704	0.0778	0.0699	0.0050
	1200	0.0818	0.0826	0.0820	0.0709	0.0827	0.0800	0.0051
2.5%	600	0.0342	0.0342	0.0342	0.0342	0.0342	0.0342	0.0000
	800	0.0438	0.0436	0.0436	0.0438	0.0435	0.0437	0.0002
	1000	0.0580	0.0613	0.0477	0.0528	0.0529	0.0545	0.0052
	1200	0.0589	0.0578	0.0632	0.0792	0.0725	0.0663	0.0092
5%	600	0.0247	0.0255	0.0247	0.0246	0.0255	0.0250	0.0005
	800	0.0393	0.0380	0.0393	0.0393	0.0379	0.0388	0.0008
	1000	0.0409	0.0448	0.0409	0.0409	0.0448	0.0424	0.0021
	1200	0.0549	0.0523	0.0588	0.0514	0.0448	0.0524	0.0052
10%	600	0.0194	0.0179	0.0160	0.0194	0.0177	0.0181	0.0014
	800	0.0316	0.0286	0.0386	0.0316	0.0286	0.0318	0.0041
	1000	0.0417	0.0454	0.0387	0.0387	0.0387	0.0407	0.0030
	1200	0.0690	0.0562	0.0534	0.0586	0.0529	0.0580	0.0065
20%	600	0.0120	0.0111	0.0120	0.0120	0.0110	0.0116	0.0005
	800	0.0227	0.0217	0.0218	0.0217	0.0216	0.0219	0.0005
	1000	0.0481	0.0482	0.0479	0.0480	0.0480	0.0480	0.0001
	1200	0.0535	0.0481	0.0473	0.0398	0.0556	0.0488	0.0062

Table A7.10: K_p values used for $K_L a$ determination from the GOP (lag) in $n\text{-C}_{10-13}$ -aqueous dispersions

$n\text{-C}_{10-13}$	Agitation	Replicates ($K_p; \text{s}^{-1}$)					Average	Standard
		1	2	3	4	5		
conc. (% v/v)	rate (rpm)							deviation
0	1000	0.0393	0.0418	0.0430	0.0445	0.0424	0.0422	0.0019
2.5	1000	0.0368	0.0391	0.0372	0.0391	0.0409	0.0386	0.0017
5	1000	0.0347	0.0370	0.0363	0.0357	0.0347	0.0357	0.0010
10	1000	0.0252	0.0259	0.0296	0.0240	0.0240	0.0257	0.0023
20	1000	0.0238	0.0239	0.0234	0.0222	0.0224	0.0231	0.0008

Table A7.11: K_La data obtained from the PSP in n -C₁₀₋₁₃-aqueous dispersions by Correia (2007)

n -C ₁₀₋₁₃ conc. (% v/v)	Agitation rate (rpm)	Replicates (K_La ; s ⁻¹)		Average	Standard deviation
		1	2		
0%	600	0.0272	0.0243	0.0258	0.0021
	800	0.0485	0.0440	0.0463	0.0032
	1000	0.0579	0.0601	0.0590	0.0016
	1200	0.0709	0.0664	0.0687	0.0032
2.5%	600	0.0253	0.0258	0.0256	0.0004
	800	0.0304	0.0327	0.0316	0.0016
	1000	0.0432	0.0457	0.0445	0.0018
	1200	0.0608	0.0618	0.0613	0.0007
5%	600	0.0235	0.0212	0.0224	0.0016
	800	0.0414	0.0421	0.0418	0.0005
	1000	0.0593	0.0614	0.0604	0.0015
	1200	0.0723	0.0720	0.0722	0.0002
10%	600	0.0183	0.0198	0.0191	0.0011
	800	0.0383	0.0365	0.0374	0.0013
	1000	0.0513	0.0514	0.0514	0.0001
	1200	0.0711	0.0694	0.0703	0.0012
20%	600	0.0128	0.0132	0.0130	0.0003
	800	0.0228	0.0224	0.0226	0.0003
	1000	0.0328	0.0325	0.0327	0.0002
	1200	0.0568	0.0569	0.0569	0.0001

Table A7.12: $K_L a$ data obtained from the GOP (no lag) in n -C₁₀₋₁₃-aqueous dispersions by Correia (2007)

n -C ₁₀₋₁₃ conc. (% v/v)	Agitation rate (rpm)	Replicates ($K_L a$; s ⁻¹)					Average	Standard deviation
		1	2	3	4	5		
0%	600	0.0265	0.0273	0.0264	0.0254	0.0257	0.0263	0.0007
	800	0.0370	0.0358	0.0345	0.0343	0.0352	0.0354	0.0011
	1000	0.0386	0.0395	0.0379	0.0377	0.0373	0.0382	0.0009
	1200	0.0368	0.0361	0.0367	0.0372	0.0368	0.0367	0.0004
2.5%	600	0.0268	0.0275	0.0255	0.0254	0.0240	0.0258	0.0014
	800	0.0365	0.0352	0.0303	0.0317	0.0300	0.0327	0.0029
	1000	0.0363	0.0350	0.0341	0.0352	0.0333	0.0348	0.0011
	1200	0.0324	0.0299	0.0329	0.0331	0.0320	0.0321	0.0013
5%	600	0.0226	0.0216	0.0212	0.0217	0.0233	0.0221	0.0009
	800	0.0307	0.0301	0.0309	0.0319	0.0261	0.0299	0.0022
	1000	0.0357	0.0360	0.0361	0.0358	0.0293	0.0346	0.0030
	1200	0.0339	0.0345	0.0342	0.0355	0.0279	0.0332	0.0030
10%	600	0.0193	0.0210	0.0204	0.0202	0.0211	0.0204	0.0007
	800	0.0335	0.0316	0.0314	0.0311	0.0304	0.0316	0.0012
	1000	0.0397	0.0391	0.0380	0.0382	0.0376	0.0385	0.0009
	1200	0.0417	0.0400	0.0392	0.0389	0.0381	0.0396	0.0014
20%	600	0.0133	0.0139	0.0129	0.0130	0.0128	0.0132	0.0004
	800	0.0225	0.0226	0.0234	0.0230	0.0221	0.0227	0.0005
	1000	0.0292	0.0297	0.0302	0.0304	0.0294	0.0298	0.0005
	1200	0.0338	0.0351	0.0343	0.0335	0.0337	0.0341	0.0006

Table A7.13: $K_L a$ data obtained from the GOP (lag) in $n\text{-C}_{14-20}$ -inert solid-aqueous dispersions

$n\text{-C}_{14-20}$ conc. (% v/v)	Agitation rate (rpm)	Solids loading (g/L)	Solids particle size (μm)	Replicates ($K_L a$; s^{-1})					Average	Standard deviation
				1	2	3	4	5		
2.5	600	1	3	0.0295	0.0266	0.0280	0.0277	0.0271	0.0278	0.0011
2.5	1200	1	3	0.0824	0.0757	0.0680	0.0752	0.0762	0.0755	0.0051
20	600	1	3	0.0180	0.0183	0.0194	0.0202	0.0199	0.0192	0.0010
20	1200	1	3	0.0367	0.0351	0.0435	0.0399	0.0424	0.0395	0.0036
2.5	600	10	3	0.0351	0.0311	0.0300	0.0317	0.0297	0.0315	0.0022
2.5	1200	10	3	0.0476	0.0500	0.0542	0.0662	0.0614	0.0559	0.0078
20	600	10	3	0.0179	0.0185	0.0185	0.0170	0.0176	0.0179	0.0006
20	1200	10	3	0.0402	0.0422	0.0425	0.0482	0.0440	0.0434	0.0030
2.5	600	1	14	0.0473	0.0329	0.0358	0.0351	0.0313	0.0365	0.0063
2.5	1200	1	14	0.0611	0.0647	0.0498	0.0553	0.0554	0.0573	0.0058
20	600	1	14	0.0137	0.0132	0.0141	0.0133	0.0125	0.0134	0.0006
20	1200	1	14	0.0314	0.0352	0.0364	0.0337	0.0395	0.0352	0.0030
2.5	600	10	14	0.0418	0.0309	0.0247	0.0288	0.0258	0.0304	0.0068
2.5	1200	10	14	0.0444	0.0417	0.0461	0.0589	0.0483	0.0479	0.0066
20	600	10	14	0.0175	0.0166	0.0166	0.0158	0.0194	0.0172	0.0014
20	1200	10	14	0.0320	0.0349	0.0419	0.0445	0.0432	0.0393	0.0055

Table A7.14: K_p values used for $K_L a$ determination from the GOP (lag) in n -C₁₄₋₂₀-inert solid-aqueous dispersions

n -C ₁₄₋₂₀ conc. (% v/v)	Agitation rate (rpm)	Solids loading (g/L)	Solids particle size (μm)	Replicates ($K_p; \text{s}^{-1}$)					Average	Standard deviation
				1	2	3	4	5		
2.5	600	1	3	0.0447	0.0433	0.0448	0.0442	0.0432	0.0440	0.0008
2.5	1200	1	3	0.0447	0.0433	0.0448	0.0442	0.0432	0.0440	0.0008
20	600	1	3	0.0424	0.0448	0.0442	0.0418	0.0421	0.0431	0.0013
20	1200	1	3	0.0424	0.0448	0.0442	0.0418	0.0421	0.0431	0.0013
2.5	600	10	3	0.0422	0.0436	0.0455	0.0445	0.0451	0.0442	0.0013
2.5	1200	10	3	0.0422	0.0436	0.0455	0.0445	0.0451	0.0442	0.0013
20	600	10	3	0.0424	0.0448	0.0442	0.0418	0.0421	0.0431	0.0013
20	1200	10	3	0.0424	0.0448	0.0442	0.0418	0.0421	0.0431	0.0013
2.5	600	1	14	0.0366	0.0376	0.0368	0.0364	0.0379	0.0371	0.0007
2.5	1200	1	14	0.0366	0.0376	0.0368	0.0364	0.0379	0.0371	0.0007
20	600	1	14	0.0391	0.0392	0.0405	0.0396	0.0398	0.0396	0.0006
20	1200	1	14	0.0391	0.0392	0.0405	0.0396	0.0398	0.0396	0.0006
2.5	600	10	14	0.0427	0.0399	0.0405	0.0396	0.0376	0.0401	0.0018
2.5	1200	10	14	0.0427	0.0399	0.0405	0.0396	0.0376	0.0401	0.0018
20	600	10	14	0.0426	0.0422	0.0413	0.0427	0.0403	0.0418	0.0010
20	1200	10	14	0.0426	0.0422	0.0413	0.0427	0.0403	0.0418	0.0010

Table A7.15: Fluid viscosity data obtained in n -C₁₄₋₂₀-inert solid-aqueous dispersions

n -C ₁₄₋₂₀ conc. (% v/v)	Solids loading (g/L)	Solids particle size (μ m)	Replicates (μ ; mPa.s)					Average	Standard deviation
			1	2	3	4	5		
2.5	1	3	1.075	1.040	1.060	1.070	1.110	1.071	0.026
20	1	3	1.170	1.325	1.300	1.325	1.320	1.288	0.067
2.5	10	3	1.145	1.170	1.170	1.250	1.230	1.193	0.045
20	10	3	1.320	1.450	1.450	1.585	1.455	1.452	0.094
2.5	1	14	1.080	1.125	1.075	1.125	1.105	1.102	0.024
20	1	14	1.155	1.120	1.075	1.100	1.070	1.104	0.035
2.5	10	14	1.130	1.055	1.165	1.195	1.145	1.138	0.052
20	10	14	1.080	1.000	1.155	1.090	1.105	1.086	0.056

Table A7.16: Fluid surface tension data obtained in n -C₁₄₋₂₀-inert solid-aqueous dispersions

n -C ₁₄₋₂₀ conc. (% v/v)	Solids loading (g/L)	Solids particle size (μm)	Replicates (σ ; mNm^{-1})					Average	Standard deviation
			1	2	3	4	5		
2.5	1	3	59.47	57.18	59.01	61.30	63.13	60.02	2.27
20	1	3	71.82	71.37	70.91	71.37	71.82	71.46	0.38
2.5	10	3	68.62	68.62	70.45	69.99	71.37	69.81	1.19
20	10	3	71.37	71.82	72.28	71.37	71.37	71.64	0.41
2.5	1	14	67.25	66.33	68.16	68.16	66.79	67.34	0.82
20	1	14	51.69	51.69	50.78	49.86	51.69	51.15	0.82
2.5	10	14	69.54	70.45	70.45	70.91	70.91	70.45	0.56
20	10	14	63.59	64.50	65.88	61.30	64.05	63.86	1.67

Table A7.17: $K_L a$ data obtained from the GOP (lag) in $n\text{-C}_{14-20}$ -yeast-aqueous dispersions

$n\text{-C}_{14-20}$ conc. (% v/v)	Agitation rate (rpm)	Yeast loading (g/L)	Replicates ($K_L a$; s^{-1})					Average	Standard deviation
			1	2	3	4	5		
2.5	600	1	0.0262	0.0267	0.0202	0.0248	0.0204	0.0237	0.0032
2.5	900	1	0.0433	0.0365	0.0373	0.0392	0.0467	0.0406	0.0043
11.25	600	1	0.0361	0.0345	0.0335	0.0336	0.0286	0.0333	0.0028
11.25	900	1	0.0385	0.0471	0.0465	0.0395	0.0358	0.0415	0.0051
2.5	600	5.5	0.0264	0.0265	0.0273	0.0255	0.0257	0.0263	0.0007
2.5	900	5.5	0.0348	0.0334	0.0333	0.0362	0.0350	0.0345	0.0012
11.25	600	5.5	0.0148	0.0153	0.0141	0.0146	0.0145	0.0147	0.0004
11.25	900	5.5	0.0256	0.0254	0.0238	0.0261	0.0250	0.0252	0.0009
6.8	750	3.25	0.0333	0.0323	0.0345	0.0345	0.0325	0.0334	0.0010

Table A7.18: K_p values used for $K_L a$ determination from the GOP (lag) in n -C₁₄₋₂₀-yeast-aqueous dispersions

n -C ₁₄₋₂₀ conc. (% v/v)	Agitation rate (rpm)	Yeast loading (g/L)	Replicates (K_p ; s ⁻¹)					Average	Standard deviation
			1	2	3	4	5		
2.5	600	1	0.0485	0.0469	0.0466	0.0504	0.0458	0.0476	0.0018
2.5	900	1	0.0384	0.0394	0.0402	0.0412	0.0434	0.0405	0.0019
11.25	600	1	0.0472	0.0466	0.0509	0.0492	0.0475	0.0483	0.0018
11.25	900	1	0.0472	0.0466	0.0509	0.0492	0.0475	0.0483	0.0018
2.5	600	5.5	0.0384	0.0394	0.0402	0.0412	0.0434	0.0405	0.0019
2.5	900	5.5	0.0384	0.0394	0.0402	0.0412	0.0434	0.0405	0.0019
11.25	600	5.5	0.0437	0.0432	0.0437	0.0439	0.0432	0.0435	0.0003
11.25	900	5.5	0.0472	0.0466	0.0509	0.0492	0.0475	0.0483	0.0018
6.8	750	3.25	0.0385	0.0411	0.0407	0.0415	0.0394	0.0402	0.0013

Table A7.19: Fluid viscosity data obtained in n -C₁₄₋₂₀-yeast-aqueous dispersions

n -C ₁₄₋₂₀	Yeast loading	Replicates (μ ; mPa.s)					Average	Standard deviation
		1	2	3	4	5		
conc. (% v/v)	(g/L)							
2.5	1	1.060	1.050	1.100	1.100	1.110	1.084	0.027
11.25	1	1.420	1.540	1.300	1.325	1.320	1.381	0.100
2.5	5.5	1.390	1.400	1.400	1.330	1.330	1.370	0.037
11.25	5.5	1.490	1.390	1.650	1.680	1.540	1.550	0.119
6.88	3.25	1.550	1.500	1.650	1.560	1.550	1.562	0.054

Table A7.20: Fluid surface tension data obtained in $n\text{-C}_{14-20}$ -yeast-aqueous dispersions

$n\text{-C}_{14-20}$	Yeast loading	Replicates (σ ; mNm^{-1})					Average	Standard
		1	2	3	4	5		
conc. (% v/v)	(g/L)							deviation
2.5	1	27.22	27.68	27.91	26.76	27.91	27.49	0.50
11.25	1	27.68	26.30	25.39	25.62	25.16	26.03	1.02
2.5	5.5	29.28	32.94	33.40	33.40	35.23	32.85	2.18
11.25	5.5	33.17	29.51	29.74	29.28	29.74	30.28	1.62
6.8	3.25	29.28	31.34	32.48	32.02	31.79	31.38	1.25

A.8: Statistical validation of experimental results

Major conclusions from this work were made statistically. Besides the statistical interpretation of results by STATISTICA for factors affecting K_p (see section 5.1.1; Figure 5.1; Figure 5.3; Figure 5.5 and Figure 5.7). K_{La} behavior in aerated agitated alkane-inert solid-aqueous dispersions and the influence of fluid viscosity and fluid surface tension in these alkane-inert solid-aqueous dispersions were quantified at 99% confidence interval using STATISTICA (see section 5.2.1; Figures 5.14 - 5.16). In addition K_{La} behavior in aerated agitated alkane-yeast-aqueous dispersions and influence of fluid viscosity and fluid surface tension in these dispersions were also quantified statistically at 99% confidence by STATISTICA (see section 5.2.2; Figures 5.28 - 5.30).

Furthermore when determining the accuracy of K_{La} measurement method, the *t-test* was used for comparing K_{La} results from the GOP (lag) and the GOP (no lag) in *n*-C₁₀₋₁₃ and *n*-C₁₄₋₂₀-aqueous dispersions for all process conditions at 99% confidence interval (see section 5.1.2; Figure 5.9 and Figure 5.10; Table A8.1 and Table A8.2). In addition to that, it was also proven statistically using a *t-test* that the differences between the GOP (lag) and the GOP (no lag) in *n*-C₁₀₋₁₃ and *n*-C₁₄₋₂₀ aqueous dispersions for all alkane concentrations significantly increased with increase in agitation rate at 99% confidence interval (see section 5.1.2; Figure 5.11; Figure 5.12; Table A8.3 and Table A8.4). This is also supported by the increase in the *F-variance ratio* with increase in agitation rate (Table A8.3 and Table A8.4). Also the *t-test* was used to compare the K_{La} results in *n*-C₁₀₋₁₃-aqueous dispersions from the PSP reported by Correia and Clarke (2009) to those from the GOP (lag) in this work and no significant difference was noted at 99% confidence interval (see section 5.1.2; Figure 5.13 and Table A8.5). Lastly the *t-test* was used to check for any variance between K_{La} results in *n*-C₁₀₋₁₃-aqueous dispersions from this work and those

obtained by Correia (2007) measured by the GOP (no lag) (see Tables A7.8 and A7.12; Figure A7.5 and Table A8.6). No significant difference was found between the K_{La} data at 99% confidence interval.

For all t -test analyses, if the modulus of $t_{stat} > t_{crit}$ for the one tail and the two tails, then the differences will be significant else the opposite holds.

Table A8.1: t -test two-sample assuming equal variances for K_{La} results from GOP (no lag) and GOP (lag) in 0-20% (v/v) n -C₁₄₋₂₀-aqueous dispersions and agitation 600-1200rpm

Statistical parameter	K_{La} (s ⁻¹) (GOP no lag)	K_{La} (s ⁻¹) (GOP lag)
Mean	0.0244	0.0357
Variance	0.0000	0.0002
Observations	120	120
Pearson correlation	0.765	
Hypothesized mean difference	0	
df	119	
t Stat	-11.927	
P(T<=t) one-tail	0.000	
t Critical one-tail	1.658	
P(T<=t) two-tail	0.000	
t Critical two-tail	1.980	

Table A8.2: t -test two-sample assuming equal variances for K_{La} results from GOP (no lag) and GOP (lag) in 0-20% (v/v) n -C₁₀₋₁₃-aqueous dispersions and agitation 600-1200rpm

Statistical parameter	K_{La} (s ⁻¹) (GOP no lag)	K_{La} (s ⁻¹) (GOP lag)
Mean	0.0297	0.0417
Variance	7.3E-05	3.3E-04
Observations	120	120
Pooled variance	0.000	
Hypothesized mean difference	0	
df	238	
t Stat	-6.579	
P(T<=t) one-tail	0.000	
t Critical one-tail	2.342	
P(T<=t) two-tail	0.000	
t Critical two-tail	2.597	

Table A8.3: *t*-test two-sample for independent results for $K_L a$ average results from GOP (no lag) and GOP (lag) in 0-20% (v/v) $n\text{-C}_{14-20}$ -aqueous dispersions and agitation 600-1200rpm

Agitation	GOP (no lag)	GOP (lag)	<i>t</i> -value	df	p	Stdev (GOP no lag)	Stdev (GOP lag)	F ratio var	p Variances
600	0.021	0.021	-0.110	8	0.915	0.006	0.005	1.641	0.643
800	0.026	0.032	-1.115	8	0.297	0.007	0.010	1.936	0.538
1000	0.029	0.041	-1.450	8	0.185	0.010	0.016	2.995	0.313
1200	0.030	0.049	-2.023	8	0.078	0.009	0.019	4.062	0.203

Table A8.4: *t*-test two-sample for independent results for $K_L a$ average results from GOP (no lag) and GOP (lag) in 0-20% (v/v) $n\text{-C}_{10-13}$ -aqueous dispersions and agitation 600-1200rpm

Agitation	GOP (no lag)	GOP (lag)	<i>t</i> -value	df	p	Stdev (GOP no lag)	Stdev (GOP lag)	F ratio var	p Variances
600	0.024	0.023	0.091	8	0.930	0.006	0.009	2.143	0.479
800	0.030	0.037	-1.233	8	0.252	0.007	0.011	2.742	0.352
1000	0.036	0.051	-2.556	8	0.034	0.007	0.012	3.559	0.246
1200	0.036	0.061	-3.994	8	0.004	0.006	0.012	3.813	0.223

Table A8.5: *t*-test two-sample assuming equal variances for average K_{La} results from GOP (lag) and PSP in 0-20% (v/v) *n*-C₁₀₋₁₃-aqueous dispersions and agitation 600-1200rpm

Statistical parameter	K_{La} (s ⁻¹) (GOP lag)	K_{La} (s ⁻¹) (PSP)
Mean	0.0438	0.0431
Variance	0.000	0.000
Observations	20	20
Pooled variance	0.000	
Hypothesized mean difference	0	
df	38	
<i>t</i> Stat	0.111	
P(T<=t) one-tail	0.456	
<i>t</i> Critical one-tail	2.429	
P(T<=t) two-tail	0.912	
<i>t</i> Critical two-tail	2.712	

Table A8.6: *t*-test two-sample assuming equal variances for K_{La} results from GOP (no lag) from this work and those reported by Correia (2007) in 0-20% (v/v) *n*-C₁₀₋₁₃-aqueous dispersions and agitation 600-1200rpm

Statistical parameter	K_{La} (s ⁻¹) (GOP no lag) this work	K_{La} (s ⁻¹) (GOP no lag) Correia (2007)
Mean	0.0297	0.0304
Variance	0.0001	0.0000
Observations	120	120
Pooled variance	6E-05	
Hypothesized mean difference	0	
df	222	
<i>t</i> Stat	-0.635	
P(T<=t) one-tail	0.263	
<i>t</i> Critical one-tail	2.343	
P(T<=t) two-tail	0.526	
<i>t</i> Critical two-tail	2.598	